Polymerization of Ethene and Ethene-co-α-Olefin: Investigations on Short- and Long-Chain Branching and Structure-Property Relationships

Dissertation

submitted to
Department of Chemistry
University of Hamburg

in partial fulfillment of the requirements
for the German academic degree
Dr. rer. nat.

Christian Piel

Hamburg 2005

Gutachter / Reviewers:	Prof. Dr. W. Kaminsky
	Prof. Dr.-Ing. W.-M. Kulicke
Disputation:	28. October 2005

Preface

The presented work was carried out in the research group of Prof. Dr. Walter Kaminsky at the Institute of Technical and Macromolecular Chemistry, University of Hamburg between September 2002 and August 2005.

My warmest thanks to Prof. Dr. Walter Kaminsky for giving me the opportunity to work freely in his laboratory, for advices, financial support, and for the interesting projects he charged me with.

I appreciate the time in the lab with all group members and thank all for taking part somehow on this work, e.g. by DSC or NMR measurements or many other things. A special thank to my lab colleagues Sascha Rulhoff, Matthias Donner, Ignacio Javier Núñez Zorriqueta, Dr. Katharina Wiemann, Dr. Marco Frediani and Dr. Fabian Müller for the warm atmosphere in the lab and the fruitful discussions, as well as the jolly times in- and outside the lab.

Many thanks to the team of the institute for all the important support and an extra thank to Klaus Horbaschk for his technical support and conversations on so many topics.

For the successful collaboration and many discussions I thank Prof. Dr. Helmut Münstedt and his research group, especially Florian Stadler. I appreciate very much the cooperation with Prof. Dr. Manfred Wilhelm and Katja Klimke. To Dr. Edgar Karssenberg many thanks for the successful cooperation in the lab work and for all the nice times at conferences, in Hamburg and Helsinki.

I gratefully acknowledge Prof. Dr. Jukka Seppälä and his group for the warm welcome, support and great time during my stay in Helsinki; many thanks to Dr. Paul Starck for his advices and the good collaboration.

The Deutsche Forschungsgemeinschaft (DFG) and Deutscher Akademischer Austauschdienst (DAAD) I thank for financial support.

A very warm thank to my parents for supporting me all the time during my studies and making this work possible at all. My dearest thanks to my lovely partner in life Tanja Seraidaris for all her support, the discussions and the broadening of my view by far not only on this thesis.

Zusammenfassung

Lineare und langkettenverzweigte high density Polyethylene mit molaren Massen M_w von 1.7 bis 1 150 kg/mol sind mit Metallocen-Katalysatoren synthetisiert worden. Abhängig von den Polymerisationsparametern wurden Molekulargewichtsverteilungen zwischen 2 und 12 erreicht. Die Detektion der Verzweigungen erfolgte durch zwei voneinander unabhängige Methoden, durch Schmelzrheologie und SEC-MALLS. Die aus den rheologischen Messungen erhaltenen Nullviskositäten η_0 deckten einen breiten Bereich von 10^{-3} bis etwa 10^8 Pas ab. Oberhalb der kritischen Molmasse von $M_c \approx 2900$ g/mol können die experimentellen Ergebnisse von linearen Polyethylenen durch die Beziehung $\eta_0 \sim M_w^{3.6}$ beschrieben werden, unabhängig von der Molekulargewichtverteilung. Es wurde beobachtet, dass die Viskositätsfunktion sehr stark von der Molekulargewichtverteilung und von dem Verzweigungsgrad beeinflusst wird. Die Molekulargewichtverteilung wird durch den Katalysatortyp und die Polymerisationsbedingungen beeinflusst. Eine Abhängigkeit des Schmelzpunktes und der Schmelzenthalpie von der Molmasse M_w wurde ebenfalls beobachtet. Neue Struktur-Eingeschaftsbeziehungen zwischen Katalysatorstruktur, Polymerisationsbedingungen und dem Verzweigungsgehalt von Polyethylenen konnten aufgestellt werden.

Copolymere aus Ethen mit 1-Octen, 1-Dodecen, 1-Octadecen und 1-Hexacosen mit Verzweigungslängen von 6 bis 26 Kohlenstoffatomen wurden mit dem Katalysatorsystem $[Ph_2C(2,7\text{-di-}^{tert}BuFlu)(Cp)]ZrCl_2/MAO$ hergestellt. Dieser Katalysator zeigt eine sehr hohe und lang anhaltende Polymerisationsaktivität. Das Einbauverhalten gegenüber Comonomeren ist sehr gut und mit Wasserstoff lässt sich die Molmasse der Polymere regulieren. Für das Polyethylen wurden etwa 0.37 bzw. 0.30 Langkettenverzweigungen pro Molekül mittels NMR und SEC-MALLS bestimmt. Rheologische Größen, wie die Nullviskosität η_0, erhöhen sich gegenüber denen von linearen Materialien mit gleichem M_w, wenn Langkettenverzweigungen vorhanden sind. Die Form der Viskositätsfunktion und der Gleichgewichtsnachgiebigkeit J_e^0 zeigen eine Abhängigkeit von Comonomergehalt und –länge im Polymer. Diese Beobachtungen konnten benutzt werden, um die verschiedenen Langkettenverzweigungsstrukturen zu erläutern. Die Proben mit dem höchsten Comonomergehalt verhielten sich wie lineare Polymere und die mit wenig Comonomergehalt wie langkettenverzweigte. Neben dem Comonomergehalt hat auch der Comonomertyp einen Einfluss auf die Langkettenverzweigungen und Materialeigenschaften. Die kristallinen Methylensequenzlängen und die lamellaren Schichtdicken der Copolymere wurden nach

Anwendung einer Technik zur fraktionierten Kristallisation in der DSC berechnet. Durch DMA Messungen konnten das Speichermodul als Indikator für Steifigkeit des Materials und das Verlustmodul zur Messung des Einflusses der Verzweigungen auf die α- und β-Relaxationen des Materials bestimmt werden. Die Ergebnisse wurden mit den Messungen von Materialdichte und Zugfestigkeiten korreliert und dadurch der Einfluss von Comonomergehalt und –typ auf die Materialeigenschaften charakterisiert. Die Hexacosen-Copolymere zeigten bemerkenswerte Materialeigenschaften, die sich deutlich von denen der bisher bekannten LLDPEs unterscheiden. Die Seitenketten kristallisieren in Form von Agglomeraten nicht nur parallel zur Hauptkette; diese Erkenntnisse ließen sich auch auf Ethen-Octadecen-Copolymere übertragen.

Drei Serien von Ethen/Propen-Copolymeren wurden mit den Katalysatoren 1) *rac*-[$Me_2Si(2\text{-}Me\text{-}4\text{-}(1\text{-}Naph)Ind)_2]ZrCl_2$ / MAO, 2) [$Me_2Si(Ind)(Flu)]ZrCl_2$ / MAO und 3) einer 1:5 Mischung aus 1 und 2, alle in einem großen Bereich von Comonomerfraktionen im Reaktor und Polymer, hergestellt. Die ^{13}C NMR Spektren der single-site Serien wurden genutzt, um mit der Direct Peak Methode die Reaktionsraten der Katalysatoren nach Markov zweiter Ordnung zu bestimmen. Die Aktivitäten und Reaktionsraten der Katalysatoren wurden dann dazu verwendet, die dual-site Serie anhand der NMR Daten zu modellieren. Mit den Ergebnissen der Modellierung konnten anschließend die DSC und SEC Daten der dual-site Serie interpretiert werden.

Summary

Linear and long-chain branched high density polyethylenes with a molar mass M_w between 1 700 and 1 150 000 g/mol were synthesized using metallocene catalyst systems. Depending on the polymerization parameters the molar mass distribution reached values ranging from 2 to 12. The branch detection took place via two independent methods, melt rheology and SEC-MALLS. The resulting zero shear-rate viscosities covered a range from 10^{-3} to around 10^{8} Pas. Above a critical molar mass of $M_c \approx 2900$ g/mol the experimental results for linear polyethylenes can be described by the relation $\eta_0 \sim M_w^{3.6}$ independently of the molar mass distribution. The viscosity function was found to be strongly influenced by the molar mass distribution and the degree of long-chain branching. The molar mass distribution was affected by the catalyst type and the polymerization conditions. A dependence of the melting point and the melting enthalpy on the molar mass was observed. New relationships between catalyst structure, polymerization conditions and the branching content of polyethylenes were established.

Copolymers of ethene and 1-octene, 1-dodecene, 1-octadecene, and 1-hexacosene were carried out using $[Ph_2C(2,7\text{-di-}^{tert}BuFlu)(Cp)]ZrCl_2/MAO$ as catalyst to obtain short-chain branched polyethylenes with branch length from 6 to 26 carbon atoms. This catalyst provides high activity and a very good comonomer and hydrogen response. For the homopolymer approximately 0.37 and 0.30 LCB/molecule were found by NMR and SEC-MALLS respectively. Rheological quantities, such as the zero shear-rate viscosity, increased with LCB as compared to linear samples of the same M_w. The shape of the viscosity function and the linear steady-state elastic compliance J_e^0 showed a dependence on comonomer content and length. These findings are used to elucidate the various long-chain branching architectures. The samples with highest comonomer content behaved like typical linear polymers in rheological experiments, while those with less comonomer were found to be long-chain branched. Besides the comonomer content, the type of comonomer has an influence on the branching structure and material properties. The crystalline methylene sequence lengths of the copolymers and lamellar thicknesses were calculated applying a DSC successive self-annealing separation technique. By DMA the storage modulus as an indicator of stiffness and loss modulus as a measure of the effect of branching on the α- and β-relaxations were studied. The results were related to the measurements of the polymer's density and tensile strength in order to determine the effect of longer side-chains on the material properties. The hexacosene copolymers have side-chains of 24 carbons and

remarkable material properties, different from conventional LLDPEs. The side-chains of these copolymers crystallize with each other and not only parallel to the backbone lamellar layer, even at low concentrations. A transfer of these results to 16 carbons side-chains in ethene/octadecene copolymers was also possible.

Three series of ethene/propene copolymers were made using the catalysts 1) *rac*-[$Me_2Si(2\text{-}Me\text{-}4\text{-}(1\text{-}Naph)Ind)_2]ZrCl_2$ / MAO, 2) [$Me_2Si(Ind)(Flu)]ZrCl_2$ / MAO and 3) a 1:5 mixture of 1 and 2, all with a broad range of (co)monomer mole fractions in the reactor and copolymers. The ^{13}C NMR spectra of the single-site series are the input of the Direct Peak Method to determine the second order Markov reactivity ratios of the catalysts used. The activities and reactivity ratios of the catalysts in the single-site experiments are used to model the dual-site series based on ^{13}C NMR data. The results of this modeling are used to interpretate the DSC and SEC data of the dual-site series.

Table of content

List of publications

Articles

This thesis is based on the following publications (**I-VI**), which are, throughout this book, referred to by their Roman numbers.

I. C. Piel, F. Stadler, J. Kaschta, S. Rulhoff, H. Münstedt, W. Kaminsky; *Structure-Property Relationships of Linear and Long-Chain Branched Metallocene High Density Polyethylenes Characterized by Shear Rheology and SEC-MALLS*; Macromol. Chem. Phys. **2005**, accepted.

II. F. Stadler, C.Piel, S. Rulhoff, W. Kaminsky, H. Münstedt; *Dependence of the zero shear-rate viscosity and the viscosity function of linear high density polyethylenes on the mass average molar mass and polydispersity*; Rheol. Acta **2005**, in press.

III. W. Kaminsky, C. Piel, K. Scharlach; *Polymerization of Ethene and Longer Chained Olefins by Metallocene Catalysis*; Macromol. Symp. **2005**, 226(1), 25-34.

IV. F. Stadler, C. Piel, K. Klimke, J. Kaschta, M. Parkinson, W. Kaminsky, M. Wilhelm, H. Münstedt; *Influence of type and content of very long comonomers on long-chain branching of ethene/α-olefin copolymers*; Macromolecules **2005**, accepted.

V. C. Piel, F.G. Karssenberg, W. Kaminsky, V.B.F. Mathot; *Single-Site and Dual-Site Metallocene Ethene/Propene Copolymerizations: Experimental and Theoretical Investigations*; Macromolecules **2005**, 38(16), 6789-6795.

VI. C. Piel, P. Starck, J.V. Seppälä, W. Kaminsky; *Thermal and Mechanical Analysis of Metallocene-Catalyzed Ethylene-α-Olefin Copolymers: The influence of length and number of the crystallizing side-chain*; submitted **2005**.

Other relevant publications:

VII. W. Kaminsky, A. Hopf, C. Piel; *C_s-symmetric hafnocene complexes for synthesis of syndiotactic polypropene*; J. Organomet. Chem. **2003**, 684, 200-205.

VIII. M. Pollard, K. Klimke, R. Graf, H.W. Spiess, M. Wilhelm, O. Sperber, C. Piel, W. Kaminsky; *Observation of Chain Branching in Polyethylene in the Solid State and Melt via ^{13}C NMR Spectroscopy and Melt NMR Relaxation Time Measurements*; Macromolecules **2004**, 37, 813-826.

IX. W. Kaminsky, C. Piel; *Tailoring polyolefins by metallocene catalysis: kinetic and mechanistic aspects;* J. Mol. Cat. A: Chemical **2004**, 213, 15-19.

X. W. Kaminsky, C. Piel, K. Wiemann; *Recent developments in metallocene catalysis;* DECHEMA Monographien **2004**, 138 (8th International Workshop on Polymer Reaction Engineering, 2004), 131-140.

XI. F.G. Karssenberg, C. Piel, A. Hopf, V.B.F. Mathot, W. Kaminsky; *Chain Microstructure of Homogeneous Ethylene-1-Alkene Copolymers and Characteristics of Single Site Catalysts using a Direct 13C NMR Peak Method. Part III: Application to Ethylene-Propylene Copolymers Showing No Inversion*; J. Pol. Sci. Part B: Polym. Phys. **2005**, in press.

XII. F.G. Karssenberg, C. Piel, A. Hopf, V.B.F. Mathot, W. Kaminsky; *Bernoullian, terminal, penultimate or third order Markov statistics?;* Macromol. Theory Simul., **2005**, 14, 295-299.

XIII. K. Klimke, M. Parkinson, C. Piel, W. Kaminsky, H.W. Spiess, M. Wilhelm; *Optimisation and Application of Polyolefin Branch Quantification by Melt-State ^{13}C NMR Spectroscopy*; submitted **2005**.

Conference contributions

A. Poster: C. Piel, M. Frediani, W. Kaminsky; *Copolymerization of ethene or propene with higher 1-olefines by single site catalysts*; EUPOC 2003 (European Polymer Conference on Stereospecific Polymerization and Stereoregular Polymers), Milano – Italy **2003**.

B. Talk: F.G. Karssenberg, C. Piel, V.B.F. Mathot and W. Kaminsky; *Towards the Modeling of Heterogeneous Catalysts Using Mixtures of Metallocenes: Theory and Experiments*; MOSPOL 2004 (International Olefin Polymerization Conference) Moscow - Russia **2004**.

C. Poster: C. Piel, W. Kaminsky; *Lineare, Kurz- und Langkettenverzweigte Polyethene Definierter Mikrostruktur mit Metallocen/MAO-Katalysatoren*; Bayer Doktoranden-Seminar, Leverkusen – Germany **2004**.

D. Poster: C. Piel, P. Starck, J. Seppälä, W. Kaminsky; *Thermal and Mechanical Analysis of Metallocene-Catalyzed Ethylene-α-Olefin Copolymers: A Comparative Study of the Side Chain Length Influence up to a length of 26 carbons*; 2nd Blue Sky Conference on Catalytic Olefin Polymerization, Sorrento - Italy **2005**.

E. Poster: C. Piel, S. Rulhoff, B. Arikan, W. Kaminsky; *Definiert langkettenverzweigte Polyolefine durch Copolymerisation mit Metallocen-Katalysatoren*; Hamburger Makromolekulares Symposium, Hamburg – Germany **2005**.

Other contributions:

F. Talk: O. Sperber, M. Frediani, W. Kaminsky, C. Piel; *Metallocene catalyzed copolymerizations of ethene and propene with higher α-olefins to yield short-, long- and ultra long branched polyolefins*; XXXVI Jahrestreffen Deutscher Katalytiker, Weimar - Germany **2003**.

G. Poster: M. Pollard, H.W. Spiess, and M. Wilhelm O. Sperber, C. Piel, W. Kaminsky; E*xpanding the Detection Limit for Side-Chain Branches in Polyethylene: 13C NMR Spin-Lattice Relaxation and NOE Buildup Directly in the Melt*; American Chemical Society, Division of Polymer Chemistry, 225th ACS National Meeting - Spring 2003, New Orleans, LA - USA **2003**. Polymer Preprints 2003, 44(1), 369.

H. Poster: M. Wilhelm, M. Pollard, R. Graf, K. Klimke, H.W. Spiess, O. Sperber, C. Piel, W. Kaminsky; *Topology in polyolefins as seen by solid-state NMR and FT-rheology*; American Chemical Society, Division of Polymer Chemistry, 226th ACS National Meeting - Fall 2003, New York City, NY – USA **2003**. Polymer Preprints 2003, 44(2), 45.

I. Poster: K. Klimke, M. Pollard, R. Graf, H.W. Spiess, O. Sperber, C. Piel, W. Kaminsky, M. Wilhelm; *Observation of Chain Branching in Polyethylene by Melt- & Solid-State 13C-NMR Spectroscopy & Melt Relaxation Time Measurements*; Makromolekulares Kolloquium, Freiburg – Germany **2004**.

J. Poster: K. Klimke, M. Pollard, R. Graf, H. W. Spiess, O. Sperber, C. Piel, W. Kaminsky, M. Wilhelm; *Optimum detection of chain branching in polyethylene in the melt- and solid-state via 13C NMR spectroscopy*; MACRO 2004 (40^{th} World Polymer Congress of the Macromolecular Division of the International Union of Pure and Applied Chemistry), Paris – France **2004**.

K. Poster: S. Rulhoff, C. Piel, B. Arikan, W. Kaminsky; *Short and Long Chain Branched Polyolefins of Defined Microstructure by Metallocene / MAO-Catalysts*; Makromolekulares Kolloquium, Freiburg – Germany **2005**.

L. Poster: F.J. Stadler, C. Piel, K. Klimke, J. Kaschta, M. Parkinson, W. Kaminsky, M. Wilhelm, H. Münstedt; *Einfluss von Comonomergehalt und –länge auf die Bildung von Langketten-verzweigungen in Ethen-/α-Olefin-Copolymeren*; Hamburger Makromolekulares Symposium, Hamburg – Germany **2005**.

M. Poster: M. Frediani, C. Piel, W. Kaminsky; *Tandem Copolymerisation: Effektive Kontrolle von Verzweigungsgrad und Molekulargewichtsverteilung*; Hamburger Makromolekulares Symposium, Hamburg – Germany **2005**.

1. Introduction

1.1 History of polyolefin catalysis

The first industrially practical polyethylene synthesis was discovered by Eric Fawcett and Reginald Gibson at ICI Chemicals in 1933. It was not until 1935 that another ICI chemist, Michael Perrin, developed the reproducible high-pressure synthesis for polyethylene, which became the basis for industrial LDPE (low density polyethylene) production beginning in 1939. Ethene was polymerized under extremely high pressure (500 - 1200 atm) and high temperatures (200 – 400 °C) to a white waxy material. The reaction had been initiated by trace oxygen contamination in the apparatus (< 3 %).[1]

Subsequent landmarks in polyethylene synthesis have centered on the development of several types of catalyst that promote ethylene polymerization at more mild temperatures and pressures. The first of these was a chromium trioxide based catalyst discovered in 1951 by Robert Banks and John Hogan at Phillips Petroleum, although it was patented later in 1958.[2] In 1953, Karl Ziegler developed a catalytic system based on titanium halides and organoaluminum compounds that worked at even milder conditions than the Phillips catalyst.[3,4] The Phillips catalyst is less expensive and easier to work with, leading to both methods being used in industrial practice. By the end of the 1950s both, the Phillips and Ziegler type catalysts were being used for HDPE production.

A third type of catalytic system, based on metallocenes, was discovered in 1976 in Germany by Walter Kaminsky and Hansjörg Sinn.[5] The Ziegler and metallocene catalyst families have since proven to be very flexible at copolymerizing ethene with other olefins and have become the basis for the wide range of polyethylene resins available today, including VLDPE (very low density PE), LLDPE, and MDPE (medium density PE).

Until recently, the metallocenes were the most active single-site catalysts for ethylene polymerization known - new catalysts are typically compared to zirconocene dichloride.

1.2 Ziegler-Natta catalysis

In 1953 Karl Ziegler developed the catalytic polymerization of ethylene.[6] Gaseous ethene was polymerized quickly to high-molecular polymers at pressures of 100, 20 or 5 atm and even at atmosphere pressure using simple producible catalysts. With this discovery,[3,4,7] based on fundamental investigations of the reaction between ethene and organometallic compounds, especially aluminum compounds, Ziegler has changed the world in a twofold way: He initiated many scientific studies in the field of catalysis using organometallic compounds and his discovery was of outstanding relevance for the industrial synthesis of polyolefins. The production of polyethylenes by polymerization of ethene under normal pressure or pressures up to 5 MPa and moderate high temperatures (up to 90 °C) using organometallic catalysts formed by mixing alkyl aluminum compounds and transition-metal chlorides, such as $TiCl_4$ in a hydrocarbon diluent (diesel oil or petrol) was transferred into an industrial process within a few months.[8] With these catalysts Natta and co-workers polymerized propylene to isotactic polypropylene. They discovered the principles of the regio- and stereospecific polymerization of 1-alkenes.[9,10] The process to synthesize isotactic polypropylene was again transferred into a industrial process within a few years because a polymer with new properties was accessible.[8] These catalysts can also be used for the copolymerization of ethene and propene to produce ethene–propene elastomers; again these were new polymers.[11]

1.3 Metallocene catalysis

1.3.1 Development of single-site catalysts

Soon after Ziegler and Natta discovered heterogeneous olefin polymerization catalysts in the mid-1950s, efforts were directed toward devising homogeneous catalyst model systems that would prove more amenable to study. In 1957, Natta and Breslow reported that the metallocene Cp_2TiCl_2 could be activated for olefin polymerization by Et_3Al or Et_2AlCl.[12-14] These soluble catalysts polymerized ethene but were inactive for propene and exhibited much lower activities than the heterogeneous systems. Reichert and Meyer reached an enhancement in the polymerization activity upon addition of water to the $Cp_2TiEtCl/AlEtCl_2$ catalyst system.[15] The situation changed dramatically in the early 1980s when Sinn and Kaminsky discovered partially hydrolyzed Me_3Al, called methylaluminoxane (MAO). MAO was able to activate group IV metallocenes for the polymerization of both ethene and α-olefins.[5,16] This discovery has stimulated a renaissance in single-site catalysis, with olefin polymerization clearly receiving the most attention.[17]

Efforts to polymerize propene were less satisfying, the product was found to be fully atactic, indicating complete lack of stereospecifity of the catalyst.[18] Besides the availability of suitable organometallic cocatalysts, the development of stereoselective, metallocene-based catalysts required the development of chiral, stereorigid metallocenes, first developed by Brintzinger in 1982.[19,20] Between 1984 and 1986, two key discoveries were made: the effect that different alkyl-substituted cyclopentadienyl ligands can induce on metallocene performances in olefin polymerization (the ligand effect)[21,22] and the discovery that stereorigid, chiral metallocene catalysts can induce enantioselectivity in α-olefin insertion.[23,24] Since then, thanks to the combined efforts of industrial and academic research groups worldwide, an impressive increase of the knowledge of, and control over, the mechanistic details of olefin insertion, chain growth, and chain release processes at the molecular level has been made.[25]

In the early 1990s supported metallocenes were introduced to enable gas phase polymerization. Also ethene/α-olefin copolymers with high comonomer content, cycloolefin copolymers and ethene/styrene copolymers became available.[26] In 1990 J. C. Stevens at Dow Chemical discovered that titanium cyclopentadienyl amido compounds (constrained geometry catalysts, CGC) are very beneficial for the copolymerization of ethene and long-chain α-olefins.[27]

Today, next to the early transition metals such as Ti, Zr and Hf, the focus of interest is also on the potential of the late transition metals like Ni, Pd, Co and Fe. As the late transition metals are characteristically less oxophilic than the early metals, they are more tolerant towards polar groups. A nickel-based catalyst system, which produces, in the absence of comonomers, highly short-chain branched polyethylene was developed by M. Brookhard.[28] Efficient new systems were developed; in nickel or palladium systems the metal is typically sandwiched between two α-di-imine ligands, while iron and cobalt are triadentate complexed with imino and pyridyl ligands.[29]

R. H. Grubbs developed another type of Ni-based catalyst.[30,31] This neutral Ni-catalyst, based on salicylaldimine ligands, is active in ethene polymerization without any co-activator and originated from the Shell higher olefin process (SHOP). Shortly thereafter another active neutral P,O-chelated nickel catalysts for polymerization of ethene in emulsion was developed by R. Soula.[32-34]

Recently, work by T. Fujita at the Mitsui corporation has demonstrated that certain iminophenolate complexes of Group IV metals show comparable high activity than the metallocenes.[35,36]

1.3.2 The role of the cocatalyst

The key to extremely high activity of single-site catalysts in polymerization is the cocatalyst. MAO is the most used one in metallocene polymerization. It is well recognized that the activation with MAO consists of two steps: alkylation of the complex by MAO or TMA (trimethylaluminium) inherent in MAO, followed by cationization with MAO. The MAO anion acts as a weakly or noncoordinating anion and is complexing the molecule. Although MAO is used in industrial processes, a number of other activators have been developed lately. Some organic boron compounds, such as trisphenylmethyltetrakis-(pentafluorophenyl)borate $[Ph_3C]^+$ $[B(C_6F_5)_4]^-$, seem to especially fulfill a role as non-coordinating, non-nucleophilic counter anion to the active cationic species. A review of cocatalyst for metal-catalyzed olefin polymerization is given by Chen and Marks.[37]

To understand the nearly unlimited versatility of metallocene complexes, it is necessary to take a closer look at the catalyst precursor and its activation process with the cocatalyst (Figure 1-1). In most cases the catalyst precursor is a metallocene dichloride complex consisting of two aromatic five-membered ring systems, which can be tethered in addition by a bridging unit (ansa metallocene complexes). The introduction of substituents at certain positions of the two aromatic ligands and/or the bridge modifies not only the steric and electronic conditions in the molecule but also the symmetry of such a metallocene dichloride complex. Another variable parameter is the metal: M = e.g. Ti, Zr, Hf.[38]

Neutral metallocene compound (L_2MCl_2) is inactive without an activator and requires a strong Lewis acid (i.e. methylaluminoxane) to form a cationic metal center, which is active in 1-olefin polymerization.

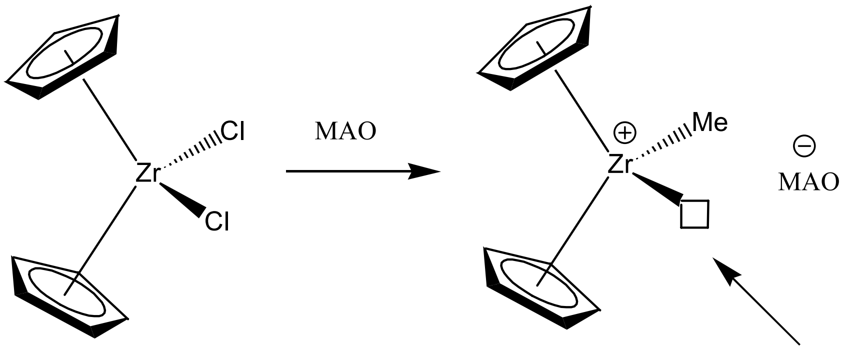

free coordination site
- cationic 14-electron species
- strong Lewis acid

Figure 1-1: Activation of the metallocene complex Cp_2ZrCl_2 by MAO.

1.3.3 Polymerization mechanism

Understanding the mechanisms and kinetics involved in the polymerization process enables one to predict the structure of the polymer formed. Propagation and termination rates determine molar mass, molar mass distribution, and, in copolymerization, comonomer content and distribution. The catalyst initiation and deactivation processes have an influence on the kinetics, and the cocatalyst may have an effect on the extent of the prevailing mechanisms.[38-40]

Propagation then proceeds by α-olefin coordination and insertion via a transition state.[39,41,42] The exact route for the monomer insertion is not completely understood. Agostic interactions appear to have an important role in the chain growth process. Kinetic studies have shown that the polymerization rate does not always follow a simple first order relationship, but often depends on the monomer concentration, indicating complex reaction pathways. Different kinetic models have been proposed to describe this kind of polymerization behavior.[39,43,**XII**]

The most common chain transfer mechanisms identified in metallocene catalyzed ethene polymerization and the corresponding end group types are presented in Figure 1-2. β-H elimination (chain transfer to the metal) and chain transfer to the monomer are generally believed to be the dominant chain transfer reactions in the olefin homopolymerization.[16] They lead to the formation of vinyl ($CH_2{=}CH{-}R$) or vinylidene ($CH_2{=}C(R'){-}R$) bond in ethene or α-olefin polymerization, respectively. Chain transfer to the aluminum (cocatalyst) is usually of minor importance in ethene polymerization. Chain transfer to the aluminum leads to the formation of an $Al-CH_2-R$ compound. The aluminum-alkyl bond is highly reactive and the treatment with hydrochloric acid and ethanol – a standard laboratory washing procedure – results in a saturated end-group in the polymer. Chain transfer to an external chain transfer agent, for example hydrogen[16], results in a saturated chain end. Hydrogen is far more reactive in metallocene-catalyzed polymerizations than in Ziegler-Natta polymerizations.[44]

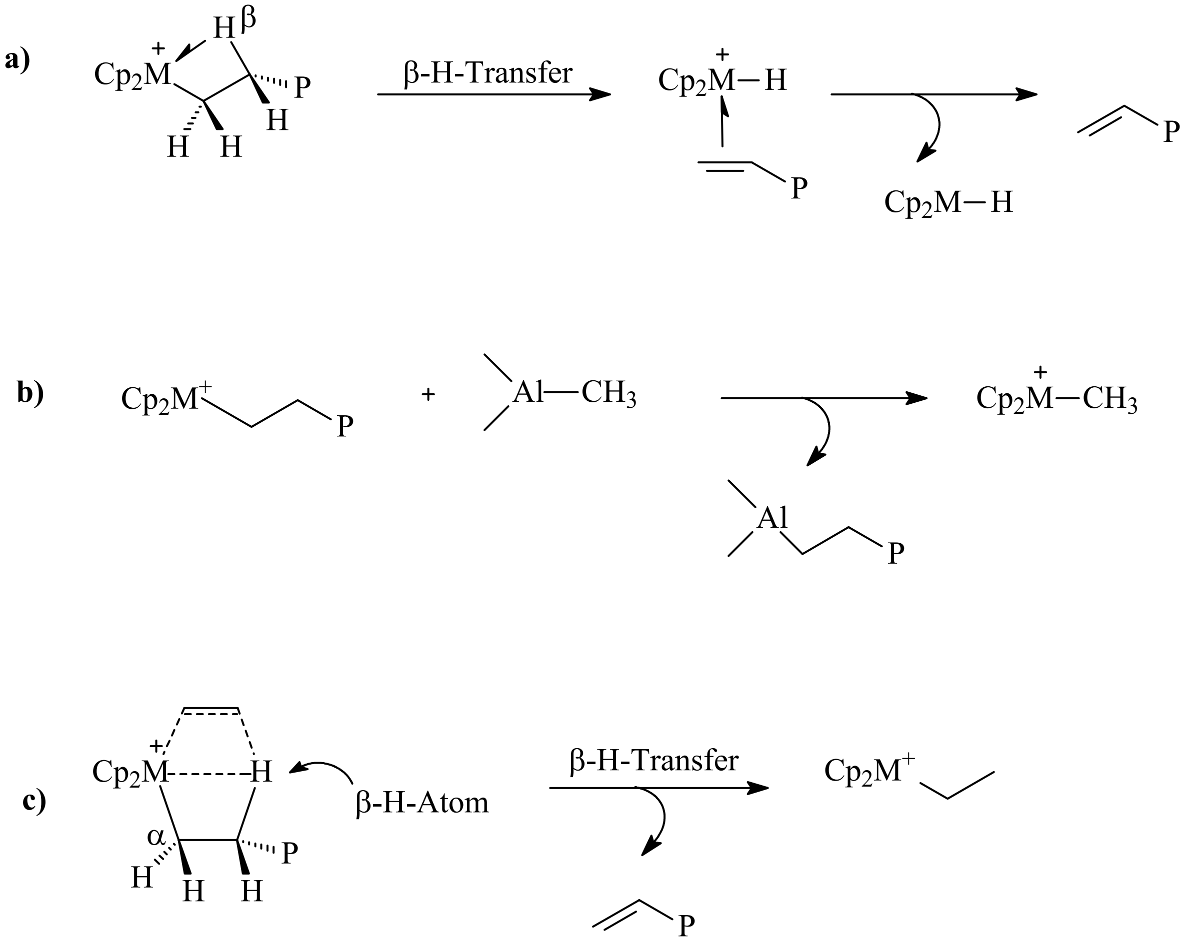

Figure 1-2: Termination reactions of the ethene polymerizations: a) β-H elimination, b) chain transfer to the cocatalyst, c) hydrogen transfer to the monomer.

In the copolymerization of ethene and α-olefin, vinylidenes and trans-vinylenes ($CH_3-R'-CH=CH-R$) account for a significant part of the end-groups. Both β-H elimination and chain transfer to the α-olefin after 1,2-insertion of the α-olefin results in the formation of a vinylidene bond. β-H elimination or chain transfer to the monomer after 2,1-insertion results in the formation of a trans-vinylene bond in the polymer chain.[45] In α-olefin (co)polymerizations a β-alkyl elimination analog to the β-H elimination may take place as termination reaction.

Isomerization reactions play an important role in the formation of regio- and stereoerrors in propene polymerization and in chain termination. The isomerization reactions contribute not only to the formation of stereo errors but also to the chain transfer. The catalyst structure and monomer concentration have a major influence on the extent of the isomerization reaction leading to the formation of the stereo errors.[39] In ethene polymerization, isomerization reactions have a less important role.

1.4 Metallocene catalyzed polyethylenes

1.4.1 Classification of polyethylenes

Polyethylene is classified into several different categories based mostly on its mechanical properties. The mechanical properties of PE depend significantly on variables such as the extent and type of branching, the crystal structure, and the molar mass.

UHMWPE (ultra high molecular weight polyethylene) is polyethylene with a molar mass of usually between 3 and 6 million grams per mol. The high molar mass results a very good packing of the chains into the crystal structure. This results in a very tough material. UHMWPE is made through metallocene catalysis polymerization.

HDPE has only little amount of short-chain branching and thus stronger intermolecular forces and tensile strength. The lack of branching is ensured by an appropriate choice of catalyst (e.g. Ziegler-Natta or metallocene catalysts) and reaction conditions.

LDPE has many more branches and branches on branches than HDPE, which means that the chains do pack into the crystal structure as well. It has therefore less strong intermolecular forces because the instantaneous-dipole induced-dipole attraction is weaker. This results in a lower tensile strength and increased ductility. LDPE is created by free radical polymerization.

LLDPE is a substantially linear polymer, with significant numbers of short branches, commonly made by copolymerization of ethylene with longer-chain olefins. It is made with Ziegler-Natta or metallocene catalysts.

UHMWPE is used in high modulus fibers and in bulletproof vests. The most common household use of HDPE is in containers for milk, liquid laundry detergent, etc; the most common household use of LDPE is in plastic bags. LLDPE is used primarily in flexible tubing and films. Recently, much research activity has focused on long-chain branched polyethylene. This is essentially HDPE, but has a small amount of very long branches. These materials combine the strength of HDPE with the processability of LDPE.

1.4.2 Material properties of metallocene polyethylene

The synthesis and characterization of polyolefins, especially polyethylenes and ethene/α-olefin copolymers synthesized using metallocene catalysts, has gained great interest in recent years. This is due to several major advantages of these systems over those produced by Ziegler-Natta (Z-N) catalysis. With metallocene catalysis, the molar mass is adjustable over a broad range[I] and the polymers show a narrow molar mass distribution (MMD).[8,26] Due to the stereo- and regiospecific nature of the catalysts, highly tactic and tailored copolymers[25,39,46] may be produced. Metallocene catalysts also have a high affinity to incorporate α-olefins into growing chains, and are even able to produce short branches in homopolymerizations.[47-49] Polymer chains containing a terminal vinyl group, created in-situ, can also act as macro-comonomers, leading to the formation of long-chain branched (LCB) polymers. In contrast, copolymerization of α-olefins with more than six carbon atoms by Z-N catalysts has proved to be difficult.

Research in the area of nanocomposites is inspired by nature, which has ‘invented’ materials with exceptional properties by combination of a hard, skeleton-like structure combined with a continuous flexible phase.[50] Analogously, the addition of fillers to a polymer matrix opens up the route to materials with completely new properties.[X]

1.4.3 Influence of the side-chains (copolymers)

Ethene copolymers with higher α-olefins, such as 1-butene, 1-hexene and 1-octene, are industrially important materials. Compared to polymers made with Ziegler-Natta catalysts, metallocene catalyzed copolymers have several advantages, the LLDPEs have excellent physical properties like high strength, high clarity and good heat sealability.[51] This is due to the narrow composition distribution and random distribution of comonomers. The amount of the comonomer and the length of the side-chains influence the material properties. The presence of short-chain branches (SCB) disturbs the crystallization kinetics; still metallocene copolymers have narrower lamellar thickness distribution than Z-N copolymers.[40] It is generally agreed that these side groups are concentrated in amorphous regions and, at most, only a small proportion of ethyl groups are located inside crystallites.[52,53] Metallocene catalysts enable the production of a new family of materials, which are eliminating the differences between the commodity and engineering polymers and between thermoplastics and elastomers. These thermoplastics are increasingly elastic and the elastomers are increasingly thermoplastic. Consequently the mechanical and physical properties of polyethylene are drastically changed by copolymerization with small amounts of α-olefins. This change will depend not only on the number of comonomer-units, but also their distribution along the chain and the nature of the side branches arising from the α-olefin. Comonomer and side-chains effects in LLDPEs are discussed in chapter 3.

Long-chain branches in polyethylene has several benefits relating to the polymer processability[54-57] since they affect the melt viscosity, temperature dependence of viscosity, melt elasticity, shear thinning, and extension thickening and they are also improving the stability of elongation dominated processes by strain hardening. The use of single-site catalysts allows a novel structure combination for PE of LCB with narrow molar mass distribution. The formation of long-chain branched metallocene polyethylenes (mPE) was first reported in patent literature in the mid-nineties.[27,58] The first scientific papers covering this topic were published a few years later.[59-61]

1.4.4 Modifying high density polyethylenes

Comparing conventional heterogeneous Ziegler-Natta to metallocene-based catalysis for the synthesis of polyolefins, it is surprising to see that the level of understanding of the catalytic species is almost opposite to the level of production. Even though the nature of the active species is rather incomprehensible in Ziegler-Natta catalysis, quantitatively, this way of synthesizing (co)polymers continues to dominate the market, mainly because of the lower production costs but also due to the favorable morphology and good processability of the materials. The polyolefins made by single-site catalysts only possess a relatively small part of the world market. Due to the narrow distribution of molar masses, which in case of most polyethylene types is unfavorable for the processing, modulations of the molecular architectures have become necessary. This was reached via two main routes: introduction of long-chain branches in polyethylenes like LDPE and (in-situ) blending. Obviously, the target is to combine the best of both, the good processability and the good mechanical properties.

1.4.4.1 Introducing long-chain branching

The first single-site catalyst reported to produce LCB-polyethylene was a constrained geometry catalyst, which is a half-metallocene.[27,58,62,63] In the first publications, it was only stated that the open structure of CGC enables LCB formation. Later it has been possible to use sterically more hindered dicyclopentadienyl catalysts for the production of LCB-polyethylene. LCB has been produced with $Cp_2ZrMe_2/B(C_6F_4)_3$[58] and Cp_2ZrCl_2/MAO[64-66]. In contrast, $(Me_5Cp)_2ZrMe_2$/MAO - catalyst resulted in a linear polymer.[44,58] In addition to these catalysts, $Et[Ind]_2ZrCl_2$/MAO and other *ansa*-metallocenes have also been reported to produce LCB polyethylene.[61,67-69] Evidence for long-chain branching in mPE was published by Wood-Adams et al. using a combination of NMR, SEC and shear rheology.[70] For the quantification of the small amount of LCB by NMR extremely long measurements up to 2 million scans were needed.

Most catalysts found to produce LCB are either half-metallocenes (constrained geometry catalysts)[27,71] or ansa-metallocenes.[64,67,68] The unbridged metallocene Cp_2ZrMe_2 system, activated with either $B(C_6F_4)_3$ or methylalumoxane (MAO), was also reported to produce long-chain branches.[**I**,58,59,66,68] Long-chain branching in metallocene catalyzed polymerizations is believed to take place via a copolymerization route, with the incorporation of a vinyl terminated polyethylene chain into a growing polymer chain.[59,72,73] Investigation into the polymerization behavior of several metallocene catalysts revealed that the termination mechanisms were catalyst specific. Depending on the catalyst structure, the termination of chain growth occurred via either β-H-elimination, hydrogen transfer to the monomer, or by chain transfer to the cocatalyst. Further research indicated that catalysts with high vinyl selectivity and good copolymerization ability were the most prominent for producing polymers with modified rheological properties.[64,**III**]

The formation of LCB depends on many different factors, including the presence of comonomers. If α,ω-dienes are incorporated, the additional terminal vinyl groups act as starting points for long-chain branching and thus result in a higher degree of LCB.[74] Initial investigations indicated that α-olefin comonomers decrease the amount of LCB, as they tend to terminate the growing chain.[75] The resulting vinylidene group at the end of a macromer is believed to be sterically hindered from reintroduction into a growing chain by the short-chain branch residing at the 2-position. Additionally, vinyl terminated polymer chains are sterically hindered from incorporation as LCB due to the short-chain branches in the growing chain and macromonomer. Thus the degree of LCB tends to decrease with increasing comonomer content.

Kokko et al.[68] showed, that for the catalyst system *rac*-$[Et(Ind)_2]ZrCl_2$/MAO, that both the temperature dependence of the viscosity and the viscosity itself decreased when introducing up to 3.4 mol-% hexadecene, suggesting a decreasing amount of LCB. The data indicated that 3.4 mol-% comonomer was not sufficient for the complete suppression of LCB. The viscosity was distinctly above the zero shear-rate viscosity of a linear polymer of equal molar mass, the activation energy of 41 kJ/mol was also much higher than that expected for a truly linear HDPE system (28 kJ/mol).[76] It was also shown that the presence of gaseous hydrogen during polymerization dramatically decreased the degree of long-chain branching using certain metallocene catalysts.[64,68] Some aspects of the processing behavior can be assessed by measuring the viscosity function in shear and extension.[77]

Long-chain branched polyethylenes are discussed in more details in chapter 2 and the influence of comonomer on LCB is described in chapter 3.

1.4.4.2 Influencing the molar mass distribution

An opportunity to modify the properties of HDPE is to produce blends. Apart from the MMD and comonomer distribution that a certain catalyst produces in polymerization in one reactor, two or more cascaded reactors with different polymerization conditions increase the possibilities to tailor polymer properties by in-situ blending of two or more structurally different polyethylenes. The bimodal process technique has been mostly used to improve processability and the mechanical properties of HDPE.[78] Bimodal polyethylene consists of two or more polymer fractions which usually differ from each other with respect to molar mass and branching (comonomer) content, and in fact, such a grade leads to intermolecular heterogeneity.[79-82] In a bimodal process, the catalyst is fed into the first reactor where the first polymer fraction is produced. After that the polymer fraction is transferred into the second reactor for production of the second polymer fraction. In some of the bimodal processes the reactor may also be operated in parallel mode.

Traditionally, bimodal polyethylene resins are produced with Ziegler-Natta type catalyst, but for specialty grades (e.g. bimodal LLDPE) the use of metallocene catalysts is slowly increasing.[78] The application areas of bimodal polyethylene are the same as for corresponding monomodal resins. However, optimizations of product-property combinations, such as the stiffness-impact balance, can result in products with higher performance. For example, without polyethylenes of controlled bimodal MMD and comonomer incorporation, development of HDPE pipe materials with better environmental stress cracking resistance (ESCR) and higher pressure classification would not have been possible.[78,80,82,83]

Multimodal polymers can also be obtained in-situ by tandem catalysis. This is claimed to be a very promising technique for the synthesis of new polyethylene, polypropylene and ethene/α-olefin copolymers. There are two possibilities to realize a dual catalytic system:[47,84,85]

- Each catalyst in the mixture generates polymers with different molar masses and molar mas distribution (type 1);
- One catalyst generates α-olefins in situ while a second catalyst copolymerizes the in situ generated α-olefins with the ethene in feed, the so called Concurrent Tandem Catalysis (type 2).

A type 1 tandem catalysis is described in chapter 4.

1.5 Polyolefins in the market

Polyethylene is cheap, flexible, durable, and chemically resistant material. Linear low density polyethylene (LLDPE) is used for making films and packaging materials, while high density polyethylene (HDPE) is used more often to make containers, plumbing, and automotive fittings.

Polyethylene is today's highest volume commodity plastic and it is the most widely utilized thermoplastic polymer. In the next years its worldwide demand is forecast to grow enormous. Figure 1-3 shows the world plastics production in 2004, polyethylene taken 32 %. Low and high density polyethylene is the material for everyday items.

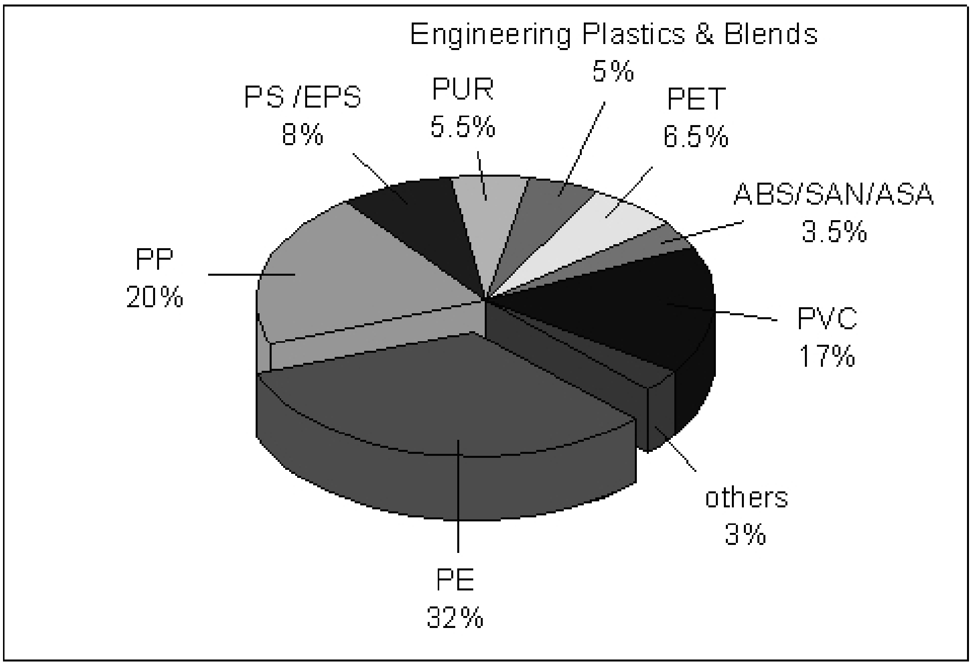

Figure 1-3: World Plastics Production, breakdown by types of plastic 2004 (tonnage in percent), Source: PlasticsEurope Deutschland, WG Statistics and Market Research.

The demand on polyolefins is still growing. The raw material is cheap and easy available, and there are plenty of different applications for polyolefin based materials. With the growing demand, the material itself has become technically more sophisticated and more application specific. Utilization of latest findings in polymer science have led to new catalysts and process innovations, which have made the required improvements in material properties possible, and in many cases also resulted in better production economy. The production and consumption of polyolefins is the most growing of all plastics (Figure 1-4), especially LLDPE and polypropylene (PP), but also HDPE.

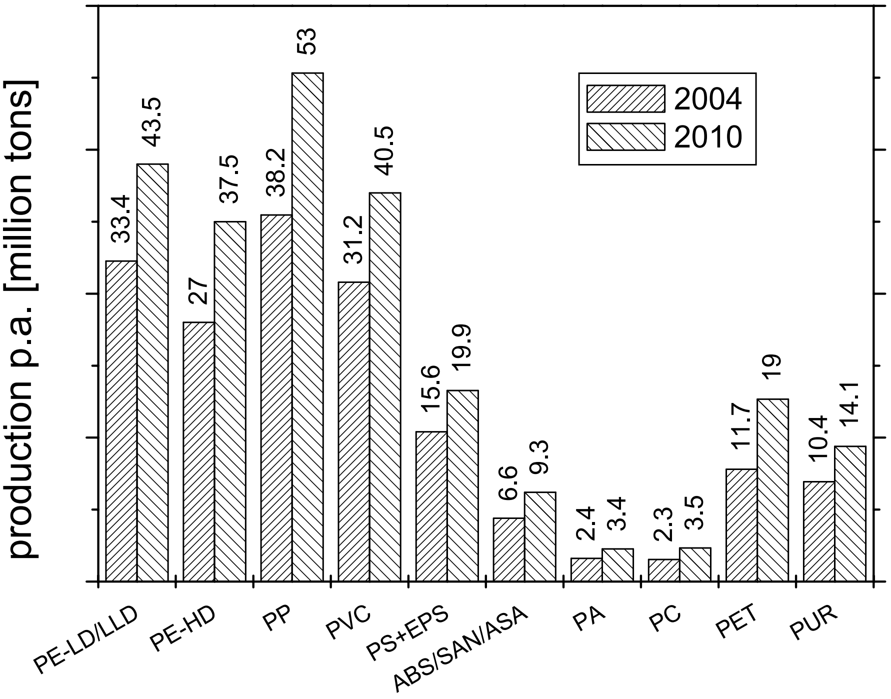

Figure 1-4: World Plastics Consumption 2004 – 2010, Source: PlasticsEurope Deutschland, WG Statistics and Market Research.

Demand for metallocene and single-site polymers advance many percent per year. Increases will be attributable to the considerable processing and performance advantages these materials hold over other conventional thermoplastics and thermoplastic elastomers (TPE). Metallocene processes allow an unprecedented degree of customization during polymerization, facilitating the cost-effective production of polymers with enhanced performance qualities such as higher strength, improved clarity and better processability. Threats to further growth include the higher cost of metallocene polymers since they are being sold into very cost-sensitive markets. Consequently, catalyst costs must be constrained and production rates optimized.[86]

Metallocene and single-site polymers are expected to account for about nine percent of the total market for polyolefin polymers in 2009 (from Global Information Inc.). Penetration rates will vary, with the highest anticipated for LLDPE and EPDM (ethene propene diene monomer) rubber. Film applications for LLDPE are particularly amenable to the performance and processing advantages offered by metallocenes (particularly their enhanced clarity and puncture resistance). Penetration rates will remain considerably lower in high density polyethylene and polypropylene, though they will be growing at a faster pace.

Recent developments in catalyst technology are revolutionizing the polyolefins industry. Specifically, INSITE single-site catalysts from Dow Chemical and EXXPOL metallocene catalysts from Exxon Mobil, along with a host of other production technology innovations (particularly gas-phase process technology from companies such as BP and Chevron Phillips, BORSTAR process by Borealis and the SPHERILENE technology from Basell) are giving resin producers significantly greater control over the manufacturing process, resulting in higher performance and custom engineered olefinic polymers.

2. Linear and long-chain branched polyethylenes

2.1 Introduction

Although metallocene catalysts have expanded the range of molar masses and molar mass distributions of polyethylenes during the last 20 years, comprehensive results regarding rheological properties of linear high density polyethylenes have not been published for the wide range of these molecular parameters attainable today.

In this work polyethylenes with a defined linear or long-chain branched topography were synthesized in order to find more relationships between catalyst structure, polymerization conditions and branch incorporation.

Three different basic methods are used for the detection of long-chain branching; Carbon-13 nuclear magnetic resonance (^{13}C NMR) spectroscopy, size exclusion chromatography with coupled multi angle laser light scattering (SEC-MALLS), and rheological measurements. Melt rheological measurements are the most sensitive methods for detecting very low concentrations of LCB. The LCB density in single-site catalyzed polyethylenes is typically in the range of 0.01 – 0.2 branch points per 1000 main-chain carbons.[67,69] In many cases, low LCB content is difficult to detect with ^{13}C NMR spectroscopic methods, even though nowadays a differentiation between side-chains of longer than six carbons is possible.**[VIII]** However, a mixture of short-chain branches and long-chain branches (usually found in LLDPE) is even harder or impossible to characterize with respect to long-chain branches because of the similar signals of SCBs and LCBs. Here SEC-MALLS and melt rheological measurements are used for branch detection.

Much attention has been paid during recent years to the influence of long-chain branches on rheological properties but in order to be able to assess their effectiveness exactly the influence of molar mass and molar mass distributions on rheological properties should be known.

Especially the dependence of the zero shear-rate viscosity η_0 on the molar mass M_w has gained growing interest years as it allows some insight into the branching structure of polymers.[70,76,87,88] Long-chain branches have similar effects as some molar mass distributions in shear flow. With the correlation between the zero shear-rate viscosity η_0 and the molar mass it is possible to separate between these two influence factors in most cases. However, in some cases zero shear-rate viscosities of long-chain branched samples fit to the η_0-M_w-correlation as well, most of these cases are high molecular LDPEs.

The dependence of the zero shear-rate viscosity η_0 on the molar mass M_w of a linear polymer is described by the equations (2-1) – (2-3).[89]

$$\eta_0 = K_1 \cdot M_w{}^{\alpha} \text{ for } M_w > M_c \qquad (2\text{-}1)$$

$$\eta_0 = K_2 \cdot M_w \text{ for } M_w < M_c \qquad (2\text{-}2)$$

$$M_c \approx 2 \cdot M_e \qquad (2\text{-}3)$$

α is reported to be between 3.4 and 3.6. K_1 and K_2 are parameters dependent on the polymer type and the temperature, M_c is a critical molar mass, which is approximately two times the entanglement molar mass M_e. According to literature M_c is around 3800 g/mol for polyethylene.[90,91] Technically relevant polymers usually have a weight-average molar mass M_w of more than $5xM_c$ because the polymers with a lower M_w are very brittle.

One prerequisite for using $\eta_0(M_w)$ for the analysis of long-chain branching is, that $\eta_0(M_w)$ is independent of the polydispersity of the polymer. Otherwise more complicated correlations would have to be used to compensate for the influence of the molar mass distribution. Wasserman and Graessley proposed such an extension of equation (2-1) by introducing an additional dependence of η_0 on M_w/M_z.[92] Such a relationship can only be established by using polyethylenes which do not contain any long-chain branches. Metallocene catalysts offer the possibility to polymerize such samples in a wide range of molecular parameters (see chapter 2.2).

In this work (see chapter 2.3 and 2.4) various linear high density metallocene catalyzed polyethylenes are characterized with respect to their viscosity functions and their molar masses and polydispersities to find out how the well characterized molecular structure is reflected to the viscosity data.

Polyethylene tends to cross-link with increasing time in the melt and cross-linking involves the formation of long-chain branches as a first step. Thus it is of great importance to ensure the thermal stability of the samples. If cross-linking can be excluded, the deviation of the viscosity function from the linear function is very sensitive to detect LCB.

From the processing point of view the viscosity function is important. The viscosity function can be determined by stressing or dynamic-mechanical-experiments, for more details about this see also publication **II**. The zero shear-rate viscosity η_0 of LCB polymers does not only depend on the M_w but also on the molecular structure. Thus no simple equation such as (2-1) is valid for non-linear chains. As a general trend small amounts of LCB will lead to an increased η_0 while large amounts of LCB (e.g. in LDPE) will decrease η_0.[76,93-95]

In order to separate between effects of the molar mass distribution and long-chain branching by shear rheology the molar mass distribution has to be measured by SEC because a broad molar mass distribution can account for the same rheological behavior. A MALLS detector attached to the SEC apparatus is able to measure the radius of gyration as a function of the molar mass $<r^2>^{0.5}$ (M) of the samples as an additional information besides the absolute molar mass. The presence of long chain branches in the polymer leads to a decrease of the radius of gyration $<r^2>^{0.5}$.[96,97] By plotting the radius of gyration as a function of the molar mass $<r^2>^{0.5}$ (M) a decrease can be detected as the deviation from a linear curve representative for each class of polymers.

A broad range of linear and long-chain branched polyethylenes were synthesized using metallocenes and constrained geometry catalyst. Some catalysts were taken which were studied before concerning long-chain branching. However, there is a lack of information available in literature how the catalyst structure and the polymerization conditions affect the formation of long-chain branches. By using also known systems definitely linear and long-chain branched polyethylenes were obtained. New structure-property relationships using two independent detection methods were established and extended to new systems based on the results. This is described in chapter 2.4 and **I**.

2.2 Polymerization behavior and polymer characteristics

2.2.1 Materials

A series of different polyethylenes were synthesized using reactor 1a and 1b. Six catalysts (CpMe$_5$)$_2$ZrCl$_2$ **(A)**, Cp$_2$ZrCl$_2$ (**E**), *rac*-[Et(Ind)$_2$]ZrCl$_2$ (**B**), [Me$_2$Si(Me$_4$Cp)(N^{tert}Bu)]TiCl$_2$ (**D**), [Ph$_2$C(2,7-di-^{tert}BuFlu)(Cp)]ZrCl$_2$ (**F**) and [Me$_2$C(Cp)$_2$]ZrCl$_2$ (**G**) together with MAO as cocatalyst were used. The polymers were analyzed by DSC 1, SEC 1 and 2, rheology and melt-state NMR (NMR 3), see chapter 6 for details. The letter **C** is kept for naming commercial grades.

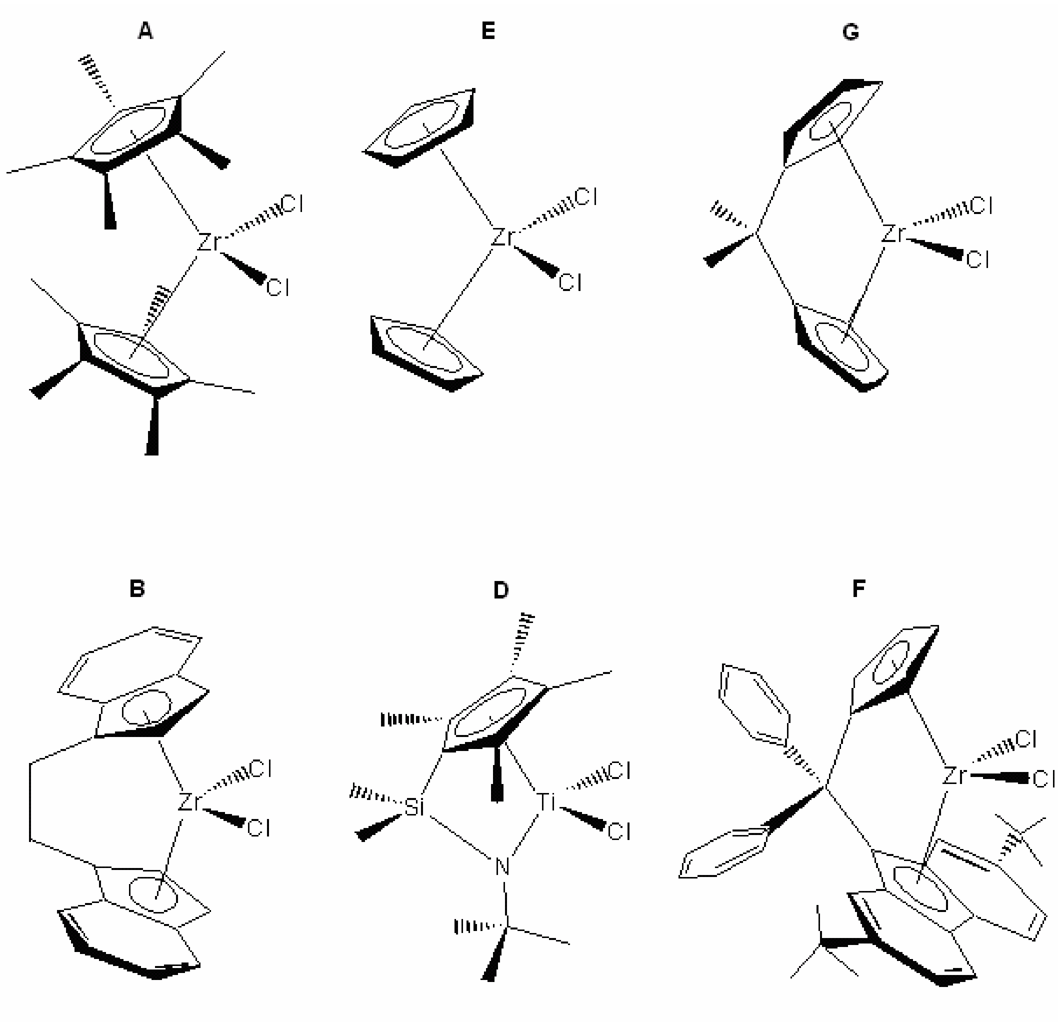

Figure 2-1: Catalyst precursors:
*(CpMe$_5$)$_2$ZrCl$_2$ **(A)**, Cp$_2$ZrCl$_2$ **(E)**, [Me$_2$C(Cp)$_2$]ZrCl$_2$ **(G)**, rac-[Et(Ind)$_2$]ZrCl$_2$ **(B)**, [Me$_2$Si(Me$_4$Cp)(N^{tert}Bu)]TiCl$_2$ **(D)**, [Ph$_2$C(2,7-di-^{tert}BuFlu)(Cp)]ZrCl$_2$ **(F)**.*

Some of the polymerizations were done under presence of hydrogen to control the molar mass of the polymer. Polymerization details are given in Table 2-1.

Table 2-1: Polymerization conditions.

#	catalyst	temp. [°C]	c(ethene)[a] [mol/l]	p(ethene)[b] [bar]	n(H_2) [mmol]	time[c] [min]	n(cat.) [µmol]	MAO [mg]	toluene [ml]
A1	A	30	0.24	2.00		60	0.20	200	200
A2	A	30	0.24	2.00		240	1.00	1000	2000
A5	A	60	0.23	2.80		240	1.25	1000	2000
A4	A	60	0.47	5.80		240	1.00	1000	2000
A6	A	60	0.41	5.00	9.0	240	0.25	1000	2000
A7	A	90	0.24	3.80		300	4.50	1000	2000
A8	A	90	0.24	3.80	8.3	75	0.20	400	400
A9	A	90	0.24	3.80	8.3	80	0.10	400	400
A3	A	90	0.24	3.80	16.6	75	0.10	400	400
E8	E	30	0.23	2.00		180	0.50	1000	2000
E1	E	30	0.23	2.00	9.0	242	0.50	1000	2000
E9	E	60	0.13	1.55		60	0.2	200	200
E2	E	60	0.13	1.55	9.0	60	0.20	200	200
E3	E	60	0.41	5.00		241	0.50	600	2000
E4	E	60	0.41	5.00	9.0	215	0.50	1000	2000
E5	E	90	0.06	1.00		45	0.25	200	200
E6	E	90	0.13	2.00		60	0.50	200	200
E7	E	90	0.13	2.00	8.3	60	0.20	200	200
B1	B	60	0.08	1.00		240	0.50	1000	2000
B2	B	60	0.25	3.00		158	0.25	1000	2000
B4	B	60	0.41	5.00		90	0.50	1000	2000
B5	B	60	0.41	5.00	9.0	241	0.25	1000	2000
B6	B	75	0.07	1.00		240	0.50	1000	2000
B7	B	75	0.22	3.00		218	0.25	1000	2000
B8	B	75	0.37	5.00		154	0.25	1000	2000
B9	B	90	0.19	3.00		190	0.25	1000	2000
D3	D	60	0.41	5.00		240	3.00	1000	2000
D4	D	60	0.41	5.00	9.0	241	1.00	1000	2000
D5	D	90	0.24	3.80		225	1.00	1000	2000
F1	F	60	0.24	2.95	9.0	243	0.48	1000	2000
F2	F	60	0.41	5.00		250	0.32	1000	2000
F3	F	60	0.41	5.00	9.0	243	0.16	1000	2000
G1	G	90	0.05	0.79		93	2.50	800	1200
G2	G	90	0.10	1.58		90	1.50	800	1200

[a] ethene concentration in toluene
[b] ethene pressure in the reactor
[c] polymerization time

2.2.2 Polymerizations

The polymerization activities and polymer characteristics are given in Table 2-2. Catalyst E and B have the highest polymerization activities of all investigated catalysts in this study. It is remarkable that the activity of catalyst A, D and F is enormously increased if hydrogen is used. Hydrogen affects the activity in different ways depending on the catalyst structure, for catalysts B and E lower activities are observed.

When considering long-chain branch formation via the copolymerization route, the choice of the catalyst and polymerization conditions plays a great role. The importance of catalyst vinyl-group selectivity for formation of LCB is described by the group of Seppälä for catalysts E, B, and other.[64,68,75] Another important factor is the polymerization reactor operating conditions. In a batch polymerization, the macromonomer concentration (here the polymer itself) increases and the monomer concentration decreases as the polymerization proceeds. The monomer concentration is constant in semi-batch polymerization. Only in the continuous stirred tank reactor system, both monomer and macromonomer concentrations are constant after the steady-state conditions are achieved. The shown polymerizations were performed as a semi-batch process. The influence of the polymerization time on the amount of branches in the polymer was observed and has to be investigated in more details (see chapter 5).

Table 2-2: Polymerization activities and polymer characteristics.

#	Activity[a]	T_m[b] [°C]	T_c[b] [°C]	ΔH [J/g]	Crystallinity[c] [%]	M_w [kg/mol]	MMD
A1	27100	140	112	174	60	665	3.0
A2	30900	140	112	137	45	923	3.8
A5	17800	142	113	170	53	403	2.6
A4	19900	142	112	176	60	564	4.3
A6	129200	136	117	232	80	72	11.6
A7	2800	135	114	217	74	179	4.0
A8	56200	131	116	227	78	28	7.8
A9	53100	131	115	228	78	19	6.5
A3	47000	129	113	237	81	17	10
E8	31300	138	112	152	52	565	2.2
E1	37600	133	116	248	85	12.7	2.1
E9	193000	138	113	173	59	221	2.1
E2	194500	128	115	244	83	6.5	2.2
E3	124900	140	109	181	62	297	2.1
E4	45600	133	117	256	88	15	2.5
E5	275100	135	117	208	71	52	2.0
E6	171500	136	115	202	69	47	2.0
E7	414200	126	112	246	84	4.7	2.5
B1	130200	139	110	179	61	147	2.2
B2	187900	141	109	217	74	93	1.9
B4	134600	138	112	208	71	100	2.0
B5	76000	135	114	202	69	67	2.1
B6	279900	135	113	196	67	106	2.5
B7	245000	138	111	171	58	76	1.8
B8	268400	138	116	196	67	69	2.0
B9	498300	135	114	226	78	66	1.8
D3	7200	140	112	156	53	560	2.1
D4	16400	136	114	199	68	74	2.0
D5	43000	140	109	177	60	365	2.6
F1	45400	140	111	172	59	102	2.0
F2	22000	136	114	151	52	1150	4.0
F3	46300	138	112	185	64	173	2.0
G1	16300	113	101	205	70	1.7	2.8
G2	25500	118	104	214	74	2.8	2.9

[a] $[\mathrm{kg_{polymer}}/(\mathrm{mol_{cat}}\cdot \mathrm{h}\cdot \mathrm{mol/l_{ethene}})]$

[b] peak temperature

[c] enthalpy of fusion of perfectly crystalline PE was taken to be 290 J/g[98]

2.2.3 Molar masses

For all polymers made by the catalysts E, B, D, F and G the expected MMD of about 2 was found. Catalyst A was found not to be thermostable for a long time and at higher temperatures. Especially at 90°C in the reactor a broadening of the MMD was observed and if hydrogen was present, a broadening in MMD occurred already at 60°C, too. The highest molar mass of this series' polymers was produced by catalyst F at 60°C and 0.41 mol/l ethene concentration. The molar masses of a comparable series in dependence of catalyst structure and hydrogen presence are given in Figure 2-2. The reduction of the molar mass by the presence of hydrogen is very much catalyst specific; it is mainly depending on the favored termination reaction, the substitution pattern and the bridge (presence).

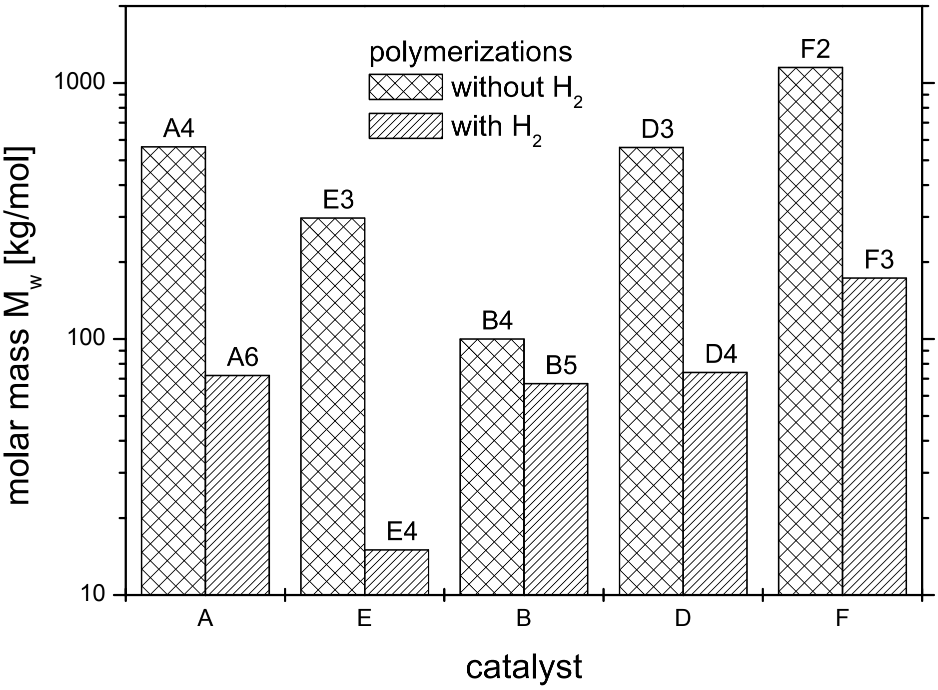

Figure 2-2: Molar masses of the polymers obtained at 60°C and 0.41 mol/l monomer concentration.

2.2.4 Thermal behavior

The melting temperature for HDPE is depending on the molar mass up to a certain point. The melting temperature is increasing with increasing molar mass up to M_w of about 100 kg/mol. After reaching a T_m of 142°C no more increase is observed (Figure 2-3). This is in agreement with the constant T_m^0 = 141.5°C[99], which is described to be the highest possible melting temperature for a polyethylene.

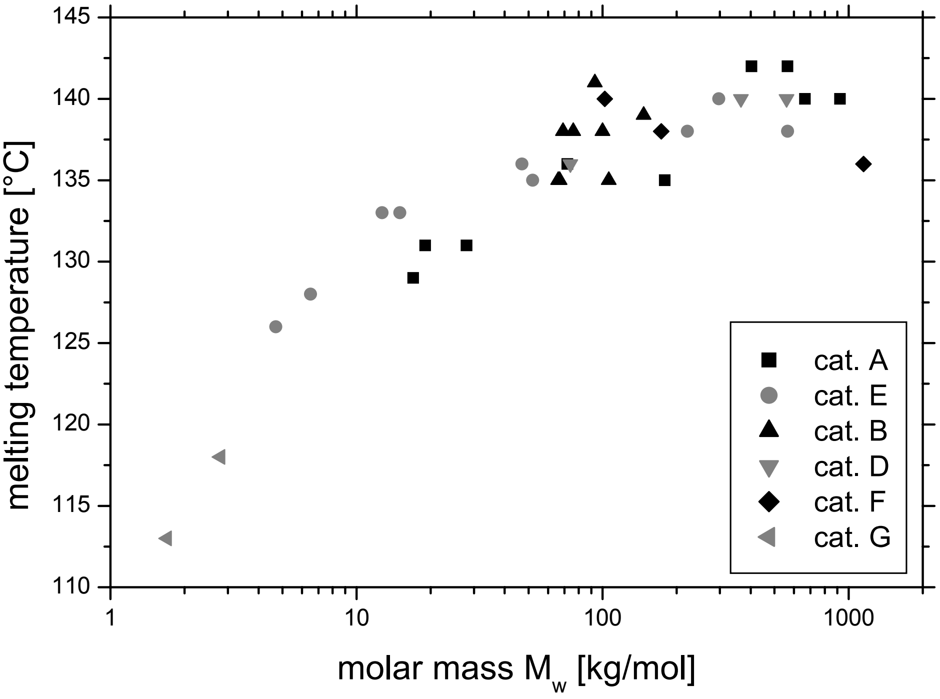

Figure 2-3: Melting temperatures of all of the investigated polyethylenes.

The crystallization temperature of the materials is between 101 and 115 °C (see Table 2-2), it is much less depending on the molar mass than the crystallinity. The melt enthalpy of the samples is decreasing with increasing molar mass. They are not depending on the type of catalyst used to produce them (Figure 2-4). A maximum of the enthalpy of melting is observed at a molar mass of about 10 000 g/mol. This can be understood by the fact that each linear chain has two end groups, which are acting as chain imperfections and thus crystallization hindrances just like short-chain branches in LLDPE. These end groups lower both crystallinity and melting point. Because the crystallinity was measured using a heating and cooling rate of 20 K/min, non-equilibrium conditions are present. As the melting and crystallization peaks of all samples are approximately the same, the crystallization time is also very similar for all samples. Due to the different viscosities of the samples (η_0 varies in a range of about 9 decades for the linear samples and even more for the LCB-samples), the time needed for an equilibrium crystallization is also very different. For the samples with a very low molar mass the crystallization time is probably sufficient to reach a quasi-equilibrium state. For the samples with the highest molar masses the chain movements are much more restrained and more time is required for the quasi-equilibrium state of crystallization.

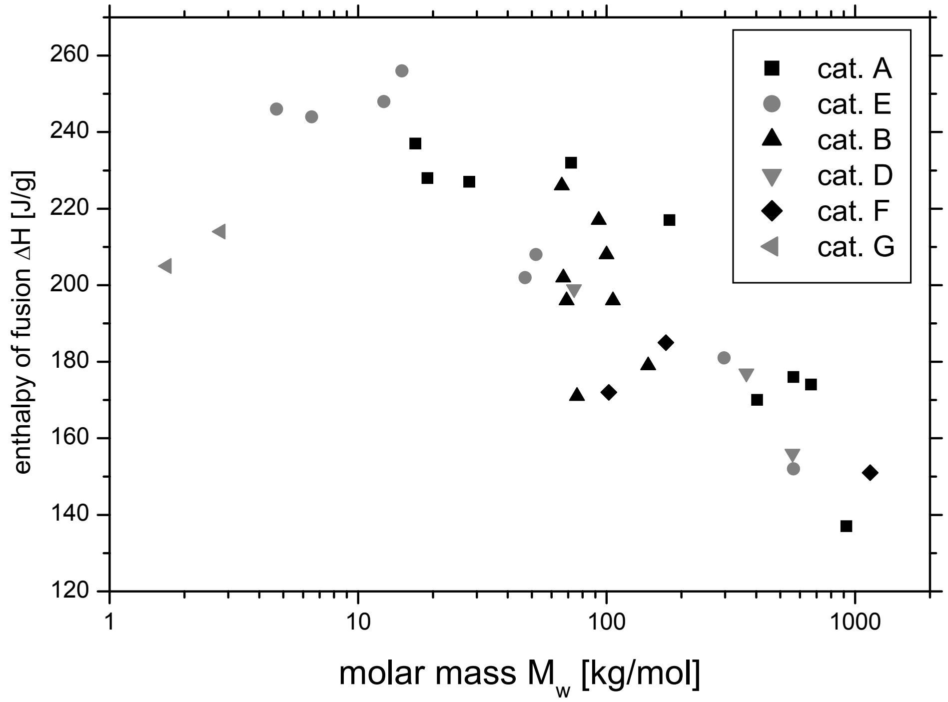

Figure 2-4: Melting enthalpy dependence on the molar mass of the polymers.

The DSC results show a strong dependence of the thermal behavior on the molar mass but not on the catalyst structure. It is therefore concluded, that none of the catalysts incorporates large numbers of short-chain branches by side reactions which would lower the melting temperature and enthalpy[100] (compare chapter 3).

2.3 Determination of the linearity of high density polyethylenes

2.3.1 Materials

Besides some few commercially available linear polyethylenes (named with C) several samples were polymerized using metallocene catalysts in laboratory scale, as described in chapter 2.2. The strictly linear materials are described in this chapter. The linearity of the samples is checked by SEC-MALLS (SEC 2), which was used in addition to obtain the absolute values of M_w. The analytical methods are described in chapter 6.4 and **II**.

2.3.2 Characterization by SEC-MALLS

The SEC-MALLS measurements were carried out by Dr. Kaschta in Erlangen. The results of the molecular characterization are given in Table 2-3. For some samples deviations from the log Gaussian-shaped MMD was observed; for some materials a low or high molar mass-shoulder was found indicating a bimodal polymer.

Table 2-3: Molecular data and zero shear-rate viscosities of the HDPE-samples.

	M_w [kg/mol]	MMD	η_0 [Pas] (at 150°C)	remarks
W1	0.24	1.0	0.0025	
W2	0.44	1.1	0.0040	
G1	2.8	2.9	0.0375	
E7	4.7	2.5	0.089	
E2	6.5	2.1	0.19	
E1	11.5	1.8	3.5	
E4	14.8	2.5	10	
A9	19	6.5	17	
A8	28	7.8	152	bimodal
C1	42	3.0	520	low molar mass shoulder
E5	52	2.0	730	
C2	114	16.0	16 130	high and low molar mass shoulder
C3	120	2.0	17 800	
A7	178	4.0	70 500	bimodal
C4	224	3.0	113 200	high molar mass shoulder
A5	403	2.6	1 570 000	high molar mass shoulder
A1	665	3.5	4 233 000	
A4	564	4.3	6 732 310	
A2	923	3.8	26 100 000	

The products W1 and 2 are waxes (W1 is heptadecane, W2 is a mixture of higher alkenes with a very narrow molar mass distribution (MMD<1.1)). Their molar mass was calculated from the chemical composition given by the manufacturers.

Some of the molar mass distributions are represented in Figure 2-5. The large range of molar masses becomes clearly visible. The curves were normalized with respect to the maximum of the peak.

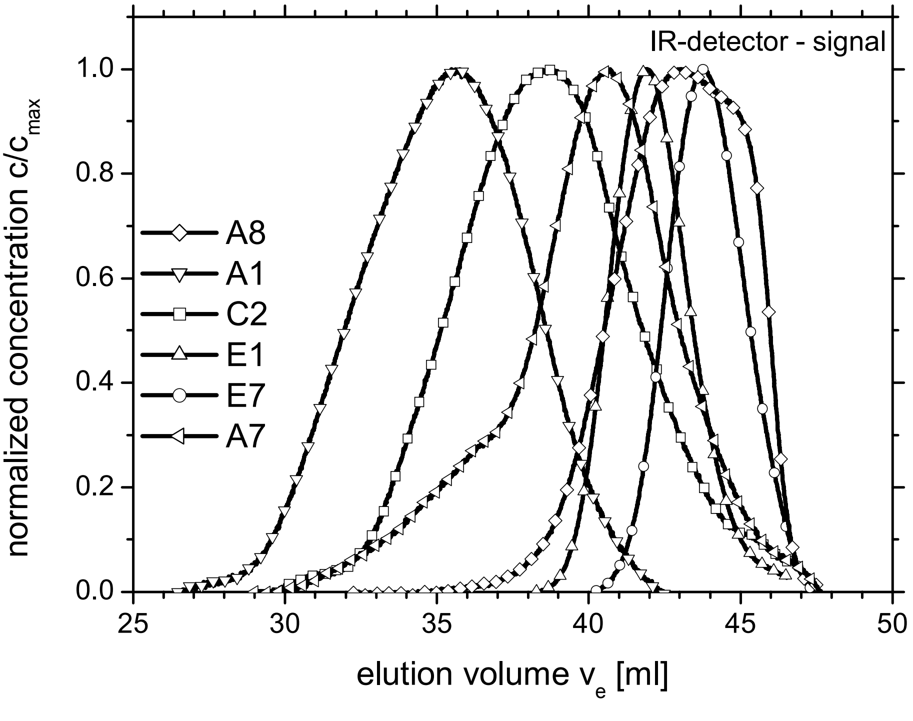

Figure 2-5: Elugrams of some resins measured with the IR-detector of SEC2.

The molar mass distributions in Figure 2-5 are shown as elugrams as this plot provides the best visualization of the bimodal molar mass distributions or the high molecular tails. Besides the absolute value of M_w the MALLS detector measures the radius of gyration. The presence of long-chain branches leads to a decrease of the radius of gyration $<r^2>^{0.5}$.

Figure 2-6 makes the linearity of some samples visible, any deviation towards higher molar masses are experimental artifacts. The first reason for that might be deviations towards $<r^2>^{0.5}$ = 20 nm (≈ 70 000 g/mol for HDPE), which are due to the physical detection limit of the MALLS. Also tiny particles are washed out of the SEC-columns, (which is part of their ageing) which might cause deviations towards larger radii of gyration at small molar masses. At high molar masses these deviations might also be caused by extremely small concentrations, which lead to artificially increased radii of gyration.

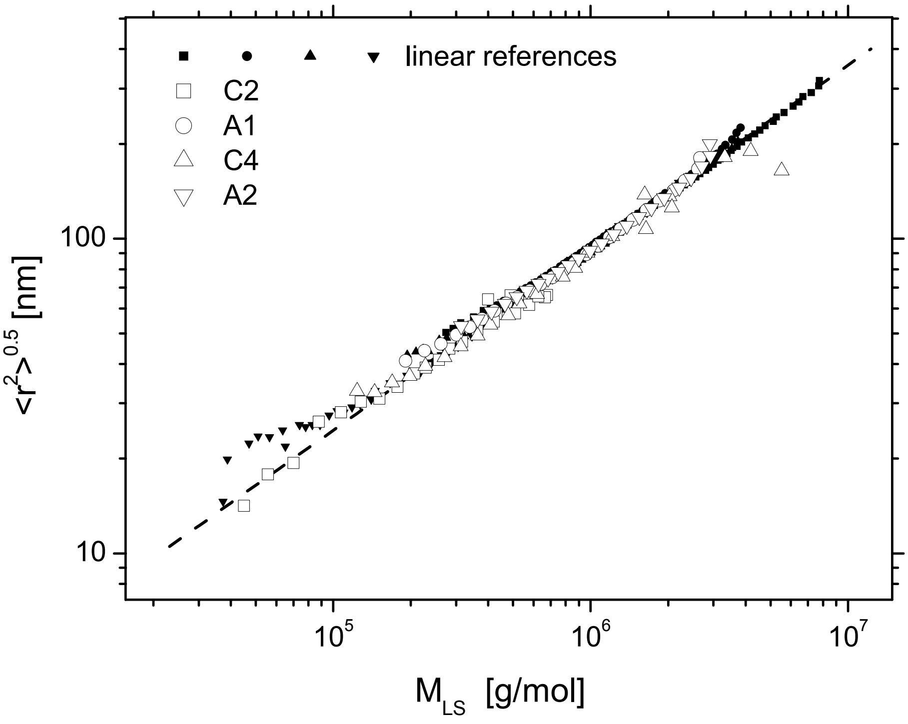

Figure 2-6: $<r^2>^{0.5}$ *(M) for several linear HDPEs.*

2.3.3 Characterization by rheology

The rheological measurements were carried out by Stadler in Erlangen. As discussed in chapter 2.1, the linearity of polyethylenes can be determined from the η_0-M_w correlation (Figure 2-7). A correlation with $\alpha = 3.6$ and $K_1 = 9 \cdot 10^{-15}$ according to equation (2-1) was found for all the samples above M_c. For the molar masses distinctly below M_c, $\alpha = 1$ and $K_2 = 9 \cdot 10^{-6}$ describe the data points sufficiently well. The critical molar mass M_c which is determined from the intersection point between the straight lines with α=3.6 and α=1 of the $\eta_0(M_w)$-plot is 2 900 g/mol.

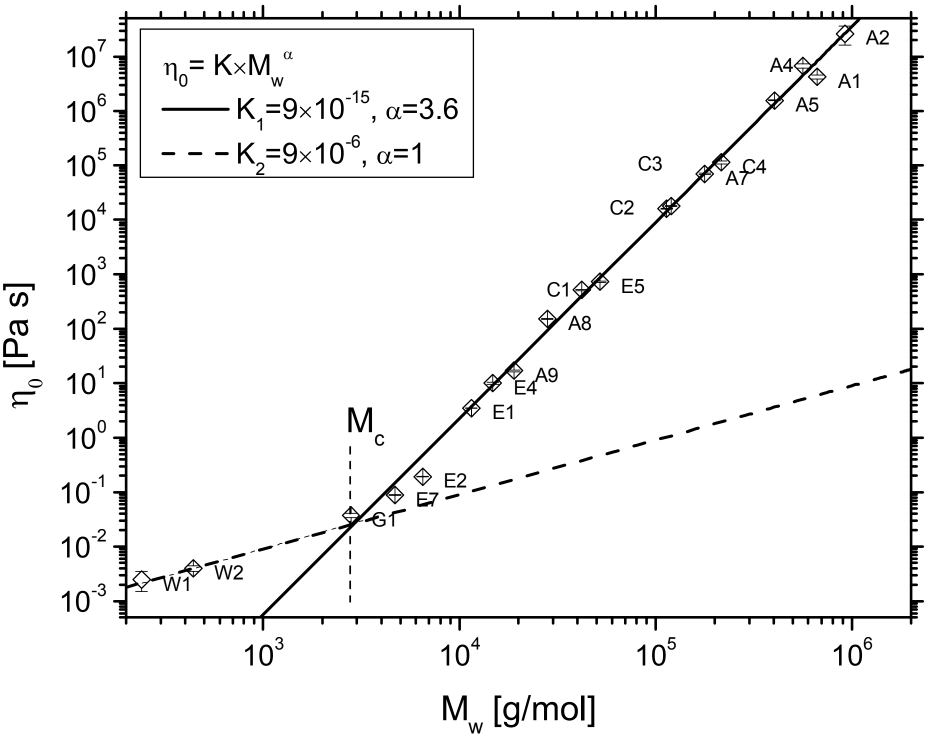

Figure 2-7: Zero shear-rate viscosity versus molar mass M_w for linear PEs.

Although some of the samples with an M_w of more than 10 000 g/mol show a high value of MMD and even a bimodal molar mass distribution (Table 2-3), no relevant deviation of those samples from the η_0-M_w-relationship is observed; $\eta_0(M_w)$ is independent of the molar mass distribution for the samples investigated.

Regarding the scatter of the measured data no systematic influence of the molecular structure can be found. Most materials (M_w>10 000 g/mol) are within an error margin of ±10% (of M_w) related to $\eta_0=9\cdot10^{-15}\cdot M_w^{3.6}$. Towards lower molar masses (M_w<10 000 g/mol) the error increases slightly because the measurement of the molar mass M_w itself becomes more prone to errors and thus the deviations from the η_0-M_w-line increase.

When looking in particular at the samples C3 and C2, which are extremely different with respect to MMD (2 and 16), it becomes obvious, that the influence of the molar mass distribution can be regarded to be negligible. This result is of importance as a deviation of

$\eta_0(M_w)$ from the relationship for linear polyethylenes gives a very sensitive hint to the existence of long-chain branches independent of the polydispersity (compare chapter 2.4).

The Carreau-Yasuda equation was applied to the viscosity functions of the samples of various molar mass distributions. Besides the zero shear-rate viscosity separately obtained from creep experiments the other three parameters of this model were determined by a best fit, this is described in detail by Stadler.[101,**II**]

2.4 Structure – property relationships for long-chain branched polyethylenes

2.4.1 Materials

All materials described in chapter 2.2 were investigated on their branching content to yield relationships between their synthesis conditions and catalysts and long-chain branching. The SEC-MALLS measurements were carried out by Dr. Kaschta and the rheological measurements by Stadler in Erlangen.

2.4.2 Branch detection by SEC-MALLS

In Figure 2-8 the molar mass distributions of polymers made with the different catalysts but under the same experimental conditions are compared. It reveals that the different catalysts produce polymers, which differ in molar mass but have comparable molar mass distributions. The exception is polymer D3 with shows a high molar mass tailing. F2 has a slightly broadened molar mass distribution.

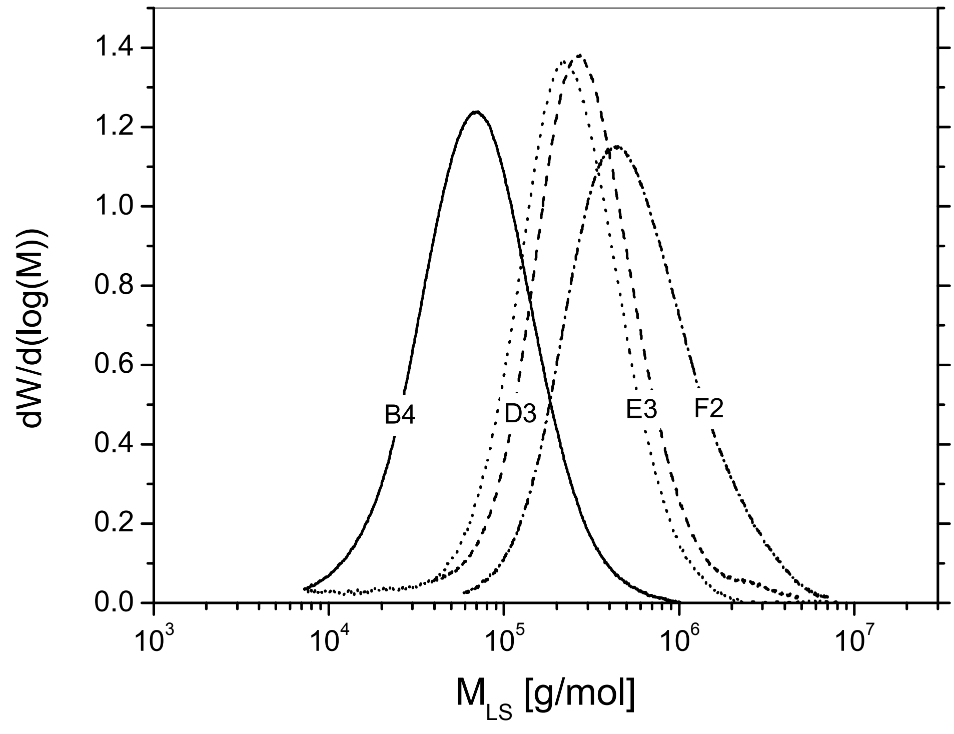

Figure 2-8: Molar mass distributions of polymers polymerized with different catalysts but under the same conditions (T_{poly}=60°C, c_{ethene}= 0.41 mol/l, no hydrogen).

The influence of the ethene concentration at a fixed polymerization temperature on the molar mass distribution and on the radius of gyration is shown in Figure 2-9 for catalyst B. An increase in ethene concentration yields in slightly decreasing molar masses but has, in accordance with the ongoing polymerization mechanism, no influence on the width of the molar mass distribution. From the radius of gyration as a function of absolute molar mass it is concluded that all polymers are long-chain branched because of the coil contraction, which is evident from the comparison with the radius of gyration of linear molecules. The polymers do not differ in their coil contraction and carry therefore long-chain branches of a similar topography.

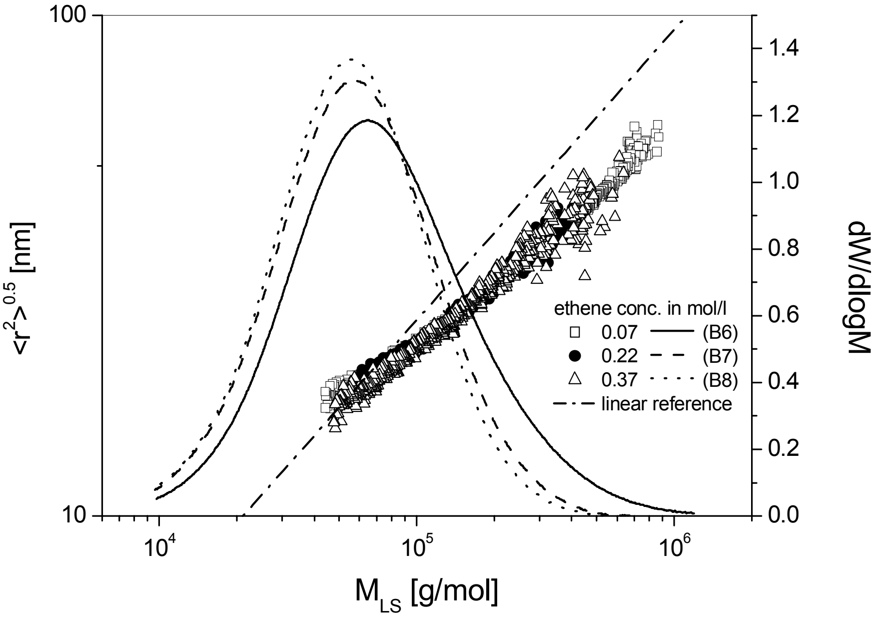

Figure 2-9: Influence of ethene concentration on molar mass and radius of gyration for catalyst B at 75 °C polymerization temperature (linear ref. is sample A2).

The effect of hydrogen on molar mass and the long-chain branching is shown in Figure 2-10 and Figure 2-11 for catalyst B and E, respectively. The influence on the molar mass varies with the different catalysts. While the decrease in molar mass is moderate for catalyst B it is very much pronounced for catalyst E. In this case, the molar mass distribution is shifted to about 20 times smaller molar masses resulting in a polymer, which is too brittle for applications.

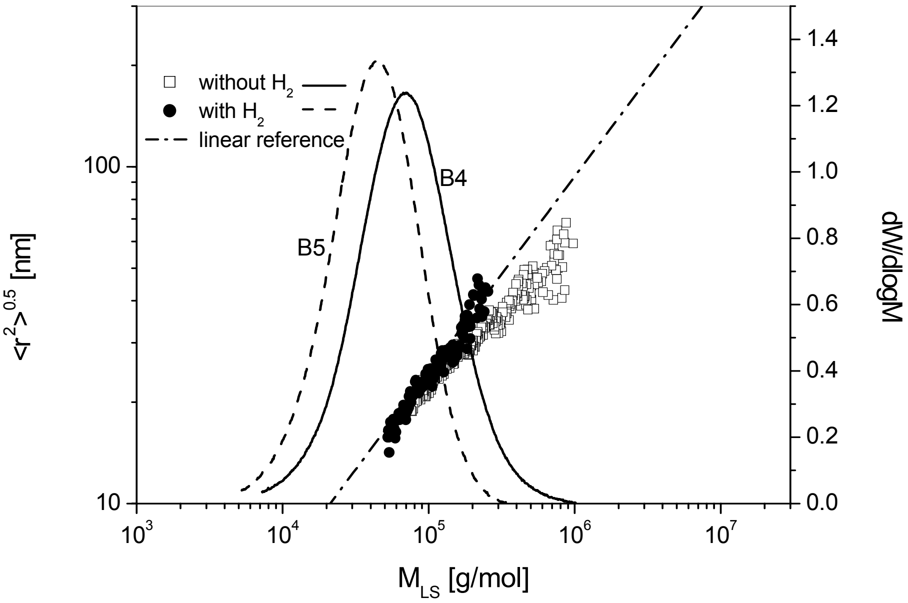

Figure 2-10: Influence of hydrogen on molar mass distribution and radius of gyration for catalyst B (B4, B5, linear ref. is sample A2).

Together with the change in molar mass a change in long-chain branching is observed. While for products produced with catalyst B without hydrogen, a long-chain branched structure could be clearly detected, LCB can hardly be found in the products of catalyst B polymerized with hydrogen (Figure 2-10), the same was observed for catalyst E (Figure 2-11). For the grade E4 the radius of gyration was so small due to the lower molar mass that it could only be detected for the high molar masses, because of the intensive showing of scatter. The mean value of the radius of gyration suggests that the polymer is linear.

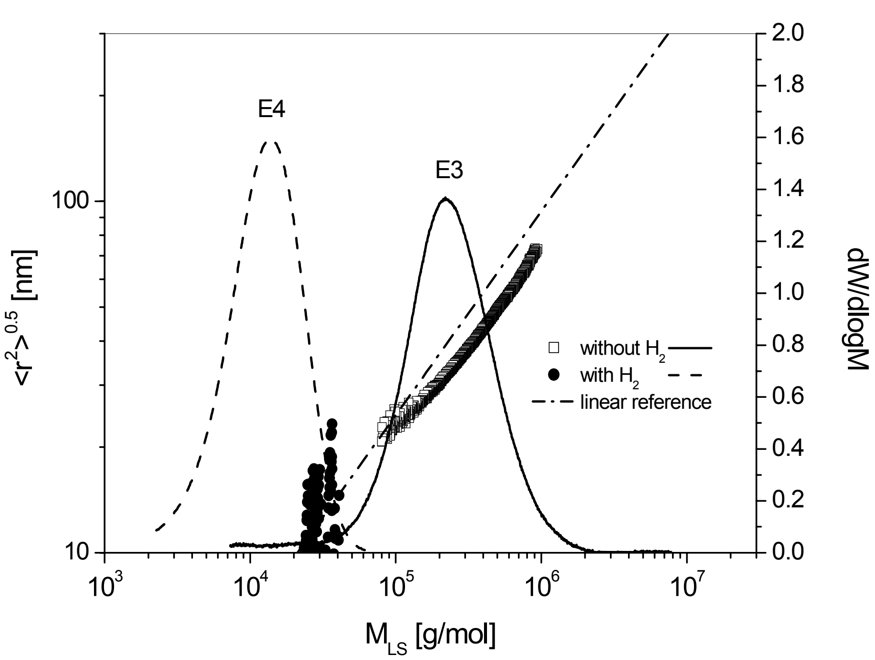

Figure 2-11: Influence of hydrogen on molar mass distribution and radius of gyration for catalyst E (E3, E4).

The molecular data concerning the branching is listed in Table 2-4 and Table 2-5. The degree of branching was evaluated from the radius of gyration. If a deviation from the linear standard is barely visible the degree of branching is set to - while a large deviation is designated with ++.

2.4.3 Branch detection by melt rheology

The mass average molar mass M_w determines the zero shear-rate viscosity η_0. The shape of the viscosity function, however, is strongly influenced by the shape of the MMD. Because of the broad range of molar masses the viscosity functions have to be reduced to be molar mass independent. This can be achieved by the η_0-M_w-correlation for linear PE.

The normalized viscosity functions of several of these samples are described in detail by Stadler.[101,I]

A broad molar mass distribution (e.g. A7 and A5) leads to a broader transition zone between the shear thinning regime at high frequencies and the limiting zero shear-rate viscosity η_0 at infinitely low frequencies. The frequency ω is linked to the shear rate g by the Cox-Merz-Rule which is valid for unfilled PE-melts. Samples with a narrow MMD (e.g. E5) show a narrow transition region.

The dependence of the zero shear-rate viscosity η_0 on the mass average molar mass M_w of these samples is discussed in chapter 2.3.3. The zero shear-rate viscosity η_0 of the linear samples is listed in Table 2-4. No long-chain branches were detected for any of those samples by SEC-MALLS or rheology. All of these samples come to lie onto a correlation $\eta_0=9\cdot 10^{-15}\cdot M_w^{3.6}$ for $M_w>M_c$ (2 900 g/mol).

Table 2-4: Rheological properties of the linear samples.

#	η_0 [Pas]	degree of branching from rheology	degree of branching from SEC-MALLS
A1	4.2×10^6	none	none
A2	6.7×10^6	none	none
A5	1.6×10^6	none	none
A4	2.6×10^7	none	none
A6	-[a]	-[a]	none
A7	70,500	none	none
A8	152	none	none
A9	3.2	none	n.d.[b]
A3	17	none	n.d.[b]
E1	3.5	none	n.d.[b]
E2	0.19	none	n.d.[b]
E4	10	none	n.d.[b]
E5	731	none	n.d.[b]
E7	0.089	none	n.d.[b]
G1	0.038	none	none
G2	0.045	none	none

[a] no rheological characterization possible due to be insufficient thermal stability

[b] not detectable (molar mass too low to measure radius of gyration)

Figure 2-12 shows the plot of the phase angle δ as a function of the complex modulus $|G^*|$. This is a very effective way to detect long-chain branches and broader molar mass distributions. The master curve was determined from several linear HDPEs and LLDPEs with a fairly narrow molar mass distribution which is shown in the small figure in Figure 2-12. This master curve is used for the detection of long-chain branches and asymmetric molar mass distributions for further analysis. More details on their origin are given in **I**. The samples

E1, E5, and A4 (A4 has a polydispersity of 4.3, but the molar mass distribution is monomodal), as well as many other mPEs with a narrow MMD, can be approximately described with a master curve (broken line), while the samples A5 and A7 have a distinct asymmetric molar mass distribution. These samples show a deviation from the master curve even at small phase angles. In Table 2-4 all linear samples are listed.

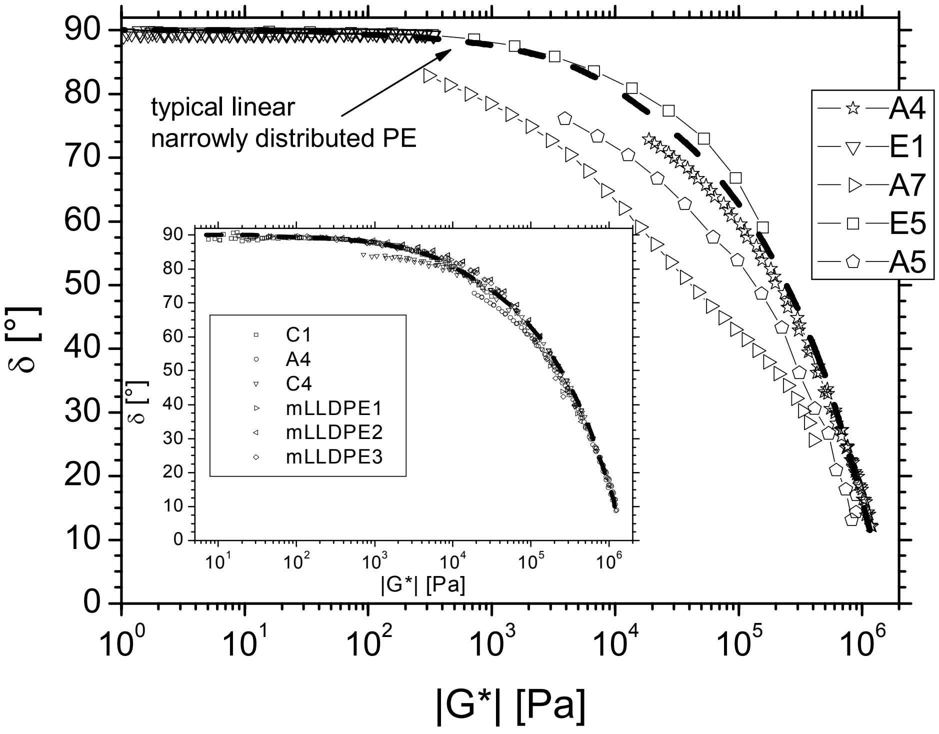

Figure 2-12: δ(|G|)-plot for some of the linear samples.*

The plot δ(|G*|) of some of the long-chain branched products is shown in Figure 2-13. All these samples were synthesized at 60°C and 0.41 mol/l ethene concentration, but different catalysts were used. A series with hydrogen presence and one sample without, for a comparison, were polymerized. The hydrogen reduces both, the molar mass and the degree of long-chain branching.

The presence of long-chain branches is revealed by the additional minimum (or shoulder in case of small degrees of LCB) caused by the additional relaxation modes of the long-chain branches. Its position depends on the molecular topography.[102]

For the hydrogen molar mass regulated samples B5 and especially D4 the difference from $\delta(|G^*|)$ of a linear resin is rather small. The SEC-MALLS data revealed no long-chain branches for those samples. Because of the small deviation from a strictly linear sample it is believed that the degree of LCB is very small, probably much below 1 LCB/molecule. The long-chain branched sample with hydrogen molar mass regulation F3 shows both, a much more distinctly long-chain branched viscosity function as well as a clear deviation from the linear standard in the SEC-MALLS. The data of this sample is described in chapter 3.3. For this sample a maximum of 0.37 LCB/molecule were found by NMR measurements.

The sample E4 is behaving like a Newtonian liquid because of its low molar mass. Thus this sample is not shown in Figure 2-13. The zero shear-rate viscosity, however, lies on the η_0-M_w-correlation established (see chapter 2.3) and indicates the linearity of this sample.

When comparing the samples synthesized without H_2, one will notice that they are deviating from the linear standard at much lower phase angles (≈35° compared to ≈65° for the samples with H_2). This can be attributed to the much higher degree of long-chain branching. F2 is deviating from the linear PE standard at the lowest phase angle followed by E3 and B4. D3 deviates at slightly higher δ but shows the onset of a much more pronounced minimum than B3 and E3.

The rheological data of the long-chain branched samples is listed in Table 2-5. The evaluation of the branching was performed based on the shape of the viscosity function, the increase of the zero shear-rate viscosity and the minimum in the phase angle δ_c. If all quantities were just slightly different from a linear polymer (δ_c>70°, η_0/η_0^{lin} <3) -- was added. The samples with the highest degree of branching were labeled ++. For none of them the zero shear-rate viscosity η_0 could be reached and for some even δ_c was not found (e.g. F2 in Figure 2-13).

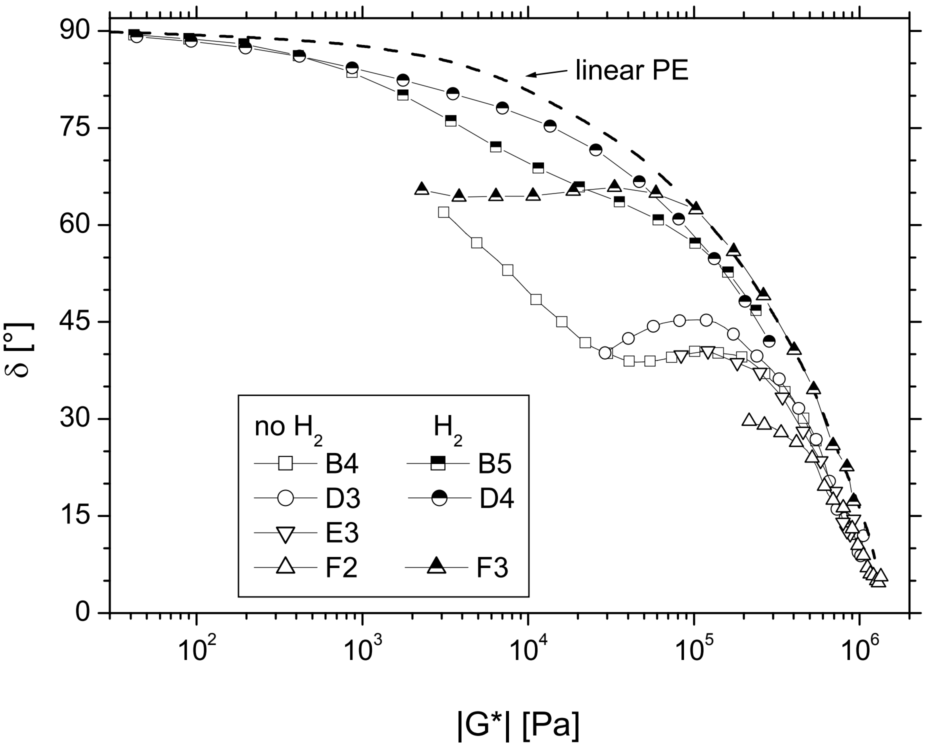

Figure 2-13: Influence of hydrogen on the phase angle as a function of the complex modulus δ(|G|) of LCB-PEs (all synthesized at 60°C and 0.41 mol/l ethene).*

Generally the branching detection by the two methods agrees fairly well despite their completely different technique. However, it is interesting to note that for some of the samples the degree of branching as detected by the two different methods differs distinctly. This can be attributed to the fact that the radius of gyration is mainly sensitive to the number of branching points,[103] while the rheological behavior depends on the extra relaxation modes added by the long-chain branches.[104] These relaxation modes depend on both the length and the number of long-chain branches. The length of the long-chain branches is corresponding with the polymers molar mass, the higher the molar mass the longer the branches are.

Thus a low degree of branching detected by SEC-MALLS and a high one by rheology means that very long long-chain branches are present.

For F2 it seems to be that it is highly branched according to the rheological measurements but almost linear according to SEC-MALLS. No gelled portion was detected for this resin by SEC-MALLS, because the injected mass was completely recovered in the detectors. A slightly crosslinked gel fraction would have explained the behavior, too. The most likely explanation is that the polymer is extremely high in molar mass. Therefore very few but extremely long long-chain branches can account for the observed behavior in the rheological measurements hinting to a highly branched structure. On the other hand these few molecules would result in a very small deviation from the behavior of linear molecules in the SEC-MALLS measurements suggesting that the polymer is linear.

Table 2-5: Rheological properties of the long-chain branched samples.

#	η_0 [Pas]	η_0/η_0^{lin}	η_{max} [Pas]	η_{max}/η_0^{lin}	δ_c [a] [°]	degree of branching from rheology	degree of branching from SEC-MALLS
E3	-	-	4.7×10^7	103	<39 (34)[b]	+	+
E6	1210	1.9	-	-	*(77)*	--	-
B1	-	-	($\approx10^8$)	≈1800	14	++	++
B2	872,000	121	-	-	35	+	+
B4	660,000	54	-	-	37	+	+
B5	4,200	2.75	-	-	68	--	none
B6	-	-	($\approx10^8$)	≈200	26	++	++
B7	40,540	12	-	-	51	+	+
B8	11,580	4.9	-	-	65	-	-
B9	6,300	3.1	-	-	69	-	+
D3	-	-	(9.0×10^7)	≈20	<36 (31)[b]	+	-
D4	4,500	1.5	-	-	*(81)*	--	none
D5	-	-	(9.0×10^6)	≈12	<27 (18)[b]	++	+
F1	30,900	3.4	-	-	72	+	+
F2	-	-	9.0×10^7	≈0.59	<30 (16)[b]	++	-
F3	445,000	6.9	-	-	63	+	+

[a] values in brackets are at the limit of this method and thus should be regarded with care

[b] no minimum reached in plot $\delta(|G^*|)$, value in brackets: estimate of δ_c

The increase of the zero shear-rate viscosity over a linear sample of equal M_w η_0/η_0^{lin} is also quite different for the samples with hydrogen molar mass regulation compared to those without (calculated according to $\eta_0^{lin}=K_1\cdot M_w^{\alpha}$ with $K_1=9\cdot10^{-15}$ and $\alpha=3.6$ [II]). The error of η_0/η_0^{lin} is ± 20% because of the high exponent α of 3.6 and the error margin of M_w which is around ±5%. For the samples synthesized with H_2 η_0/η_0^{lin} is close to 1. While η_0/η_0^{lin} is just above the error margin of the η_0-M_w-correlation for D4 (η_0/η_0^{lin} = 1.46), B5 has a slightly higher value of 2.75. The value for η_0/η_0^{lin} of F3 is much higher with 6.9.

The very high molar mass resins produced with catalyst D (D3), E (E3) and F (F2) show very high viscosities. For those samples it was not possible to reach the zero shear-rate viscosity because of the extremely long relaxation times. It was, however, possible to determine the zero shear-rate viscosity of B4 with 665,000 Pas which leads to a zero shear-rate viscosity increase η_0/η_0^{lin} of 53. The maximum viscosities η_{max} of D3, E3, and F2 were found to be around 10^8 Pas. The zero shear-rate viscosity of these samples is believed to be much higher than the maximum viscosity. Thus the increase of maximum viscosity η_{max} observed for those samples is plotted as a function of η_0^{lin}. The detection of the actual zero shear-rate viscosity of these samples would have taken at least several days if not months and is prevented by the insufficient thermal stability.

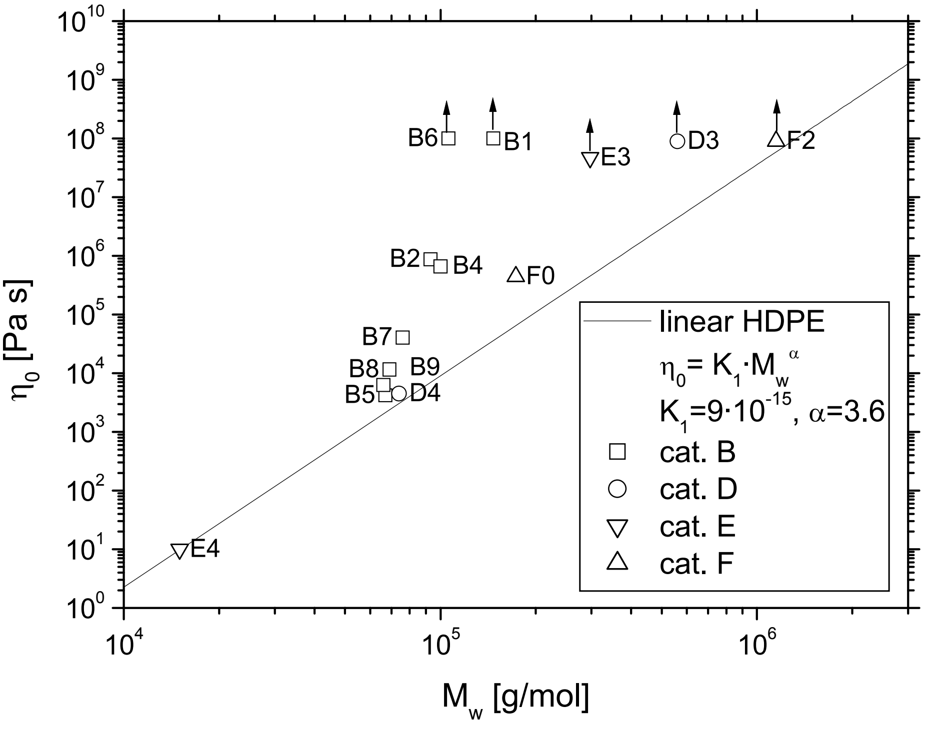

Figure 2-14: Zero shear-rate viscosity versus molar mass M_w for LCB-PEs.

Figure 2-14 shows the zero shear-rate viscosity of some long-chain branched polymers in dependence on their molar mass. All these materials are above the line on which all the linear samples lie. The boxed values are polymerizations under presence of hydrogen. For some products it was, due to extreme long relaxation times, not possible, to determine η_0. The measurement would take longer than the materials are thermostable. In those cases the maximal measured zero shear-rate viscosity is given instead (Table 2-5, Figure 2-14), η_0 is higher than η_{max}, so an arrow in the figures indicates the direction of the assumed values.

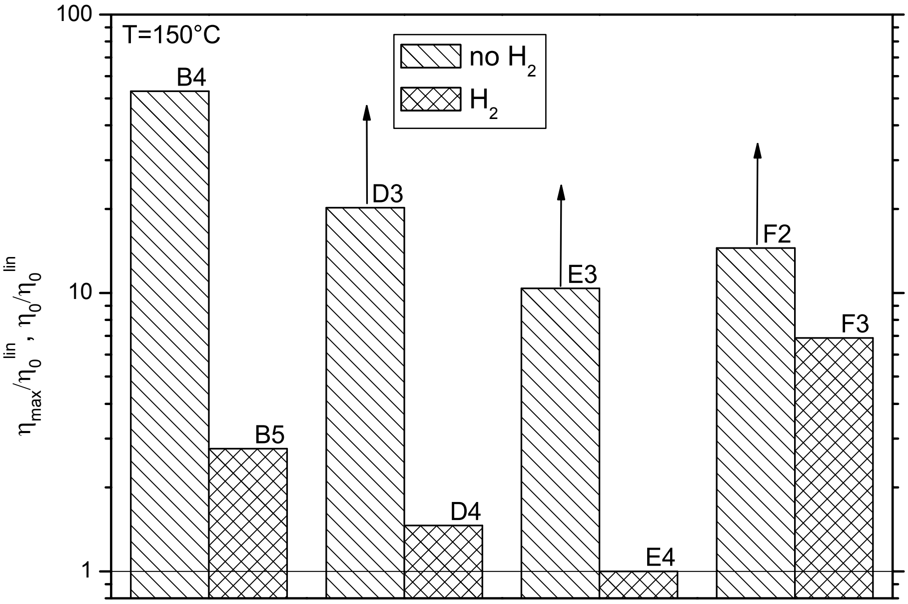

Figure 2-15: Influence of hydrogen on the zero shear-rate viscosity increase η_0/η_0^{lin} *of LCB-PEs (all synthesized at 60°C and 0.41 mol/l ethene), arrows indicate that* η_0 *is not reached.*

Besides the influence of the catalyst and hydrogen on the rheological properties of a polymer also the influence of monomer concentration (pressure) and polymerization temperature was tested.

The influence of the polymerization pressure and temperature was tested with the catalyst B. Despite the similarities in the synthesis conditions (just the ethene concentration was varied), the viscosity functions are very much dissimilar. The differences between the different viscosity functions are rather small for the high frequencies, while the differences are increasing towards lower ω. The difference between B8 and B6 is a factor of 70.5 at ω=0.01 s^{-1} while the factor for B7 lies in between. The viscosity function is described in more detail in **I**.

Because the degree of branching is identical for these samples as detected by SEC-MALLS, the molar mass M_w has to play an important role, too. On one hand a longer polymer chain has longer long-chain branches, which lengthens the relaxation times and on the other hand is the number of long-chain branches per 1 000 C constant, which means that samples with a higher molar mass carry more long-chain branches. Thus these differences are primarily attributed to the higher molar mass of B6 compared to B8.

These differences can be found for a polymerization temperature of 60°C as well. The lower polymerization temperatures yield higher M_w and thus higher viscosities. Therefore, the relaxation times are longer. These differences are only clearly visible in very long creep tests.

Figure 2-16 shows the increase of the zero shear-rate viscosity η_0/η_0^{lin} for the catalyst B-series. As a general trend η_0/η_0^{lin} decreases with increasing temperature. The second trend is the decrease of η_0/η_0^{lin} with increasing pressure i.e. increasing comonomer concentration. Interestingly, the ratio between the different polymerization pressures is about the same for a polymerization temperature of 60°C and 75°C, although it is not possible to reach the zero shear-rate viscosity for the series with a pressure of 1 bar.

Even the maximum viscosity η_{max} lies much more above the zero shear-rate viscosity of a linear polymer of equal molar mass η_0^{lin} than the samples with a pressure of 3 bar. Thus, η_0/η_0^{lin} of the series with 1 bar has even higher values than the η_{max}/η_0^{lin}. That means there is a decrease in inserting long-chain branches during the polymerization with increasing reaction temperature and/or increasing reaction pressure.

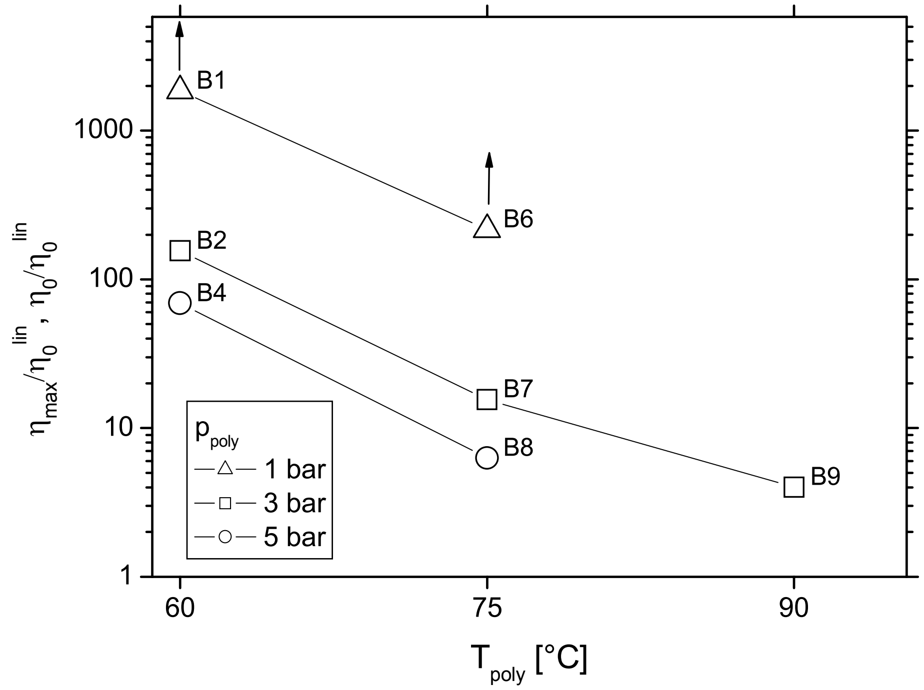

Figure 2-16: Increase of the zero shear-rate viscosity η_0/η_0^{lin} *for the series polymerized with catalyst B for different polymerization conditions.*

The dependence of the rheological properties on the polymerization conditions is presented for polymers made with catalyst B in Figure 2-17. The lower the polymerization temperature and pressure is, the larger is the deviation from the linear standard curve. For the samples with a low polymerization temperature and pressure a clear minimum is evident while the other samples have only a shoulder, which is barely observable for B9.

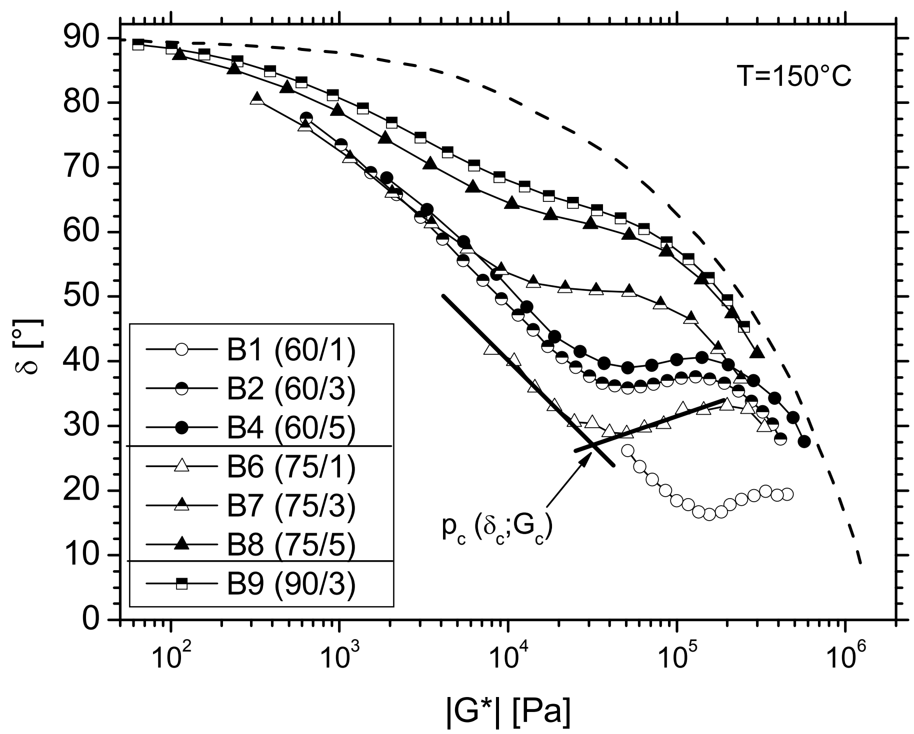

Figure 2-17: δ(|G|)-plot for the series polymerized with catalyst B (the numbers in brackets indicate polymerization temperature and pressure).*

Another possibility of visualizing the differences between the different polymerization conditions as is to determine p_c from the δ(|G*|) plot. According to the definition of Trinkle et al.[102], the only difference is that |G*| is not normalized on G_N^0, which is not necessary because only PEs, which all have the same G_N^0, are under investigation, which all have the same G_N^0. p_c has a coordinate $|G^*|_c$ [Pa] in x-direction and δ_c [°] in y-direction. δ_c is a measure of the branching topography[102]. It is determined by the two tangents laid into the inflection points on both sides of the minimum or shoulder. Figure 2-18 shows the dependence of δ_c on the polymerization temperature and pressure. The error bars are estimates of the error of determining δ_c, which is dependent on the shape of the δ(|G*|)-function and the statistical error of δ, which increases with decreasing δ.

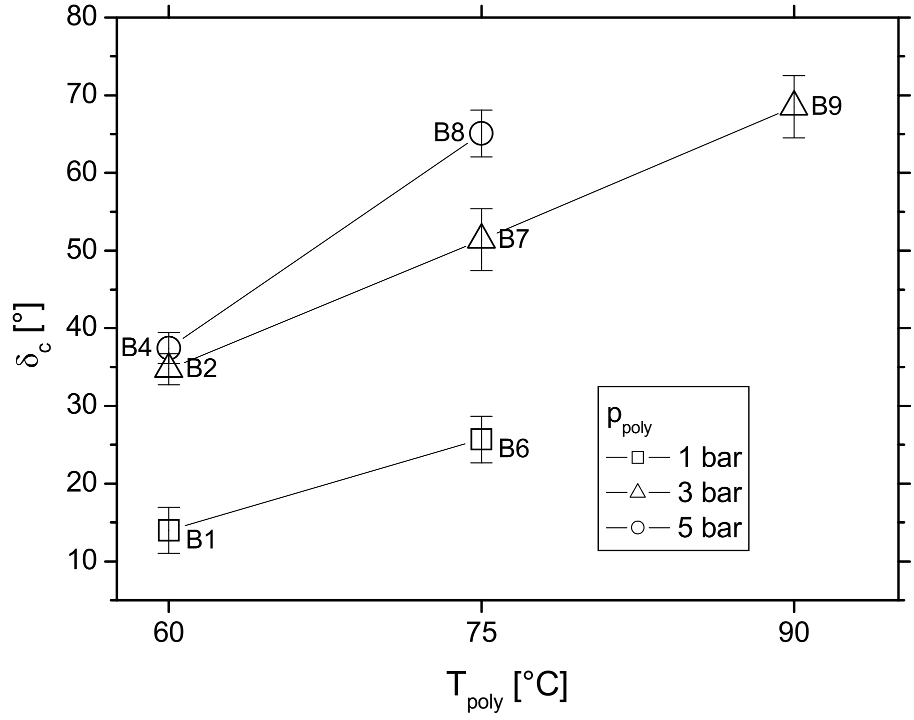

Figure 2-18: $\delta_c(T_{poly})$ for the series polymerized with catalyst B (T=150°C).

It is evident that the dependence of δ_c on the polymerization temperature decreases with increasing polymerization pressure. This leads to the conclusion that a lower polymerization temperature causes larger long-chain branched structures which increase the relaxation time. Therefore, the zero shear-rate viscosity can not be determined for those resins with frequency sweeps down to $\omega = 0.01\ s^{-1}$, while this is possible for the resins synthesized at higher temperatures.

2.5 Conclusion

A variety of linear and long-chain branched polymers covering a vast range of molar masses and molar mass distributions was synthesized using six different metallocene catalysts A-F. This study focuses on the formation of LCB comparing catalyst structures and polymerization conditions.

The thermal behavior of the materials shows a strong dependence on the molar mass concerning the melting temperature and melt enthalpy. The crystallization temperature is nearly constant over the whole range of investigated polyethylenes. It is remarkable that there is no influence of the catalyst structure, although the polymer microstructures strongly depend on the polymerization conditions and the catalyst structure.

The molecular characterization of the samples showed that the number of long-chain branches per molecule is increasing with molar mass for all branched samples. The number of LCB/1000C remained approximately constant. The degree of branching in these materials was found to differ over a range from no branches to highly branched. The catalyst structure and polymerization conditions are the contributors to these changes. Both methods, SEC-MALLS and shear rheology give relative information about the branching of the chains. The number of long-chain branches in these polymers was found to be between 0.1 and 3 branches per 10 000 monomer units.

The rheological characterization was carried out mainly with frequency sweeps. The zero shear-rate viscosity η_0 was measured by creep tests if it was not possible to obtain it by frequency sweeps.

The viscosity functions and the zero shear-rate viscosities η_0 of a series of linear polyethylenes with different molar mass distributions were measured by creep experiments and correlated to the molar mass M_w measured by SEC-MALLS.

The resulting $\lg(\eta_0)$-$\lg(M_w)$-plot can be described by a linear function with a slope of 3.6 for mass average molar mass greater than the critical molar mass, which was determined to be $M_c \approx 2900$ g/mol. An unambiguous dependence of the zero shear-rate viscosity on the molar mass distribution was not observed. It is concluded that the η_0-M_w-correlation is independent of the molar mass distribution within the experimental error. This finding is of particular importance as a deviation of η_0 from $\eta_0(M_w)$ valid for linear polyethylenes can be used for a qualitative analysis of long-chain branching.

A clear dependence of the viscosity function on the MMD was found, especially on the weight average molar mass M_w for the linear products. The LCB-resins showed a much more diverse behavior. For the products polymerized with catalyst B a dependence of $|\eta^*|(\omega)$ and δ ($|G^*|$) on polymerization temperature and the monomer concentration was observed. Interestingly the dependence of δ_c (T_{poly}) decreases with increasing pressure.

The formation mechanism of the LCB has been described as a reincorporation of a vinyl unsaturated polymer-chain into a different growing polymer-chain. However, this reincorporation mechanism requires that the growing polymer-chain is terminated by β-hydrogen abstraction and that the catalyst is able to reincorporate the large vinyl ended polymer chain. Hydrogen as chain termination agent also lowers the amount of long-chain branches besides its influence on the molar mass.

Catalyst A forms exclusively linear polyethylenes while catalyst E under very certain conditions, especially without hydrogen (see materials E3, E6, E8, E9), is also able to produce LCB-PE. At polymerization temperature of 90°C a certain monomer concentration is necessary to form a very low amount of LCBs, at 60°C the highest amount of branches was observed and at 30°C also some branches were detected. For catalyst G a similar behavior can be expected, when the monomer concentration is higher and the polymerization temperature is lower than that used here, LCB will most likely occur. Comparing the catalysts A and E the substitution pattern destines if LCB can be formed. We explain this with a more open aperture gap size of catalyst E and therefore we expect LCB to be formed by catalyst G in even larger numbers. In general the more open the active side is, the better higher α-olefins can be incorporated into the growing chain. With hydrogen no LCB was observed and an increase in polymerization temperature decreases the amount of LCB.

Catalyst B and D produce only a few or no long-chain branches, when hydrogen is present. Under all other conditions the polymers are long-chain branched. Using catalyst B the LCB content is decreasing with increasing polymerization temperature (with catalyst E there is a maximum at 60°C), although here the degree of branching is higher at lower monomer concentrations. With catalyst D at 90°C even a higher amount of branches is detected than at 60°C. Catalyst B shows much higher activities than catalyst D, therefore a higher reactivity ratio for ethene can be assumed and a lower branching degree will be reached.

Catalyst F is producing LCBs in a remarkable amount although hydrogen is present. This catalyst is producing the highest degree of branching in this series in the presence of H_2.

Higher monomer concentration leads to more branches. The influence of hydrogen is less distinct than for the other catalyst systems. The chain termination mechanism via β-hydrogen elimination is believed to be so pronounced, that the vinyl content of the polymer is still high enough even with hydrogen present in the reactor.

The results of this study underline the widely accepted mechanism for the formation of LCB via the copolymerization route.

Generally, the results of SEC-MALLS and rheology concerning the branch detection are in good agreement. However, for sample F2 a totally contrary result was found. This might be due to very small amounts of chains with ultra long branches which affect the rheology very much, but their concentration is too low to be detected by SEC-MALLS.

As final conclusion the following order of affinity to create long-chain branches in polyethylenes for the catalysts can be given: F, D, B, E, A. Catalyst G can not be classified in this series because the obtained molar masses were too low. The differences in electron density and aperture gap size among the active center depend on the ligand systems and strongly affect the comonomer incorporation behavior and the formation of LCB. Also by changing the polymerization the formation of LCB can be controlled. The influence of monomer concentration, polymerization temperature, and hydrogen is varying and very specific to the catalyst systems.

3. Short-chain branched polyethylenes

3.1 Introduction

LLDPEs with side-chains longer than 18 carbons have not been described in literature. Copolymers of ethene and 1-octene, 1-decene, 1-dodecene, 1-octadecene, and 1-hexacosene (α-olefin wax fraction with over 91 wt.-% of hexacosene and octacosene, see Appendix 8.2) were carried out using [Ph_2C(2,7-di-^{tert}BuFlu)(Cp)]$ZrCl_2$/MAO as catalyst to obtain short-chain branched polyethylenes with branch length from 6 to 26 carbon atoms. This catalyst provides high activity and a very good comonomer and hydrogen response[**I**,**III**] (see chapter 2.2 and 3.2), which was also observed before for ethene/propene copolymerizations[**VII**,**IX**,**XI**,105].

The investigation of the influence of comonomer content and comonomer size on long-chain branching using melt-state NMR, SEC-MALLS and linear viscoelastic shear rheology is presented in chapter 3.3 and reference **IV**. The combination of these methods was found to be a very powerful method to characterize LCB in short-chain branched metallocene polyethylenes (LCB-mLLDPE), with its chemical composition, as well as solution and melt properties. Although the influences of comonomer and hydrogen on LCB have previously been separately investigated, their combined interaction has not been studied so far. Melt-state NMR was used to quantify the comonomer content in the copolymers and the degree of LCB in the homopolymer. Due to the lack of chemical shift resolution LCB was defined as branches of ≥ C4, as also found in literature[70]. Studies on the increase of the side-chain detection limits and other optimizations are done by solid-state and melt-state NMR by Pollard and Klimke.[**VIII, XIII**]

The influence of length and amount of the side-chains on crystallization and mechanical properties of the materials is described in chapter 3.4 and reference **VI**. The amount of comonomer in the copolymer within one series and the molar mass of the copolymer remain constant.

3.2 Comonomer influence on polymerizations and polymer characteristics

3.2.1 Materials

A series of ethene/α-olefin copolymers is synthesized using the metallocene $[Ph_2C(2,7\text{-di-}^{tert}BuFlu)(Cp)]ZrCl_2$ (catalyst F, Figure 2-1) as catalyst precursor and methylalumoxane as cocatalyst. The lengths of the side-chains in the obtained LLDPEs are 6 carbons (1-octene), 8 carbons (1-decene), 10 carbons (1-dodecene), 16 carbons (1-octadecene) and 24 carbons (1-hexacosene). All polymers were synthesized under similar conditions. In addition, a homopolymer F0 was made (it is the material F3 in chapter 2). All polymers were synthesized under similar conditions, for the copolymerizations a total monomer concentration of 0.5 mol/l was set. The polymerizations were carried out at 60°C reactor temperature and at the presence of 0.5 bar (9 mmol) hydrogen. More experimental details are described in chapter 6 and given in Table 3-1. For these series of polymerizations reactor 1b was used and the analytics were done on DSC 1, SEC 1 and NMR 1.

Table 3-1: Experimental setup for the ethene/1-olefin copolymerizations and polymerization activities.

polymer	comonomer	feed [mol-%]	c(ethene) [mol/l]	p(ethene) [bar]	activity $[kg_{polymer}/(mol_{Zr}\cdot h\cdot mol/l_{monomer})]$
F0	-	0	0.410	5.00	45400
F8A	octene	10	0.450	5.52	90100
F8B	octene	15	0.425	5.21	127000
F8C	octene	20	0.400	4.90	100000
F10A	decene	10	0.450	5.52	74000
F10B	decene	15	0.425	5.21	77000
F12A	dodecene	10	0.450	5.52	38000
F12B	dodecene	15	0.425	5.21	90000
F18A	octadecene	5	0.475	5.82	90800
F18D	octadecene	10	0.450	5.52	123000
F18B	octadecene	15	0.425	5.21	109000
F18C	octadecene	20	0.400	4.90	107000
F26A	hexacosene	5	0.475	5.82	117000
F26D	hexacosene	10	0.450	5.52	168000
F26B	hexacosene	15	0.425	5.21	96000
F26C	hexacosene	20	0.400	4.90	52000

3.2.2 Results and discussion

3.2.2.1 Activity

In all experiments the activities were very high and reached 168 000 $kg_{polymer}/(mol_{Zr} \cdot h \cdot mol/l_{monomer})$. Surprisingly, the copolymerization with the waxy hexacosene gave the highest activity of all. For all copolymerizations an increase in the activity was observed up to a certain comonomer concentration in feed. It reaches a maximum that is much higher than the activity of the ethene homopolymerization and decreases, if more than about 10 mol-% of comonomer was in the reactor feed. This comonomer effect was observed often in literature for many metallocene catalyzed ethene/α-olefin copolymerizations.[17,106,107] Seppälä et al. describe this as a participation of the comonomer on the activation of the active center.[108,109] This leads to a decrease of the activation energy for the insertion of a monomer into the carbon – metal bond and thereby facilitate the chain grows and the chain transfer reactions. This phenomenon is very much catalyst and comonomer specific. For ethene/propene copolymerizations in solution it was furthermore found, that the comonomer effect is also lowered with higher ethene concentration in feed.[110]

Figure 3-1 shows the activity in dependence of the polymerization time for runs F18A (5 mol-% comonomer in feed), F18C (10 mol-% comonomer in feed) and F18D (20 mol-% comonomer in feed). After 10 – 20 minutes, the maximum of the polymerization activity is reached, and then a slow decrease can be observed. The activity course is the same for all comparable copolymerization runs, depending on the feed ratio of the monomers. Even after a polymerization time of 4 hours, there is still a remarkable activity.

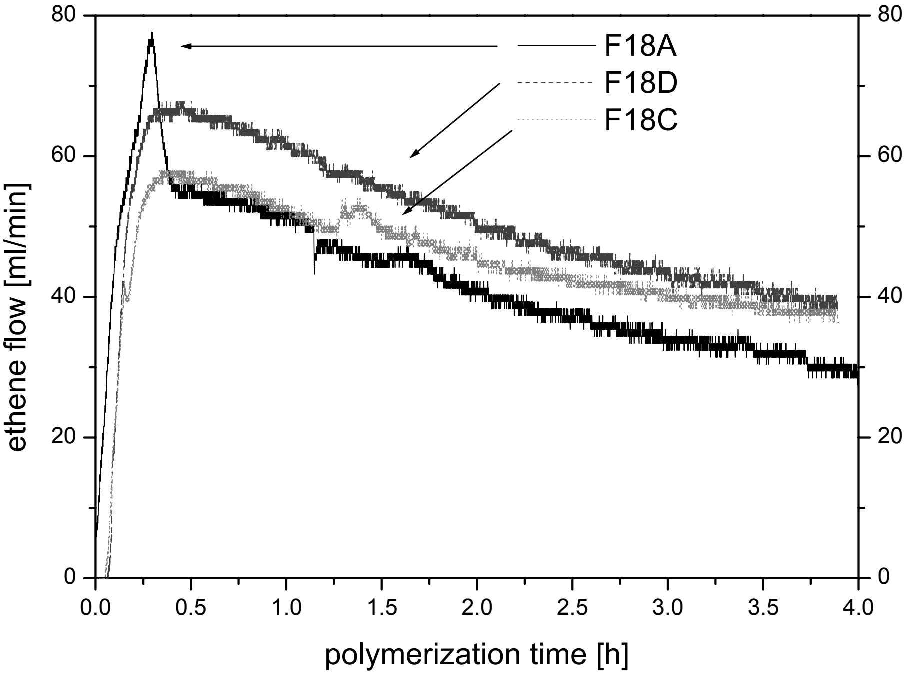

Figure 3-1: Ethene consumption during the polymerization runs for F18A, F18C and F18D

3.2.2.2 Comonomer incorporation

Using the catalyst F, the content of the α-olefin in the polymer was nearly a tenth of that in the starting feed for all different olefins. Even the hexacosene with 26 carbon atoms was inserted in a similar way (see Figure 3-2 and Table 3-2). This catalyst provides, as it was also shown in chapter 2.4 for LCB in HDPE, a high affinity to incorporate α-olefins of any length. In this series, the comonomer was distributed over the polymer chain in a statistical way. No comonomer – comonomer diades were found by NMR investigations for this incorporation rates.

The comonomer content was calculated with equation (3-1), using I(*), the integration area of the branching carbon signal, and $I(\delta,\delta^+)$, the integration area of the main signal of the CH_2-chain. The chemical shifts and denotation of the carbons are given in VIII and literature[111] (compare also Figure 3-8).

$$n_c = \frac{I(*)}{I(\delta,\delta^+)} \cdot 1000 \cdot 0.2 \quad [\text{mol-\%}] \tag{3-1}$$

$$w_c = \frac{n_c \cdot m_c}{n_c \cdot m_c + (100 - n_c) \cdot 28} \cdot 100 \quad [\text{wt.-\%}] \tag{3-2}$$

The average molar mass m_c of the hexacosene was taken to be 378 g/mol.

Table 3-2: Polymer characteristics of the copolymerization series determined by DSC 1, SEC 1 and NMR 1.

#	n_c[a] [mol-%]	w_c[b] [wt.-%]	T_c [°C]	T_m [°C]	cristallinity[c] [%]	M_w [kg/mol]	MMD
F0	0	0	111	140	60	146	2.48
F8A	0.98	4.0	100	120	34	252	1.77
F8B	1.47	5.6	96	116	38	204	1.99
F8C	2.24	8.4	88	112	28	165	2.08
F10A	0.87	4.2	102	120	45	183	2.14
F10B	1.35	6.4	97	116	32	177	2.08
F12A	0.53	3.1	101	120	34	191	1.99
F12B	1.56	8.7	96	116	46	169	2.04
F18A	0.32	2.8	108	128	45	211	2.24
F18D	0.78	6.6	100	122	42	185	1.98
F18B	1.19	9.8	98	117	38	194	1.97
F18C	1.88	14.7	87	116	34	182	1.98
F26A	0.22	2.9	106	129	47	216	1.97
F26D	0.82	10.1	99	125	40	218	1.96
F26B	1.19	14	98	116	33	184	2.19
F26C	1.72	19.3	91	113	26	209	1.90

a) mole fraction of comonomer in the polymer
b) weight fraction of comonomer in the polymer
c) enthalpy of fusion of a perfectly crystalline PE was taken to be 290 J/g[98]

The comonomer weight fraction in a copolymer with 1 mol-% of hexacosene is about 12 wt.-%, while it is in a copolymer with 1 mol-% of 1-octene only 4 wt.-% (compare Figure 3-3). Although the incorporation rate is similar for different comonomers, the mechanical properties of the materials will be influenced by the much higher weight content of the longer α-olefins in the copolymers. This is discussed in more details in chapter 3.4.

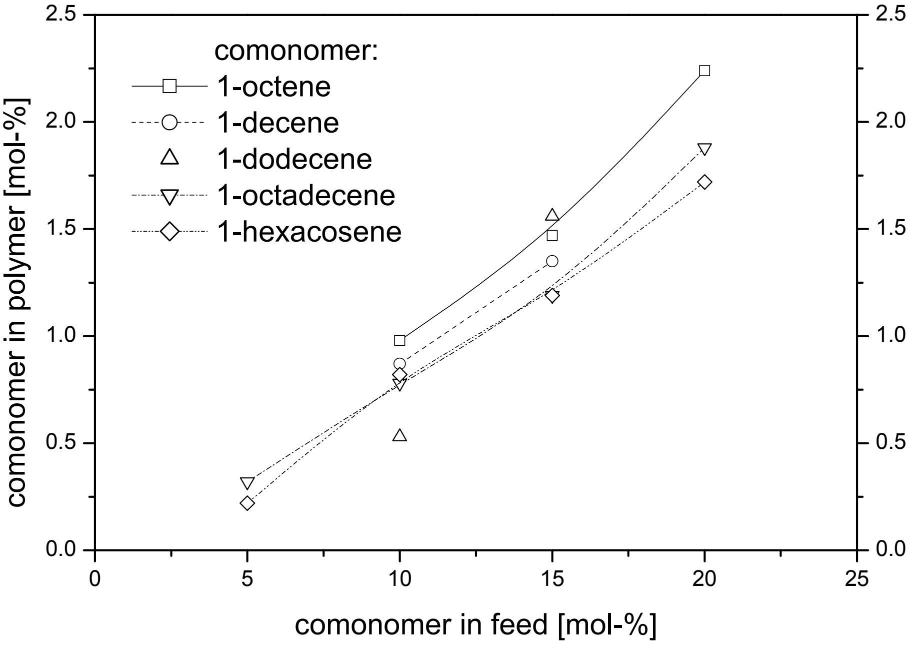

Figure 3-2: Comonomer incorporations for all LLDPEs of this series, lines are added for guidance only.

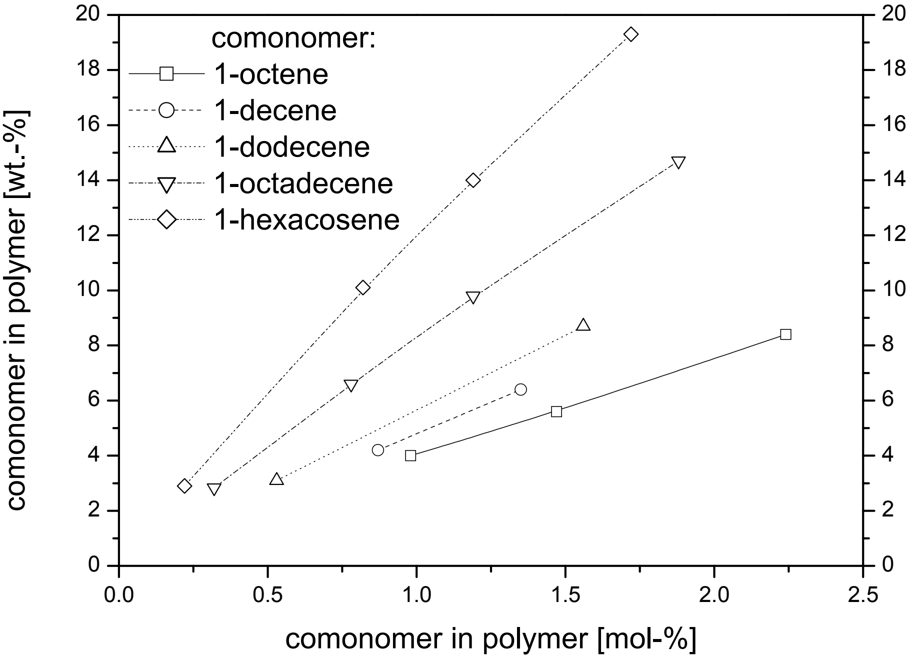

Figure 3-3: Molar versus weight fraction of comonomer in the LLDPEs, lines are added for guidance only.

3.2.2.3 Molar masses

The molar mass of the copolymer was controlled by the addition of hydrogen to be between 150 and 250 kg/mol, it is slightly dependent on the ethene concentration. As expected for metallocene catalysis, the polydispersity is narrow and about 2. The catalyst F shows a very good hydrogen response. As observed for polyethylenes (chapter 2), for ethene/α-olefin copolymers the molar masses can be reduced in dependence of the hydrogen concentration in feed. From Figure 3-4 can be seen that the molar masses are not depending on the type of comonomer used, just on the incorporation rate.

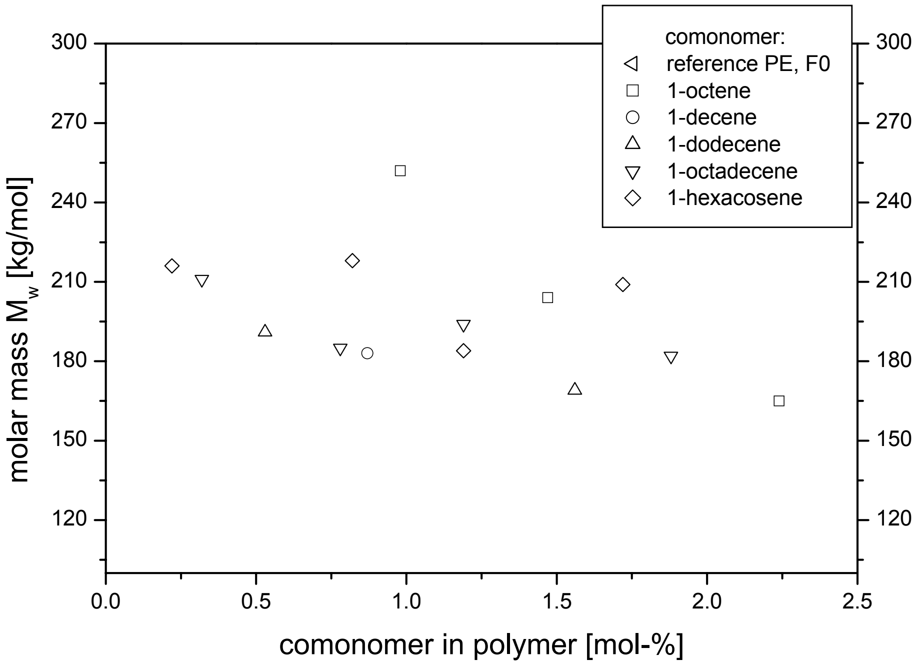

Figure 3-4: Molar mass M_w versus comonomer concentration in the polymer.

3.2.2.4 Thermal behavior

There is a strong dependence of the melting temperature on the molar ratio of the α-olefin in the copolymer. The melting temperature decreases from 130 °C to 112 °C at a comonomer content of 2.3 mol-% for all copolymers. No effect of the side-chain length on both, the melting temperature and the crystallization temperature was found (Figure 3-5 and

Figure 3-6). The crystallization temperature is decreasing linearly with increasing comonomer content but independent of the comonomer type.

For all of the ethene/hexacosene copolymers a second melting peak is observed whose intensity in the DSC curve is depending on the incorporation rate of the comonomer. The second melting peak occurs at 53 °C and can be assigned to the crystalline side-chains in the polymers; it is the same melting temperature the pure comonomer has (see Figure 3-16). Due to several washing and recrystallization procedures, remaining hexacosene in the materials can be excluded. The influence of the side-chains on the polymers is discussed in chapter 3.4.

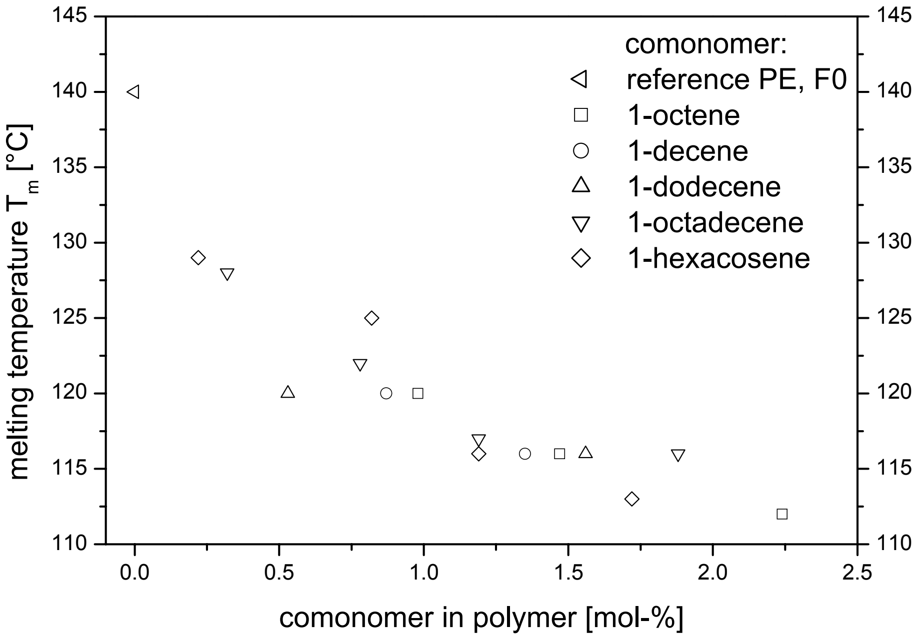

Figure 3-5: Melting temperatures of the LLDPEs versus incorporation.

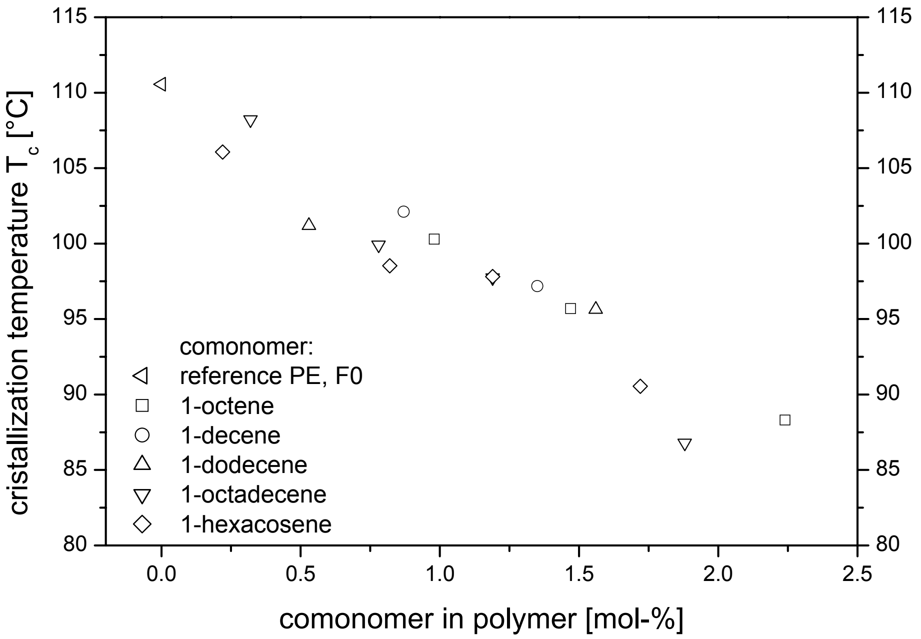

Figure 3-6: LLDPE's crystallization temperatures versus comonomer molar content.

In the case of random ethene copolymers, the melting point depression is not caused by molar mass variations but by MSL variation. Keating recrystallized the commercially available hydrocarbons and measured the subsequent melting point.[112] The plot of ln(CH_2 molar fraction) against 1/T shows a linear relationship (equation (3-9)). From this curve the MSL of fractionated ethene copolymers can be assigned from the melting temperatures of the fractions, which is applied and explained in more detail in chapter 3.4.3.2.2. Figure 3-7 shows that the relationship is valid for all the LLDPEs made in this study. Here all melting temperatures of the polymers of chapter 3 are plotted against their CH_2 molar fraction. The linear fit leads to the equation shown in Figure 3-7, which is very close to and thereby in accordance with the one by Keating. Small deviations on that equation were also found by others.[113,114]

This underlines again that the melting temperature of LLDPEs is depending only on the CH_2 molar fraction of the material and not on the type of comonomer after a certain molar mass is reached (compare Figure 2-3).

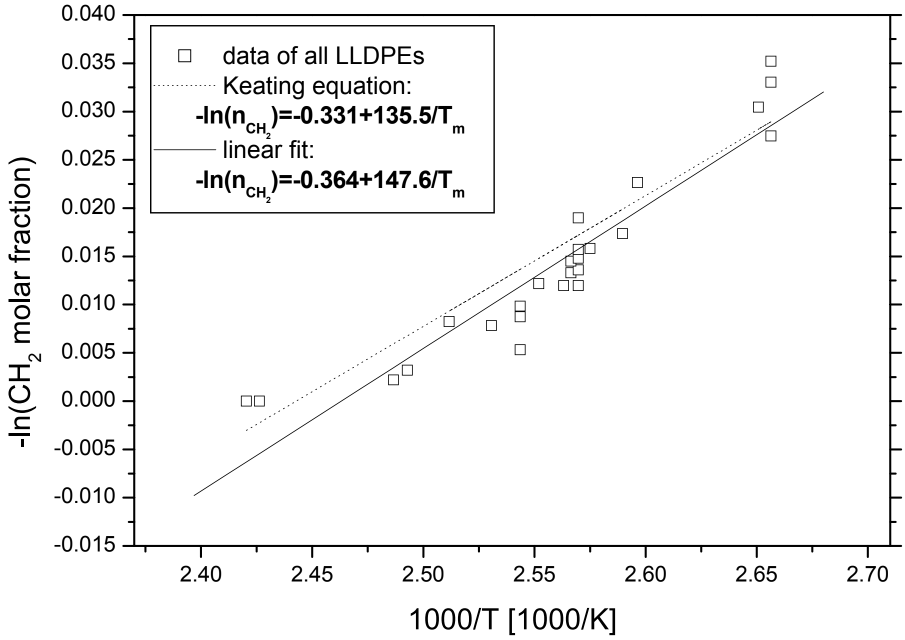

Figure 3-7: Relationship of comonomer incorporation and melting temperature.

3.3 Comonomer influence on long-chain branching

3.3.1 Materials and molecular characterization

To investigate the influence of the monomer length and amount on the long-chain branching in the polymer, the materials F0, F8A - F8C, F18A - F18C, F26A - F26C (see Table 3-1, chapter 3.2) are characterized in more detail by SEC-MALLS (SEC 2), melt rheology and melt-state NMR (NMR 3). The SEC-MALLS measurements were carried out by Dr. Kaschta and the rheological measurements by Stadler in Erlangen, the NMR measurements by Klimke in Mainz. The equipment is described in chapter 6 and reference **IV**. All products were found to be stable for at least 20 hours at 150°C, with some stable for more than 70 hours.

3.3.2 Results and discussion

3.3.2.1 Melt-state NMR

An estimation of comonomer incorporation was achieved by integration of the signals of the quantitative proton-decoupled, ^{13}C melt-state NMR (compare Figure 3-8). The ratio of integrals associated with a branch site to that of the bulk backbone CH_2 sites (A_{bulk}) allows direct access to the degree of incorporation. Although the actual CH branch site (*) is resolved at 38.3 ppm, the three sites adjacent to this (α) at 34.6 ppm are used for branch quantification due to their increased sensitivity. The comonomer incorporation, in units of mol-% (n_c) and wt.-% (w_c), was calculated from the relative area of the α peak at 34.6 ppm (A_α) to that of the bulk peak at 30 ppm (A_{bulk}) using:

$$n_c = 100 \cdot 2 \cdot \frac{\frac{1}{3} A_\alpha}{A_{bulk} + \frac{1}{3} A_\alpha \cdot \left(4 - n_\delta - n_4\right)} \quad [mol - \%] \tag{3-3}$$

$$w_c = \frac{n_c \cdot l}{n_c(l-2)+2} [\text{wt.-\%}] \tag{3-4}$$

where n_δ and n_4 are the number of δ and 4 sites per branch and l is the total number of carbons in the comonomer. The integral A_{bulk} does not solely represent the sites of the backbone. In addition to the backbone δ sites the branch δ sites (for branches of more than 7 carbons in length), the 4 site (for branches of more than 6 carbons in length) and all γ sites were also encompassed into this integral. With the α, β and * sites of the backbone also neglected A_{bulk} needed to be corrected inorder to represent the true backbone. For the missing *, two α and two β sites per branch $5A_{br}$ was added to A_{bulk}, while for the additional γ site from the branch $1A_{br}$ was subtracted. Additionally, where applicable, the number (n) of additional δ and 4 sites along the branch also had to be compensated for, thus $(n_\delta + n_4)A_{br}$ were substracted from A_{bulk}.

A number of assumptions are made when using the area of this peak as an internal standard representing the backbone. Due to the broad base of the peak at 30 ppm in the melt-state, the integral range is limited by neighboring peaks at 32.2 and 37.2 ppm. This leads to an underestimation of A_{bulk} and correspondingly to an overestimation of the branching. However, when considering the relative sizes of the areas in question (see Figure 3-8), the differences between the true and approximated values of A_{bulk} are small, and propagate into only minor deviations in calculated comonomer incorporation.

Considering these sources of error, the comonomer incorporations as determined by melt-state NMR are given to one decimal place. Repeating the branch quantification for a low (F26A) and high (F18C) incorporation sample twenty times gave a relative standard deviation in branch content of 2.0 and 2.9 %, respectively. Further analysis of these and other systems using NMR techniques is given by Pollard[VIII] and Klimke[IV,XIII,115].

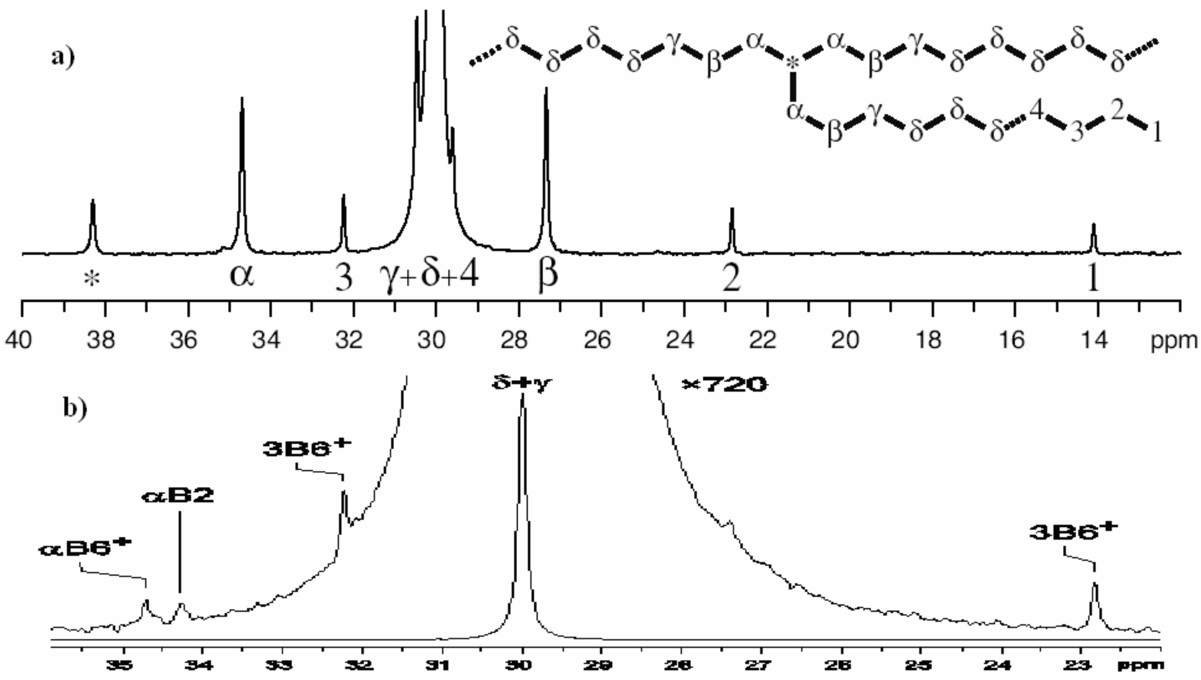

Figure 3-8: a) Typical melt-state ^{13}C NMR spectrum and assignment of polyethylene containing branches of six carbons in length or longer. (F18C: 13.7 branches per 1000 backbone carbons); b) Melt-state spectrum of the homopolymer showing 8 ethyl and 6 hexyl or longer branches per 100 000 CH_2. (F0: 78 000 scans).

For the homopolymer F0 the higher number of scans (78 000) allowed for the determination of lower branch contents. Due to the broad nature of the 'foot' of the bulk peak, all CH_2 sites are incorporated into A_{bulk}, including the α branch sites. Separate integration of the branch sites only (A_{br}) allows the branch content (B_{br}) per CH_2 to be calculated from the ratio $B_{br}=A_{br}/A_{bulk}$. It should be noted that for ethyl branches $A_{br}=1/2A_{\alpha}$ whereas for hexyl and longer branches $A_{br}=1/3A_{\alpha}$.

Under these conditions approximately 0.03 mol-% branching was still seen. Such branches may occur in metallocene catalyzed homopolymerizations via isomerisation reactions, although these are less important for polyethylenes than for polypropylenes. The degree of branching was found to be approximately evenly distributed between ethyl and hexyl or longer branches, corresponding to 0.8 and 0.6/10 000 CH_2 respectively. Thus the average molecule of F0 had approximately 0.37 branches of 6 or more carbons. With no comonomer used, this number was taken as an upper limit of the possible amount of LCB present. It should be stated that the absolute number of LCB cannot be determined by melt-state NMR as no chemical shift distinction is seen between branches of 6 carbons in length and those of the entanglement molar mass. However, only branches greater than M_e are considered long-chain branches relevant for processing.

Table 3-3: Results of analytical and rheological characterizations of PE and copolymer samples.

sample	comonomer [C_nH_{2n}]	n_c ^{a} [mol-%]	w_c ^{a} [wt.-%]	M_w^{b} [kg/mol]	M_n^{b} [kg/mol]	MMD^{b}	η_0^{c} [kPa s]	J_e^0 [10^{-4} Pa^{-1}]
F0	-	0.012 (<C2) /0.016 (>C2)^{d}	-	173	85	2.0	445	12
F8A	8	1.1	4.3	240	112	2.1	1224	18^{e}
F8B	8	1.8	6.8	190	92	2.0	440	11
F8C	8	2.7	10.0	152	76	2.0	51	2.2
F18A	18	0.4	3.5	183	80	2.3	498	15
F18B	18	1.5	12.1	167	84	1.9	164	6.4 ^{e}
F18C	18	2.2	16.8	159	79	1.9	55	1.4
F26A	26	0.5	6.1	185	89	2.1	450	11
F26B	26	1.6	17.4	194	82	2.1	284	7.6 ^{e}
F26C	26	2.3	23.4	175	78	2.1	87	1.6

$^{a)}$ As determined by melt-state NMR
$^{b)}$ Determined by SEC 2
$^{c)}$ at 150°C
$^{d)}$ Branches >C2 are taken to be the upper limit of the long-chain branch content (0.37 LCB/molecule)
$^{e)}$ linear steady-state of elastic recovery compliance J_e^0 not proven to be reached, see reference **IV**

It is evident that only a fraction (10%) of the feed (see Table 3-1) is incorporated into the polymer (Table 3-3). Although the maximum comonomer content of F26C seems small the comonomer accounts for more than 23 wt.-% of the sample, due to hexacosene having approximately 13 times the molar mass of ethene. For the F8 and F18 copolymers the amount of comonomer plays a less decisive role concerning weight fraction (compare chapter 3.2 and Figure 3-3).

3.3.2.2 SEC-MALLS

The distributions of molar mass of the three polyethene-co-octenes F8A, F8B and F8C are shown in Figure 3-9. The molar mass distribution of all the polymers is of about 2, typical of metallocene catalysis. The products differ only in their molar masses, with none showing a high molar mass component.

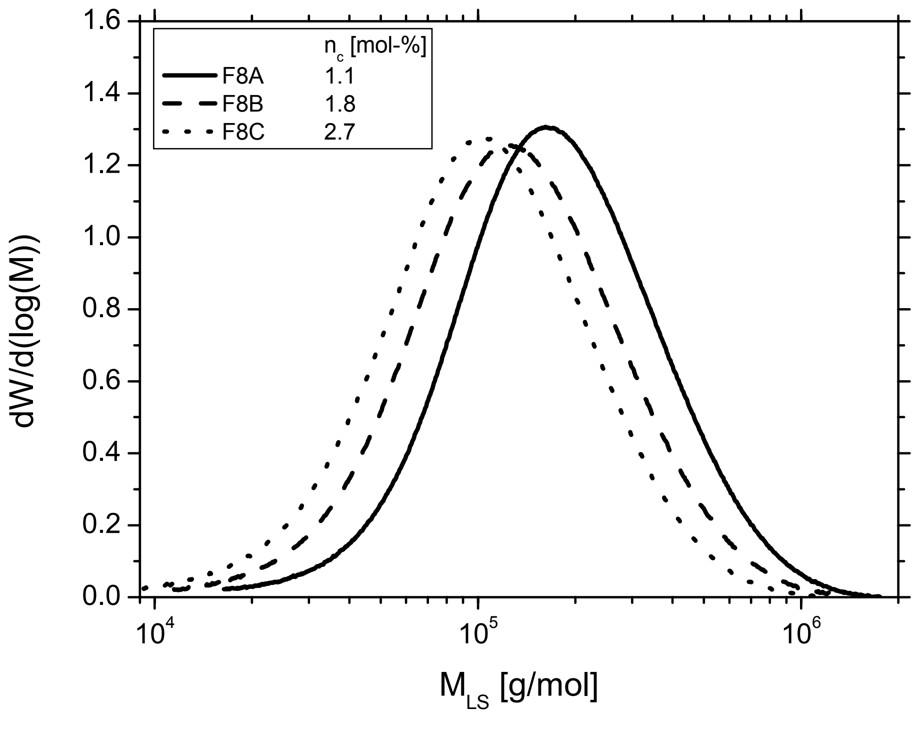

Figure 3-9: Molar mass distribution of the polymers F8A, F8B and F8C.

When the radius of gyration of F0 was compared to a known linear reference A2 (see chapter 2.3), evidence for LCB was found (Figure 3-10). The straight trend line for the linear sample in Figure 3-10 can be described by

$$< r^2 >^{0.5} = 0.024 \cdot M^{0.58} \tag{3-5}$$

This exponent is published by Tackx and Tacx, too.[116]

The radius of gyration of F0 deviates from the linear reference for molar masses above 400 kg/mol, tending towards smaller values, thus indicating a contraction of the coils in solution. Such a contraction is typical of long-chain branched molecules.

Using the Zimm-Stockmayer theory[117] the average number of three functional branch points per molecule was estimated. If these are assumed to be identical with the number of LCB for F0, a value of 0.3 LCB per molecule can be given, which is in good agreement with the upper limit of 0.37 LCB/molecule determined by NMR.

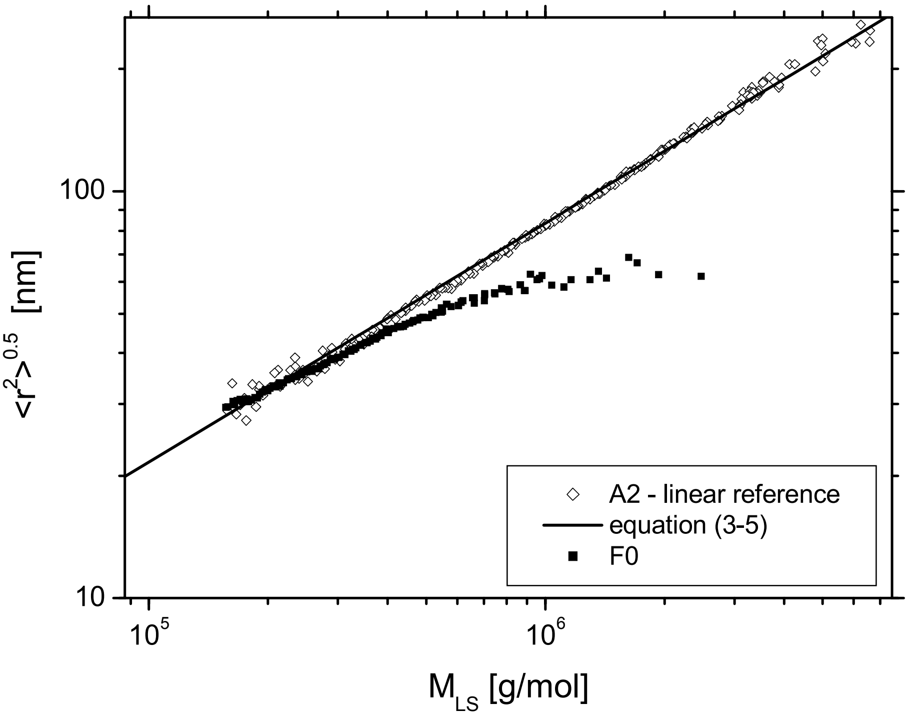

Figure 3-10: Radius of gyration as a function of absolute molar mass for a linear reference polymer (A2) and the homopolymer (F0).

The influence of comonomer type and concentration on the long-chain branching was analyzed based on the comparison of the radii of gyration. From Figure 3-11 it can clearly be seen that the radius of gyration of all copolymers with the lowest comonomer contents deviates from the linear reference above molar masses of 400 kg/mol. Thus, it can be concluded that F8A, F18A and F26A possess long-chain branches. The deviation is smaller than that of the homopolymer F0 (Figure 3-10). It can be concluded that these samples are less branched than F0. As the amount of LCB determined for F0 was already small, the amount of LCB in the copolymers was expected to be even lower.

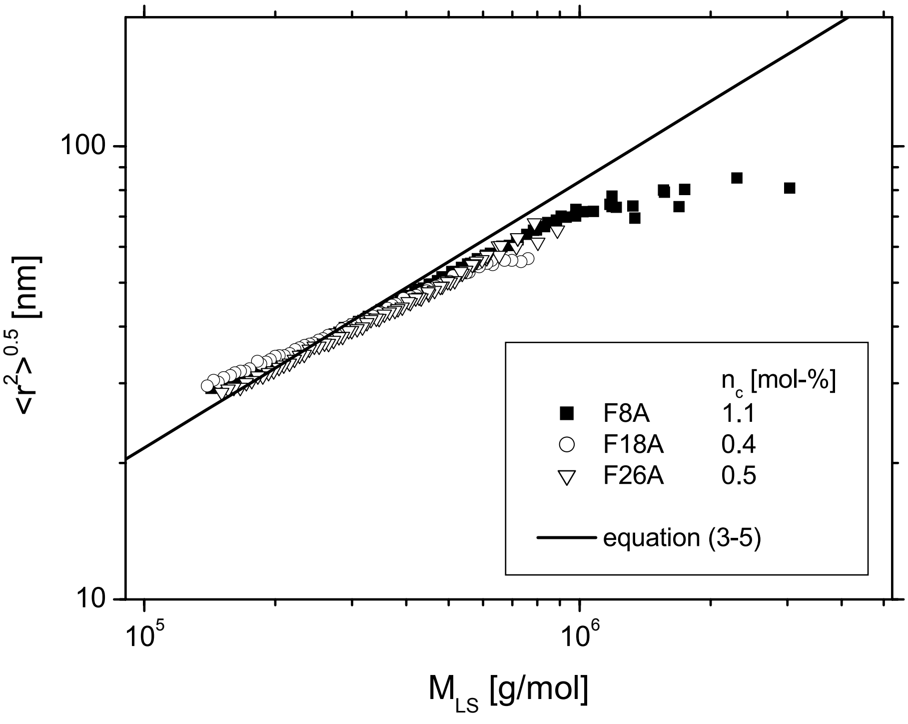

Figure 3-11: Radius of gyration as a function of molar mass for copolymers with lowest comonomer content.

The deviation from the linear behavior at smaller molar masses is mainly due to the physical limitations of the MALLS. At low molar masses the MALLS has a detection limit of about 20 nm due to the wavelength of the laser used.

Additionally, the decrease of the radius of gyration by short-chain branches also has to be taken into consideration, with significant effects often seen for comonomer contents larger than 20 wt.-%.[118] However, with the comonomer contents smaller than this value for most copolymers studied, with the exception of F26C, these effects are thought to be small. One of the fundamental questions arising from the Zimm-Stockmayer-Theory is the minimum length of a side-chain to be counted as a long-chain branch, i.e. which is the minimum length of a side-chain leading to a decrease in the radius of gyration - even for small concentrations. Even the comonomer hexacosene does not decrease the radius of gyration (as found for the linear sample F26C).

For the octene based copolymers the deviation from linear behavior became less pronounced with increasing comonomer content, with no deviation seen for F8C (Figure 3-12). A similar behavior was found for the longer α-olefins copolymers.

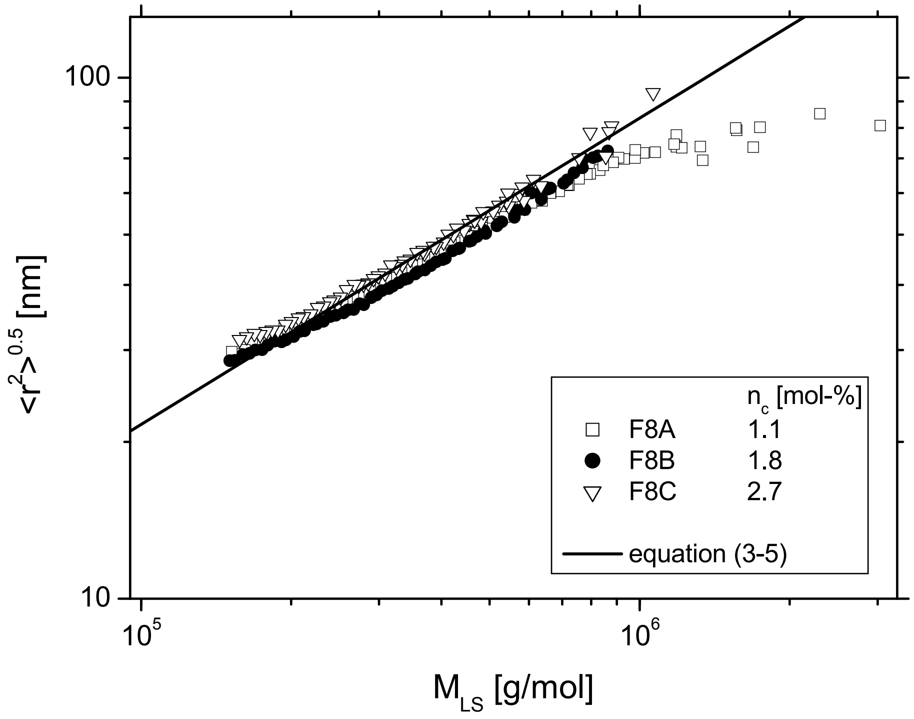

Figure 3-12: Radius of gyration as function of molar mass for the octene copolymers.

From the SEC-MALLS measurements it was concluded that the catalyst F produced LCB, even when α-olefins of greater then 8 carbons in length were used as comonomers. The incorporation of LCB was only found for copolymers containing low comonomer content. With a maximum LCB content of only 0.61 LCB/10 000 CH_2 determined for F0, the question arise whether the amount of LCB in the samples with a high comonomer content is below the detection threshold of the SEC-MALLS or whether long-chain branches are not generated at all. To gain deeper insight into the existence of LCB in the polymers, rheological measurements were performed, as they are very sensitive with respect to very small amounts of LCB.

3.3.2.3 Rheological characterization

Long-chain branching influences a number of linear and non-linear rheological properties. These include the viscosity function, and the dependence of the zero shear-rate viscosity on the absolute molar mass. The dependence of the phase angle on the complex modulus is significantly influenced by presence of LCB. Long-chain branched systems also show increased linear steady-state elastic compliances J_e^0. Most of these rheological properties are dependent on both LCB and molar mass distribution. An exception is the function $\eta_0(M_w)$, which only shows a weak influence of the molar mass distribution and may be assumed to be independent of the molar mass distribution (compare chapter 2.3). All of these rheological properties were used to investigate the presence of LCB in the polymers, with the MMD effect safely ignored due to their similar polydispersity (Table 3-3).

The dependences $\eta_0(M_w)$ and $\delta(|G^*|)$ are described here, the others are described by Stadler in literature[**IV**,101].

3.3.2.3.1 Zero shear-rate viscosity η_0

For the zero shear-rate viscosity η_0, as described in chapter 2.3, it has been shown on linear PE that equation (2-1) is independent of the polydispersity, within experimental error, for MMD between 2-16 (relevant for all systems here presented) and M_w between 0.4-923 kg/mol. At 150°C the material constants were found to be $K_1 = 9 \cdot 10^{-15}$ and $\alpha = 3.6$ for η_0 in Pa·s and M_w in g/mol. Substantial deviation from this simple relationship occurs with the presence of LCB. For long-chain branches mLLDPE and mHDPE the zero shear-rate viscosity was typically found to be greater than η_0^{lin}, calculated using equation (2-1) for a linear sample of the same molar mass.[76]

The zero shear-rate viscosity was measured for all samples by means of creep experiments and the correlation of η_0 and M_w is shown in Figure 3-13. The zero shear-rate viscosities of the samples F0, F8A, F18A, F8B, and F18B are distinctly above the η_0-M_w-line established for linear polyethylenes. For F8A the ratio η_0/η_0^{lin} is also indicated.

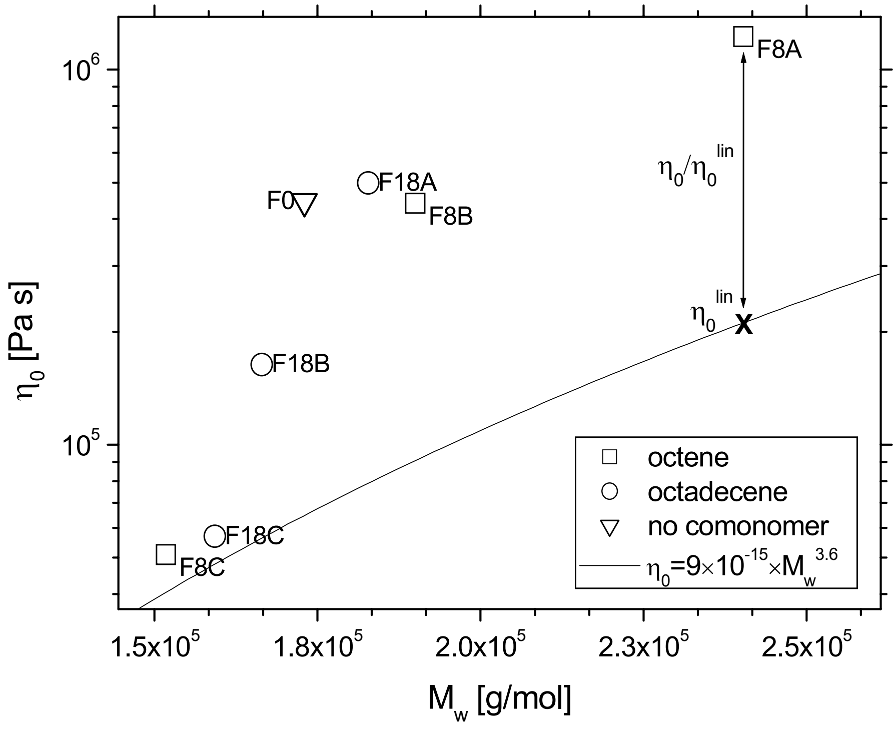

Figure 3-13: Zero shear-rate viscosity η_0 as a function of molar mass M_w for the homopolymer and octene/octadecene copolymers.

The ratio η_0/η_0^{lin} provides a more intuitive representation of the influence of the LCB on the samples, due to their different molar masses, than zero shear-rate viscosity η_0 alone. The ratio η_0/η_0^{lin} clearly shows the influence of LCB as a function of the comonomer content and feed (Figure 3-14).

Generally, η_0/η_0^{lin} was found to decrease with increasing feed and comonomer content as well, approaching the ratio of 1 for purely linear systems. The highest increase of the zero shear-rate viscosity was observed for F0 with $\eta_0/\eta_0^{lin} \approx 6.9$. The copolymers with the lowest comonomer content (F8A, F18A and F26A) show an increase of η_0 between 6.3-5.5. The copolymers with medium comonomer contents exhibit values of 4.8 and 3.0 for F8B and F18B/F26B, respectively.

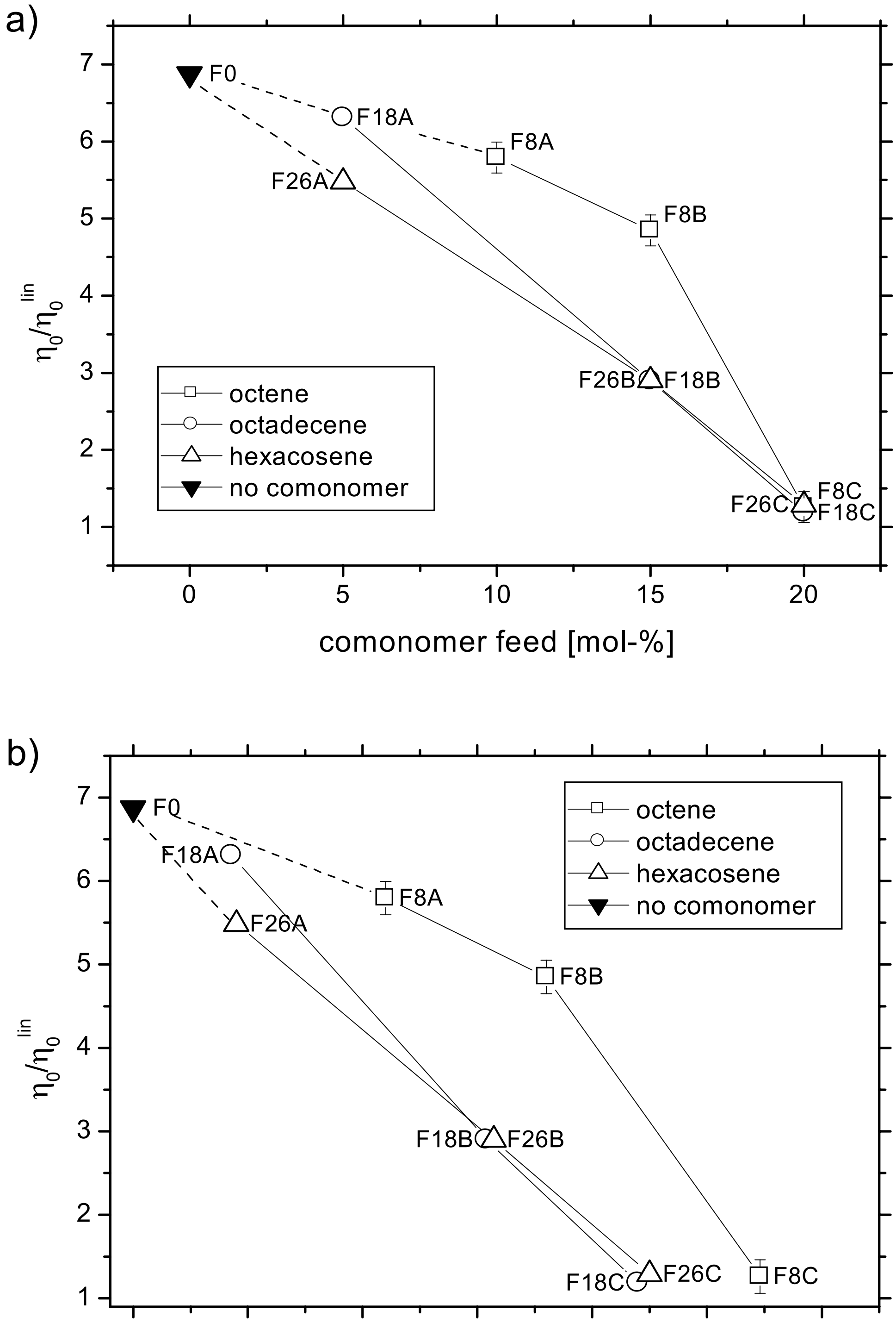

Figure 3-14: Ratio of zero shear-rate viscosity η_0/η_0^{lin} as a function of comonomer feed (a) and content (b), respectively. The approximate experimental error of η_0/η_0^{lin} is about ± 20% (shown for octene series) assuming ±5% error in M_w.

It is evident that each comonomer has a different influence on η_0/η_0^{lin} as a function of feed and content. In general the incorporation of LCB into the growing chain can be influenced either by the comonomer feed concentration or by the already incorporated comonomer. In the first case the influence is mainly due to diffusion and kinetic effects. It can formally be considered a terpolymerization reaction; ethene, the comonomer and the LCB-forming macromer are acting as competing reactants. For all copolymerizations an increase of the polymerization activity was observed up to a certain comonomer concentration in the feed (compare chapter 3.2). The activity reached a maximum much higher than that of the ethene homopolymerization and decreased when more than about 10 mol-% of comonomer was in the reactor feed. This comonomer effect was observed often in literature for many metallocene catalyzed ethene/α-olefin copolymerizations.[17,106,107] Seppälä et al. ascribe this to a participation of the comonomer on the activation of the active center.[108,109] This leads to a decrease of the activation energy for the insertion of a monomer into the carbon – metal bond and thereby facilitate the chain grows and the chain transfer reactions. This phenomenon is very catalyst and comonomer specific. For ethene/propene copolymerizations in solution it was furthermore found, that the comonomer effect is also lowered with higher ethene concentration in feed.[110] Figure 2-14a shows for the comomoner feed a decreasing effect on the LCB incorporation with increasing comonomer concentration. Looking at the influence of the reaction mixture there is a less pronounced difference between the comonomer types used, most important is their amount in solution. In contrast to that the various comonomers act very differently after insertion into the polymer chain, with the steric hindrance of the polymer side-chains strongly determining LCB formation (Figure 3-14b). For example, although F26C and F8B have approximately the same comonomer content (1.9 mol-%), each sample exhibited significantly different viscosity ratios of approximately 5 and 1, respectively, the latter lying on the $\eta_0(M_w)$ trend line for linear PE (Figure 3-13). The octadecene (F18) and hexacosene (F26) copolymers did not show a large difference in η_0/η_0^{lin} as a function of the comonomer content n_c. When comparing octadecene and hexacosene copolymers, the comonomer length is not found to play an important role in LCB incorporation. However, comparing octene and octadecene (or hexacosene) polymers, the LCB incorporation is obviously different. Thus the additional 10 carbons of octadecene have a distinct effect on η_0/η_0^{lin} while the additional 8 carbons between octadecene and hexacosene do not strongly influence this quantity.

As all high comonomer content samples (F8C, F18C and F26C) are found to lie at $\eta_0/\eta_0^{lin} \approx 1$, it can be concluded that these samples are predominantly linear. This finding is in good agreement with the SEC-MALLS experiments. The effect between the different samples, however, is much clearer than by SEC-MALLS as the effects are much larger than the small deviations of the radius of gyration of the branched samples from the linear standard.

3.3.2.3.2 |G*|-δ-plot

The phase angle δ as a function of the absolute value of the complex modulus $|G^*|$ is another versatile tool for getting insight into the molecular structure, having the advantage that no normalization with respect to the molar mass is needed.

However, characterization of LCB by the |G*|-δ-plot is only possible if the shape of the molar mass distribution is known. Bimodal or very broad molar mass distributions show a behavior similar to that of LCB. For all the materials having a polydispersity of around 2 these limitations do not apply. For linear systems the dependence of the phase angle δ with |G*| is found to sharply increase at small phase angles, and approach a plateau upon reaching the limiting phase angle of 90°.

A typical linear behavior was seen for F26C (Figure 3-15), with the strongest indication of LCB observed for F0. The lower comonomer content hexacosene copolymers, F26A and F26B, also show slight deviations from the linear reference and F26C, suggesting LCB contents between those found in F26C and F0. It can thus be concluded that F0 had the highest degree of LCB followed by F26A and F26B, while F26C showed no indication of LCB. Similar trends with comonomer content were found for the octene and octadecene copolymers.

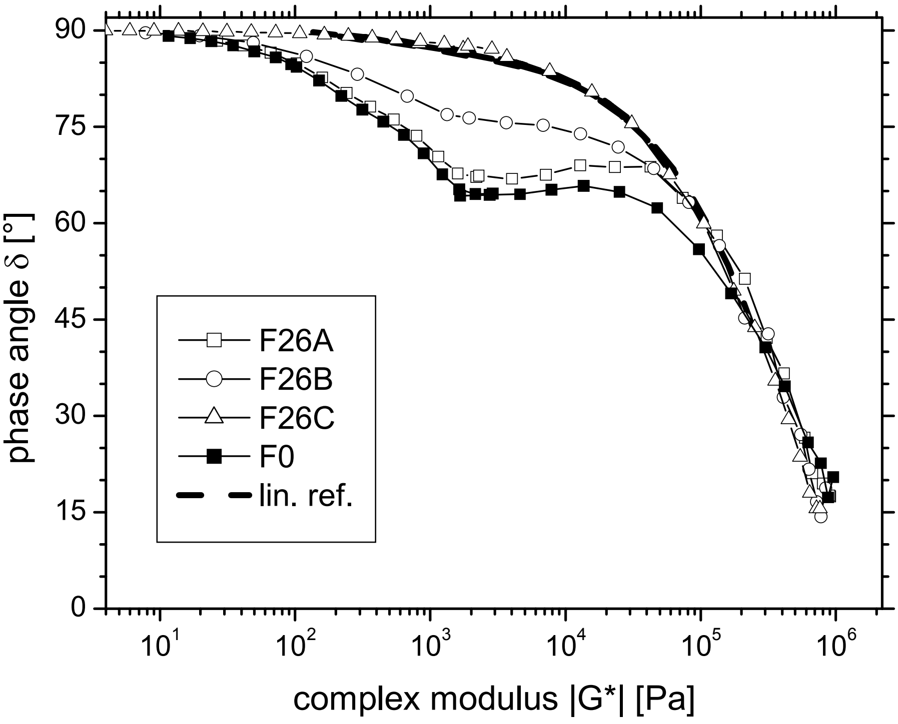

Figure 3-15: δ(|G|) plot for the samples of the hexacosene series, linear reference*[76]*, and the homopolymer F0.*

3.4 Comonomer influence on crystallization and mechanical properties

3.4.1 Chain heterogeneity analysis

Thermal fractionation techniques offer quick and practical ways to evaluate chain heterogeneities in semicrystalline thermoplastic materials by employing carefully designed thermal cycles in a DSC. These techniques are particularly useful to study the degree and distribution of short-chain branches produced by the copolymerization of ethene with α-olefins. Thermal fractionation provides an alternative to experimentally more time consuming and complicated fractionation techniques that involve preparative or analytical fractionation in solution. In a recent review by Müller and Arnal[113], a particular emphasis is made on the two techniques most commonly applied in the literature: step crystallization from the melt (SC) and successive self-nucleation and annealing (SSA). The numerous applications that have been recently developed are also reviewed.[113]

Segregation studies by stepwise annealing using DSC have been applied on different types of Ziegler-Natta[114,119-122] and metallocene catalyzed ethene copolymers[114,121-124]. The results show that differences in the ethylene sequence distributions can be seen when the polymers are annealed in steps at successively lower temperatures. The multiple endothermic peaks observed in the melting curves after this treatment correspond to a fraction of segregated molecules which crystallized at a certain temperature.

Dynamic mechanical analysis (DMA) is a very useful tool to characterize relaxations in both amorphous and semicrystalline copolymers. The influence of the structure and morphology on the dynamic mechanical behavior of polyethylenes has been discussed in a number of publications. [123-129] An understanding of the principles involved is of value in predicting the response of these polymers in various product applications. In general, linear and branched polyethylenes exhibit up to three transitions, labeled α, β and γ in order of decreasing temperature. The mechanism of these relaxation processes have been discussed in terms of the crystalline and amorphous phases present[130] and in many cases of a third interfacial phase[131-134] that is of intermediate character and may have some structural order.[135,136]

3.4.2 Materials and analytics

The polymerizations of these series were all done under very similar conditions and the copolymers obtained differ only in the length and number of the side-chains. Two series of copolymers were synthesized, containing ca. 1.5 mol-% and ca. 3 mol-% of comonomer, respectively. In addition a reference polyethylene was made to compare the properties of copolymers to the pure PE. The influence of the side-chains in amount and length on the material properties of the LLDPE is investigated. The experimental details are given in Table 3-4. The polymerizations were carried out in reactor 3 and the analytics were done on DSC 2, NMR 2, and SEC 3. DMA and tensile measurements were performed and in addition the material's densities were determined. Details on the experimental procedure and used equipment are described in chapter 6.

Table 3-4: Experimental details. The copolymers are denoted with a running number and the carbon length of the comonomer.

	#	comonomer	feed[a] [mol-%]	yield [g]	activity[b]	conv.[c] [%]
reference	1PE	none	0	21.9	55 000	0
series 1	2C8	1-octene	15	21.2	15 000	10.1
	3C12	1-dodecene	15	20.7	20 000	8.8
	4C18	1-octadecene	15	22.9	26 000	8.8
	5C26	1-hexacosene	15	20.8	21 000	7.1
series 2	6C8	1-octene	30	18.5	37 000	8.8
	7C12	1-dodecene	30	15.7	33 000	7.3
	8C18	1-octadecene	30	25.1	37 000	9.8
	9C26	1-hexacosene	30	23.0	23 000	7.7

a) comonomer content in feed
b) $[\mathrm{kg_{polymer}}\cdot(\mathrm{mol_{Zr}}\cdot \mathrm{h}\cdot \mathrm{mol/l_{monomer}})^{-1}]$
c) conversion of the comonomer

All polymerizations were catalyzed by the catalyst precursor $[\mathrm{Ph_2C(2,7\text{-}di\text{-}{}^{tert}BuFlu)(Cp)]ZrCl_2}$ (F, Figure 2-1) and methylalumoxane (MAO) as cocatalyst.

3.4.3 Results and discussion

3.4.3.1 Polymer densities

The density of the pure polyethylene is the highest and it is decreasing with increasing comonomer content, as expected for LLDPEs. If 1-hexacosene is used as comonomer, the density is behaving contrarily and is higher for both copolymers than for the other LLDPEs. An influence of the side-chains on the density is obvious, crystallization can be assumed and will be underlined in the following. The influence of the molar masses, given in Table 3-5, on our investigations is negligible within a certain area and checked by another series of polymers with higher masses. The here observed trends for ethene/octene, ethene/dodecene and ethene/octadecene copolymers are the same than Yoon et al.[128] determined from metallocene catalyzed LLDPEs like ethene/hexene, ethene/dodecene and ethene/octadecene copolymers. In DSC thermograms the melting peak shifted to a lower temperature zone with decreasing copolymer density without a significant loss in peak sharpness. The density of LLDPE was a decreasing function of mole fraction of α-olefin, and the decrease was more pronounced as the molar mass of the incorporated α-olefin increased.

Table 3-5: Polymer characteristics of reference PE and series 1 and 2.

	#	incorporation[a] [mol-%]	[wt.-%]	M_w [kg/mol]	MMD	T_m[b] [°C]	T_c[c] [°C]	cryst.[d] [%]	density [kg/m^3]
reference	1PE	0	0	368	2.13	139.0	115.6	65.6	939.7
series 1	2C8	1.57	6.00	321	2.19	115.2	100.6	41.3	912.8
	3C12	1.44	8.09	316	2.05	116.5	100.2	40.5	910.9
	4C18	1.32	10.79	328	2.08	116.5	102.9	41.3	915.5
	5C26	1.21	14.21	352	2.22	118.7	99.7	42.9	917.4
series 2	6C8	3.25	11.83	269	2.02	103.3	85.4	31.3	902.0
	7C12	3.46	17.73	280	1.94	103.3	86.1	31.1	903.6
	8C18	3.00	21.82	276	1.98	104.1	86.9	30.0	905.7
	9C26	2.71	27.35	335	2.00	103.3	85.9	40.2	921.6

a) comonomer content in polymer
b) melting peak temperature
c) cystallization peak temperature
d) enthalpy of fusion of perfectly crystalline PE was taken to be 290 J/g[137]

3.4.3.2 Microstructure of the copolymers

3.4.3.2.1 NMR study

The comonomer content was calculated with equation (3-6), the branching carbon signal, I(*), and all the resolved secondary carbon signals of the polymer backbone are used. It was corrected by substraction of the side-chain carbons, $n_{com.}$-7, which are included in the integration area of the main signal of the CH_2-chain, $I(\delta,\delta^+)$. In our measurements, we were able to resolve five backbone carbons and five side-chain carbons. The chemical shifts and nomenclature are taken in accordance with Pollard[VIII] from Randall.[111]

$$n_c = \frac{I(*)}{I(\alpha) + I(\beta) + I(\gamma) + [I(\delta,\delta^+) - (c_n - 7) \cdot I(*)]} \cdot 1000 \cdot 0.2 \quad [\text{mol - \%}] \qquad (3\text{-}6)$$

where $I(\alpha)$ is the integrated peak area of carbon α etc. and c_n is the number of carbons of the comonomer.

The molar fraction of the incorporated comonomer into the polymer chain is rather similar for all polymers within one series. Although the difference in the weight fraction (calculated by equation (3-2)) between the various comonomers is very pronounced; both are given in Table 3-5. The longer comonomers have a much higher contribution on the polymer's weight.

3.4.3.2.2 DSC analysis

All the copolymers show rather similar melting behavior (see Table 3-5); the melting and crystallization temperatures are almost the same. For the ethene / 1-hexacocene copolymers (5C26, 9C26) a 2nd melting peak at T_m = 53 °C appeared, which is very pronounced in case of higher comonomer content. In Figure 3-16 melting curves of these two polymers and the melting curve of 1-hexacosene are shown, the 2nd melting peak of the copolymers is originated by the comonomer 1-hexacosene. The pure 1-hexacosene shows two melting peaks, one at 37.3 °C and one at 52.6 °C. The zoomed area in Figure 3-16 makes visible that also for the polymer containing a low amount of 1-hexacosene a 2nd melting peak occurs. In order to be sure that no impurities like not incorporated comonomer caused this, the polymer was recrystallized several times, and the intensity of the 2nd peak did not change. The side-chains crystallize mainly between themselves. The intensity of the side-chain melting peaks is depending on the molar fraction of comonomer. From that we believe that the side-chains are crystallizing in kinds of agglomerates and not separated parallel to the polymer main-chain.

Walter et al. found for ethene/eicosene copolymers similar melting behavior.[138] The melting temperature decreased with increasing incorporation of 1-eicosene (0-50 mol-%) and side-chain crystallization occurred at 1-eicosene content over 39 mol-%. With 1-hexacosene very much less comonomer is necessary to see this effect.

In general the crystallinity of a LLDPE is decreasing with higher comonomer content and this is also the case with the copolymers of these series containing octene, dodecene and octadecene. Interestingly, the 1-hexacosene copolymers again are different and the crystallinity is increased for polymer 9C26.

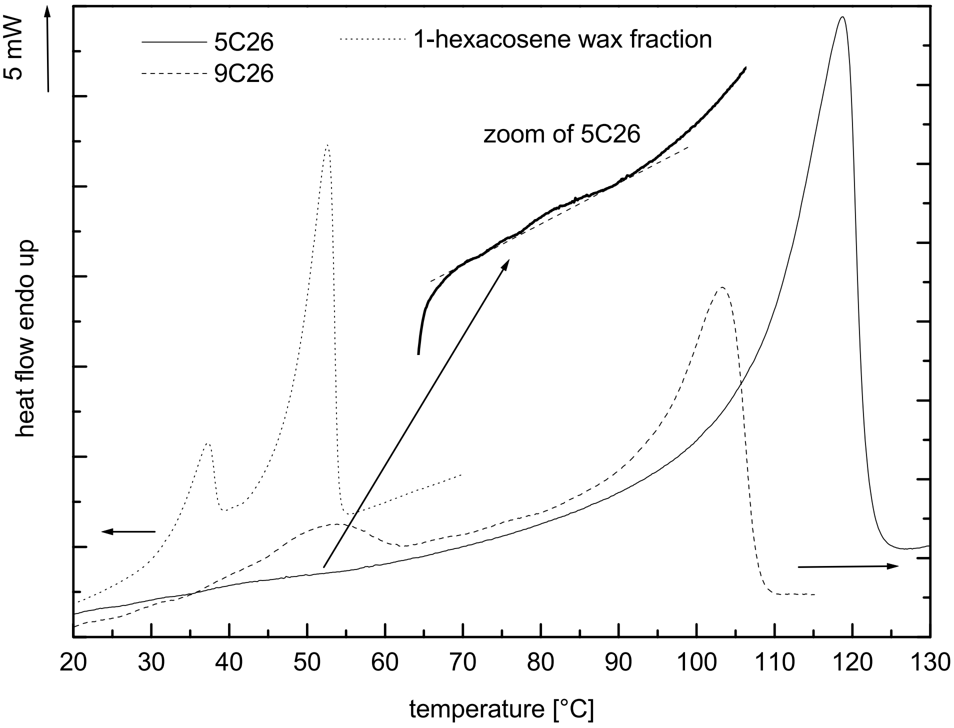

Figure 3-16: Melting curves of virgin 5C26, 9C26 and 1-hexacosene.

The thermal fractionation technique SSA was applied on all the samples to get information on the comonomer distribution. The most important parameters in using the SSA method are the first T_s temperature to be used, the temperature interval between T_s temperatures, the permanence time at T_s and the heating rates during the thermal conditioning steps.[139] A spacing of 3 °C instead of 6 °C had probably given a slightly better separation and more peaks, but increases in the measuring time were enormous. An increase in holding time does not promote higher number of signals, but more perfect crystals are expected at higher time consumption.[122,140] The melting curves obtained after the SSA treatment of the LLDPEs are plotted in Figure 3-17. As for the untreated samples the melting peaks of series 1 are again higher than those of series 2. The shapes of the curves are similar within each series, but the two copolymers 8C18 and 9C26 exhibit an additional smaller peak in the high temperature region. These peaks are most probably species corresponding to the fractions with the thickest lamellae within the distribution produced by the SSA treatment. Although, as described further on, it is found that the average lamellar thickness of 9C26 is lower than for others.

Theoretical equations are employed to quantitatively compare particular results with theory for the crystallization and melting of random copolymers. These theoretical equations are derived from an equilibrium theory. Therefore, predictions derived from the equations represent a limit typically not approached by real random copolymers.

To get quantitative information out of the SSA measurements the curves have to be analyzed by peak picking, calculating a relative index (DI[141]) for each peak and / or integrating each peak. We substracted from every DSC thermogram a baseline (from x=40 to x=130 °C), calculated the peak areas and divided them by the highest peak to get a relative value for comparison and further calculations.

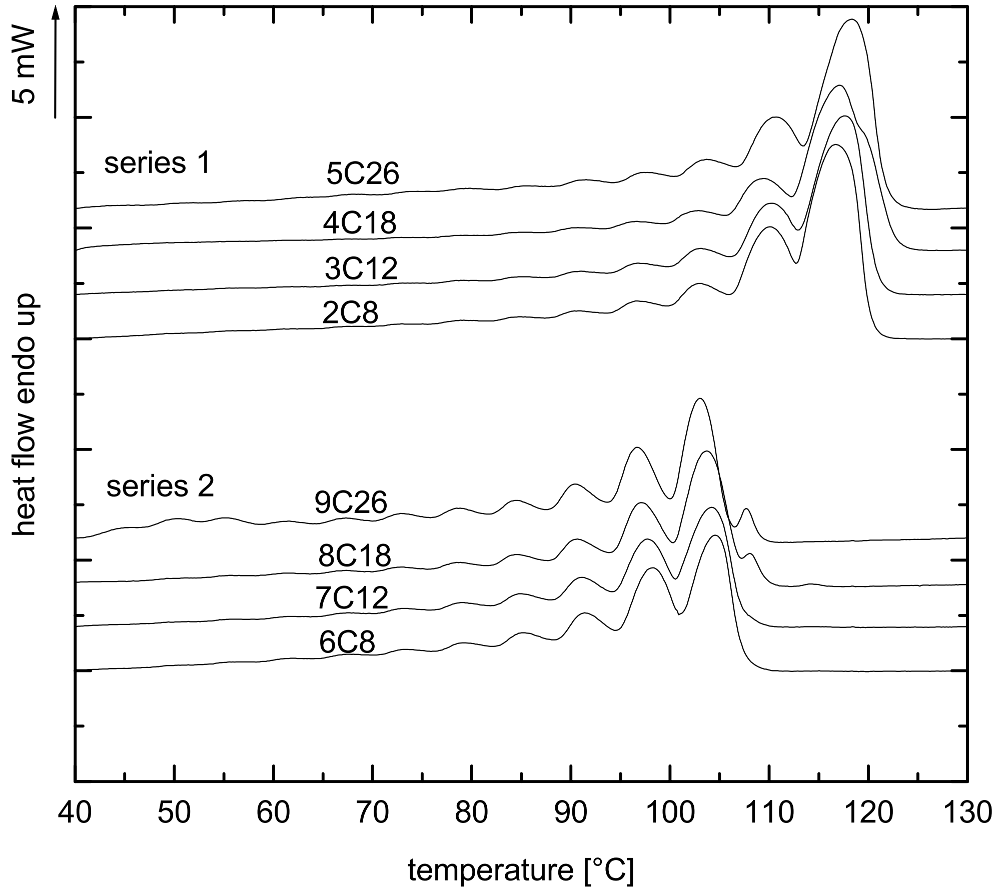

Figure 3-17: Melting curves of LLDPEs after SSA treatment.

The lamellar thickness, L_c, of the crystals can be estimated using the Gibbs-Thomson equation (3-7) from a melting temperature T_m. This equation is useful as a rough guide for estimating L_c. The returned values of L_c are too small for any temperature $T_m(L_c)$, other than the final melting temperature of crystals, T_m^f, formed in the isothermal crystallization.[142] Also the Flory equation (3-8) is only applicable to equilibrium melting of copolymers, which requires infinitely thick crystals of composition X_e to observe the copolymer melting temperature T_m^c. Because the very thick copolymer crystals do not exist, T_m^c is unobservable. This is in contradistinction to the equilibrium melting temperature T_m^0 for homopolymers (X_e=1); that temperature may be approached from homopolymers, for which essentially infinitely thick crystals do exist.[142,143]

$$T_m = T_m^c \cdot \left(1 - \frac{2\sigma_e}{\Delta H_u L_c}\right) \qquad (3\text{-}7)$$

In (3-7) $\sigma_e = 0.09$ J/m^2 is the basal surface free energy, $\Delta H_u = 2.96 \cdot 10^8$ J/m^3 is the volumetric heat of fusion, $T_m^0 = 418.7$ K is the equilibrium melting temperature of PE, R = 8.314 Pa·m^3·K^{-1}·mol^{-1}, and T_m^c of a copolymer with X_e is obtained from the following equation:

$$\frac{1}{T_m^c} = \frac{1}{T_m^0} - \frac{R}{\Delta H_u} \ln X_e \qquad (3\text{-}8)$$

The ethylene sequence length (ESL) can be calculated from each lamellar thickness, if it is assumed that an ethylene unit is 0.254 nm long.[142] Flory's theory of melting can also be used for calculating the number of consecutive carbons in the crystalline area and from that the lamellar thickness. A comparison of the different calculations is given by Zhang et al.[144] Alternatively, and used in this study, ESL or methylene sequence length (MSL) for each fraction can be obtained with Keating's method (compare to the chapter 3.2.2.4).[112] In the case of random ethylene copolymers, the melting point depression is not caused by molar mass variations but by MSL variation. They recrystallized the commercially available hydrocarbons with the same program and measured the subsequent melting point. The plot of ln(CH_2 molar fraction) against 1/T shows a linear relationship (equation (3-9)), and from this curve, the MSL of fractionated ethene copolymers can be assigned from the melting temperatures of the fractions.

$$-\ln(CH_2 molarfraction) = -0.331 + 135.5 / T_m \qquad (3\text{-}9)$$

The statistical terms arithmetic mean $\overline{L}_n$, weighted mean $\overline{L}_w$ and the broadness index were also introduced by Keating et al.[112] to describe the polydispersity of MSL in ethene copolymers.

$$\overline{L}_n = \frac{n_1 L_1 + n_2 L_2 + \ldots + n_i L_i}{n_1 + n_2 + \ldots + n_i} = \sum f_i L_i$$
$$\overline{L}_w = \frac{n_1 L_1^2 + n_2 L_2^2 + \ldots + n_i L_i^2}{n_1 L_1 + n_2 L_2 + \ldots + n_i L_i} = \frac{\sum f_i L_i^2}{\sum f_i L_i} \qquad (3\text{-}10)$$
$$I = \frac{\overline{L}_w}{\overline{L}_n}$$

where n_i is the normalized peak area, and L_i is the MSL, ESL or lamellar thickness for each fraction.

From the ethylene molar fraction the methylene sequence length and degree of branching can be easily calculated using equation (3-11) and (3-12)[145] or, with the data from NMR measurements, it can be used vice versa.

$$MSL = \frac{2 \cdot X}{1 - X} \qquad (3\text{-}11)$$

where MSL is the methylene sequence length (number of carbons) and X is the CH_2 molar fraction.

$$C = \frac{1000}{MSL + i + 1} \qquad (3\text{-}12)$$

where C is SCB/1000TC and i is number carbons in side-chain (e.g. octene: i = 6).

To differ between the different branching calculations it is named SCB/1000C as short-chain branches per 1000 backbone carbons, and SCB/1000TC as short-chain branches per 1000 carbons of the polymer in total. The calculated C is the number of branches per 1000 carbons in total of the polymer (SCB/1000TC), the branching per 1000 carbons backbone (SCB/1000C), like it was calculated from NMR data (equation (3-6)), can be obtained using equation (3-12) and i = 0.

The lamellar thickness of each fraction of each LLDPE was calculated by equation (3-7) and the number average of theses values (equation (3-10)) are given in Table 3-6. The molar fractions of the comonomer, the methylene sequence length and the degree of branching are calculated from NMR and DSC data and are also given in Table 3-6. From the NMR data the branching per 1000 carbons in total can be achieved by equation (3-13).

$$SCB/1000TC = \frac{I(*)}{I(\alpha)+I(\beta)+I(\gamma)+I(\delta,\delta^{+})+I(1)+I(2)+I(3)+I(4)}\cdot 1000 \qquad (3\text{-}13)$$

Table 3-6: Branching information by NMR and DSC-SSA.

	#	NMR n_c [mol-%]	SCB/ 1000TC[a]	SCB/ 1000C[b]	MSL[c]	DSC n_c [mol-%][d]	SCB/ 1000TC[e]	SCB/ 1000C[f]	MSL[g]	L_c[h]
series 1	2C8	1.57	7.6	7.9	120	1.78	12.5	11.5	86	7.01
	3C12	1.44	6.7	7.2	128	1.66	11.3	10.8	92	7.30
	4C18	1.32	6.0	6.6	134	1.66	10.2	10.8	92	7.36
	5C26	1.21	5.3	6.1	140	1.47	9.8	10.9	91	7.25
series 2	6C8	3.25	15.2	16.2	55	2.85	17.6	18.2	54	5.06
	7C12	3.46	14.8	17.3	47	2.85	16.6	18.5	53	5.01
	8C18	3.00	12.3	15.0	50	2.78	15.3	18.2	54	5.09
	9C26	2.71	10.2	13.6	49	2.85	14.1	19.2	51	4.83

[a] Number average SCB per 1000 carbons in total, equation (3-13)
[b] number average SCB per 1000 backbone carbons, SCB/1000C = equation (3-6) / 0.2
[c] number average MSL from NMR using equation (3-11) and (3-10)
[d] equation (3-9) from virgin melting curve peak, comonomer molar fraction = 1 - CH_2 molar fraction
[e] number average SCB per 1000 carbons in total, equation (3-9), (3-11), (3-12), (3-10)
[f] number average SCB per 1000 backbone carbons, equation (3-9), (3-11), (3-12), (3-10); i=0
[g] number average MSL from DSC using equation (3-9), (3-11) and (3-10)
[h] number average lamellar thickness, equation (3-7) and (3-10), [nm]

Differential scanning calorimetry is a powerful and fast tool to determine comonomer content in LLDPEs, if the right calibration is available. Comparing the two different methods there are only slight differences in the calculated molar fraction of comonomer. If an integration of the DSC curves is used in calculation, a correction becomes necessary. The calculated values for the branching and for the methylene sequence length, presented in Table 3-6, differ from the NMR data, particular for series 1 with low comonomer incorporation. The DSC heat flow depends on the amount of material melted at a certain temperature. The specific heat capacity also depends on temperature, and this represents another problem that should be taken into account. The peak area at lower temperatures is less intensive than at higher temperature and therefore the number average values are, depending on the calculations, too high SCB/1000TC or SCB/1000C and too low MSL. A way to correct this was described recently in a review article by Müller et al.[113] Here we forego to do these corrections because the relative differences within and between these two series would not change and this is the main focus of our work.

The average lamellar thicknesses of the LLDPEs are thicker if the copolymers are containing less comonomer. For material 9C26 a lower average lamellar thickness was calculated than for the other materials in series 2. Here comes into account that the side-chains show also a melting peak at lower temperature. This increased the peak area in the SSA curves with lower lamellar thicknesses and thereby lowers the average value.

Figure 3-18 shows the relationships of short-chain branching and MSL to lamellar thickness. The comonomer chain length has for both series no influence on the MSL; the MSL is just influenced by the lamellar thickness and vice versa. On the other hand the degree of branching is strongly influenced by the comonomer type. Longer side-chains lead to lower branching per 1000 carbons in total and thereby influence different the lamellar thickness. This is most pronounced for high branching (low lamellar thickness) and higher comonomer incorporation.

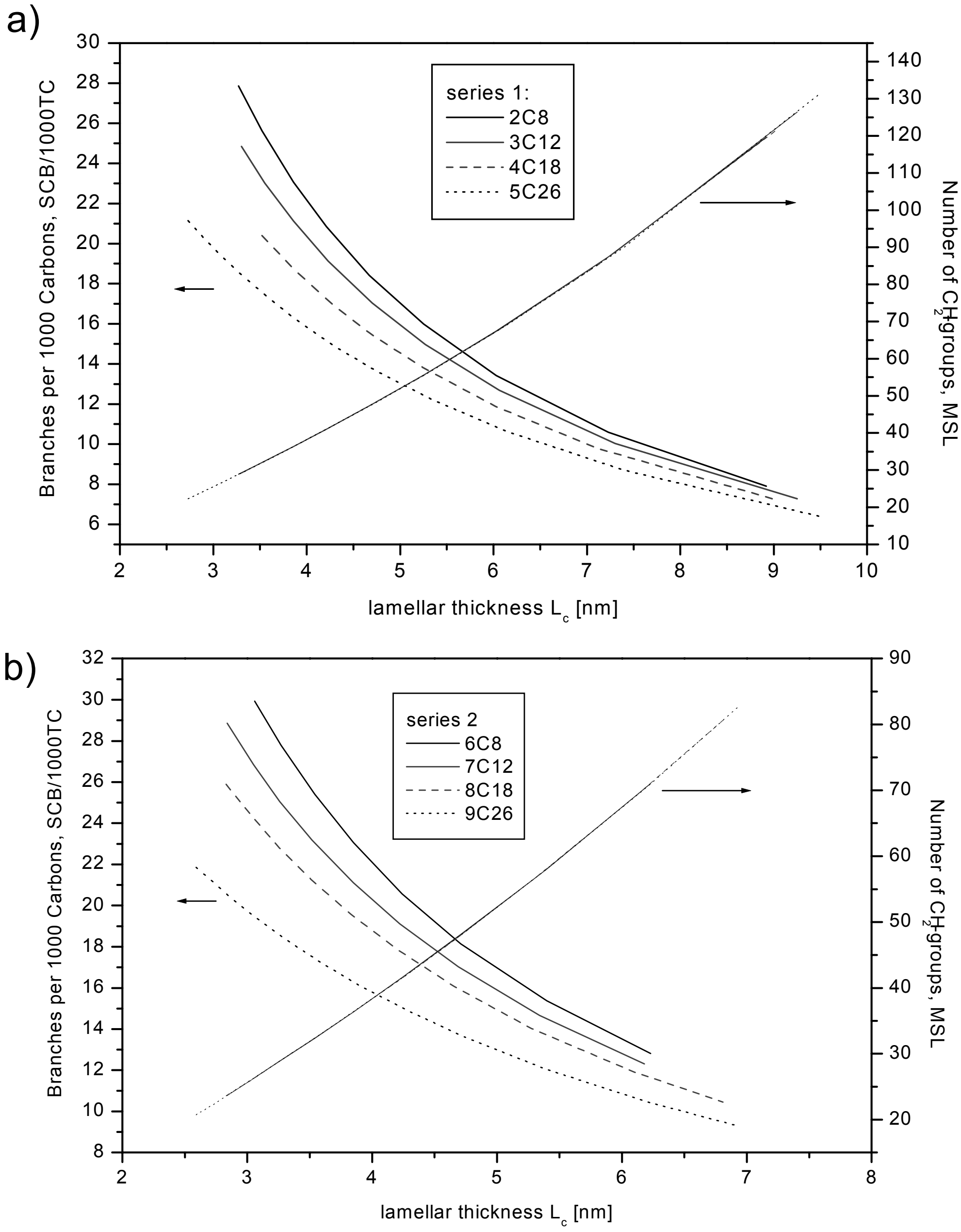

Figure 3-18: Relationships of short-chain branching (SCB/1000TC) and methylene sequence length (MSL) to lamellar thickness for the ethylene copolymers (determined by DSC); a) series 1, b) series 2.

3.4.3.2.3 Mechanical properties

3.4.3.2.3.1 Dynamic mechanical analysis

The results of the mechanical tests on both LLDPE series and the homopolymer, PE, are summarized in Table 3-7. The storage modulus of the copolymers of series 1 is generally higher than for corresponding copolymers of series 2. As expected, lower density leads to lower moduli values. The higher the comonomer content is in the copolymers, the more amorphous (less stiff) the material is in the case of the octene, dodecene and octadecene copolymers. In each series octene and dodecene copolymers have rather similar properties. Poly(ethene-co-octadecene) at high enough comonomer incorporation shows a deviating behavior in the temperature range from -30 to +30 °C (series 2). The hexacosene copolymers, however, exhibit in both series a very different behavior compared to the other copolymers. Especially in the range from -30 to +60 °C the hexacosene copolymers are much stiffer. This is due to the crystalline side-chains ($C_{24}H_{49}$), which toughen the material. When the crystalline side-chain agglomerations are starting to melt (at about 20 °C) the storage modulus curves are coming closer to the others again. At a temperature of about 60 °C all side-chains are molten and the material behaves like the other copolymers (see Figure 3-19).

Table 3-7: Material properties of DMA and tensile tests.

		DMA		stress-strain behavior				
	#	stor. mod.[a]	T_g[b]	Young's modulus	yield stress	tensile strain at yield	break stress	break strain
		[MPa]	[°C]	[MPa]	[MPa]	[%]	[MPa]	[%]
ref.	1PE	494	n.d.[c]	318 ± 2	20.3 ± 0.1	23	36 ± 2	1023 ± 44
series 1	2C8	108	-32.0	86 ± 3	n.d.	n.d.	24 ± 3	819 ± 74
	3C12	115	-35.2	89 ± 2	n.d.	n.d.	24 ± 2	828 ± 49
	4C18	83	-28.3	97 ± 2	n.d.	n.d.	30 ± 3	1025 ± 145
	5C26	177	-15.5	132 ± 4	10.4 ± 0.2	26	26 ± 3	725 ± 58
series 2	6C8	46	-37.7	30 ± 2	n.d.	n.d.	n.d.	n.d.
	7C12	43	-37.5	31 ± 1	n.d.	n.d.	n.d.	n.d.
	8C18	65	-25.5	47 ± 2	n.d.	n.d.	n.d.	n.d.
	9C26	152	-27.2	152 ± 3	11.8 ± 0.2	20	26 ± 1	674 ± 27

a) storage modulus at 25 °C

b) maximum, taken from loss modulus curve

c) not detected

In series 2, the octadecene copolymer 8C18 shows within a certain area (from -30 to +45 °C) also a deviation from the shorter chained LLDPEs. The greater stiffness is in this case also most probably a result from crystalline side-chains and thereby the material is less amorphous and stiffer at these temperatures.

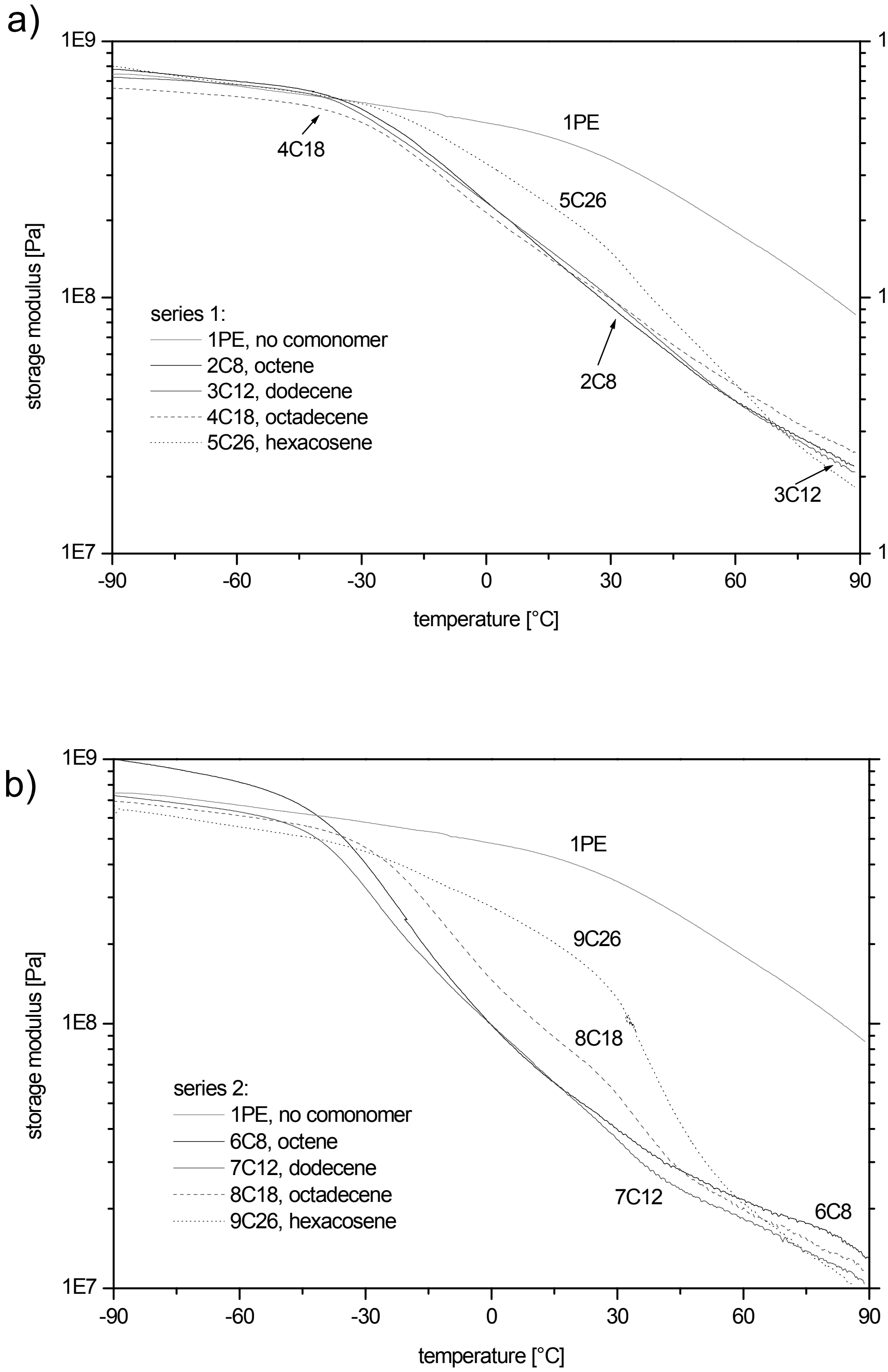

Figure 3-19: Storage modulus curves of the LLDPE a) series 1 and b) series 2 and the reference PE.

The glass transition temperatures (T_g), determined from the peak maximum of the loss modulus curves are given in Table 3-7. The T_gs of polyethene-co-octene and polyethene-co-dodecene are in both series rather similar, but for the octadecene copolymers they are much higher. In series 2 the β-transition regions are much more pronounced due to their higher comonomer content. The fact that the 1-octadecene copolymer 8C18 (series 2) has a higher transition temperature than copolymer 4C18 (series 1) has been explained by a possible lateral crystallization of the relatively long branches of 1-octadiene.[126] The T_g of the hexacosene-copolymer 5C26 (series 1) is rather high, -15.5 °C, and the transition rather weak, this is in accordance with its higher crystallinity and density values compared to the other copolymers of this series. At a higher hexacosene incorporation (series 2), T_g decreased to a temperature close to the T_g of the corresponding ethene/octadecene copolymer 8C18. As in the storage modulus, we notice temperature dependence of the loss modulus (see Figure 3-20). When all crystalline side-chains are molten the copolymer 9C26 behaves like the other copolymers. Again, after these conclusions, the same trend comes clear for the ethene/octadecene copolymer 8C18. Obviously the side-chains are long enough and concentrated enough to affect the material properties different from conventional LLDPEs.

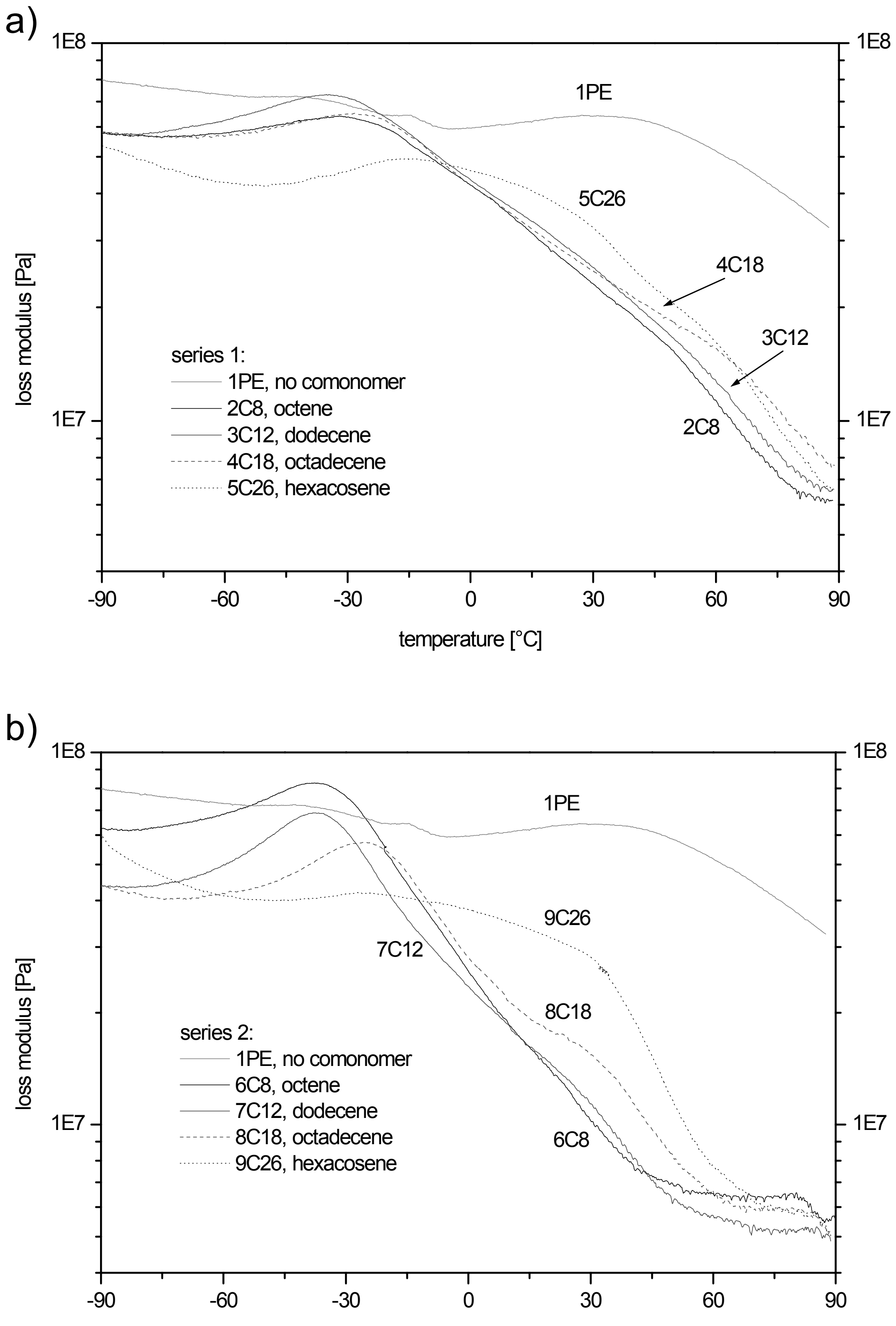

Figure 3-20: Loss modulus curves of the LLDPE a) series 1 and b) series 2 and the reference PE.

Clas et al.[129] observed also by DMA a deviating behavior between homogeneous ethene/butene, ethene/octene and ethene/octadecene copolymers, synthesized with vanadium catalysts: The intensity of the β-transition increases with comonomer content in 1-butene and 1-octene copolymers and also with the amount of interfacial material present. In ethene/1-octadecene copolymers this intensity is comparatively low, even though there is about 20% interfacial material present. In another more recent study by Starck et al.[124] on metallocene catalyzed ethene - α-olefin copolymers it was shown that for 1-octadecene copolymers the intensity of the β-transition in the loss modulus curves did not increase with increasing branching in contrast to the situation for 1-octene and 1-tetradecene copolymers. The DMA measurements confirmed the decrease in crystallinity at increasing comonomer incorporation; the deviations from the stiffness curve of conventional HDPE were greatest for the copolymers containing larger amounts of 1-tetradecene or 1-octadecene as comonomer. There were deviations from these trends observed for some 1-octadecene copolymers and this was assumed to be due to crystallization of $C_{16}H_{33}$ branches.[124]

In this study the loss tangent (tan δ) plots (see Figure 3-21) of the copolymers showed that the α-transitions for the polymers of series 1 appear at higher temperatures than for those of series 2. This is in accordance with studies by Benavente et al.[126] on ethene/1-octadecene copolymers, which showed that the temperature of the α-transition decreases with the increase in comonomer content due to the reduction in crystal size. The α-transition of the homopolymer, 1PE, did not display a clear maximum, which is a consequence of larger size crystals present in this polymer. Figure 3-21 shows a very pronounced α-transition region for the hexacosene copolymer 9C26, which is in accordance with its high crystallinity. The near total absence of a β-transition peak of 9C26 and 5C26, respectively, is a further indication of the presence of crystallizing side-chains in the ethylene-hexacosene copolymers.

In previous work[146] on ethene/octadecene copolymers the use of Cross Polarization Magic Angle Spinning (CPMAS) ^{13}C NMR, Raman spectroscopy and x-ray diffraction indicated that side branches of 1-octadecene participates in the crystalline structure. However, Benavente et al.[126] claim that it is not quite clear if the side branches of 1-octadecene really can participate in the crystalline structure of these copolymers of low comonomer contents, although such possibility exists for copolymers of very high comonomer content. Anyway, according to our studies the long $C_{24}H_{49}$ branches of the ethene/hexacosene copolymers crystallize more easily than the shorter $C_{16}H_{33}$ branches of the ethene/octadecene copolymers.

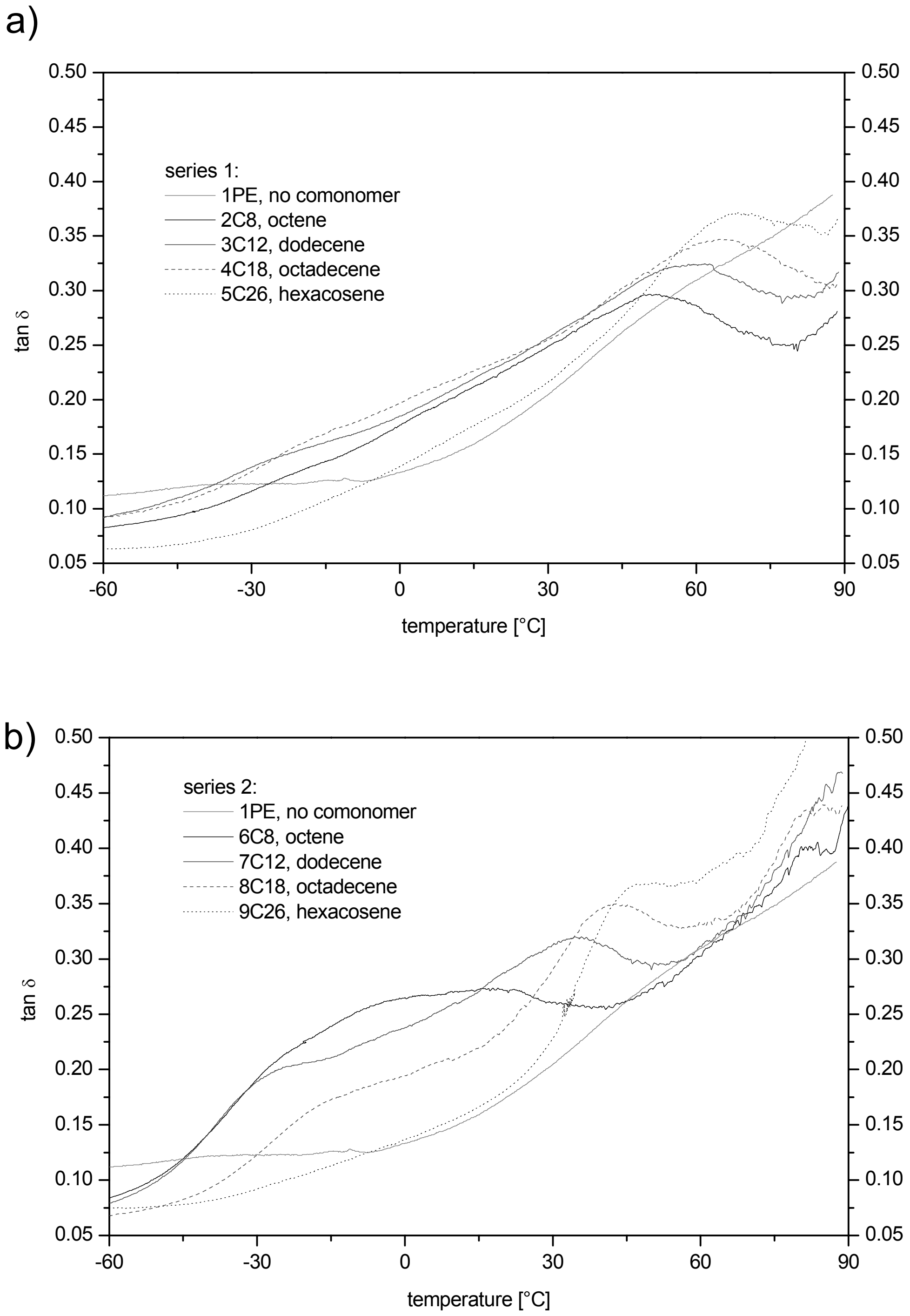

Figure 3-21: Loss tangent curve of the LLDPE a) series 1 and b) series 2 and the reference PE.

3.4.3.2.3.2 Tensile tests

The Young’s modulus and yield points of all polymers are listed in Table 3-7. The Young’s modulus is the highest for pure PE and it is decreasing with increasing comonomer content meaning increasing elasticity. Many of these copolymers do not have a yield point, they show an elastic behavior. The two octadecene copolymers 4C18 and 8C18 are slightly stiffer than the corresponding octene and dodecene copolymers in both series. The hexacosene copolymers behave completely different: They show yield points, which is more pronounced for the one with higher number of side-chains. That means that the material’s stiffness is increasing with increasing comonomer content, which is the complete opposite of the so far known for LLDPEs. Among all copolymers, 9C26 is the stiffest material, although it has about 3 mol-% of comonomer incorporated. This is due to more crystalline areas in the polymer. In Figure 3-22 the stress-strain experiments of the LLDPEs and the reference polyethylene are plotted. Break stress and break strain are also presented in Table 3-7. The same trends as described earlier become visible here. The LLDPEs with higher olefin concentrations are so elastic that the test bars did not break unless a deformation of the whole specimen took place. The material 9C26 is not that elastic, it breaks at lower stress than the corresponding 5C26. The standard deviation of these break points is rather high, although at least five different samples were measured. This is due to the forming technique of the specimens. In this study the test bars are compression molded and not extruded and injection molded. There are slight differences in structure and form of the specimens of each polymer sample. They are not affecting the Young’s modulus or yield points but cause a higher variation of data at higher strains.

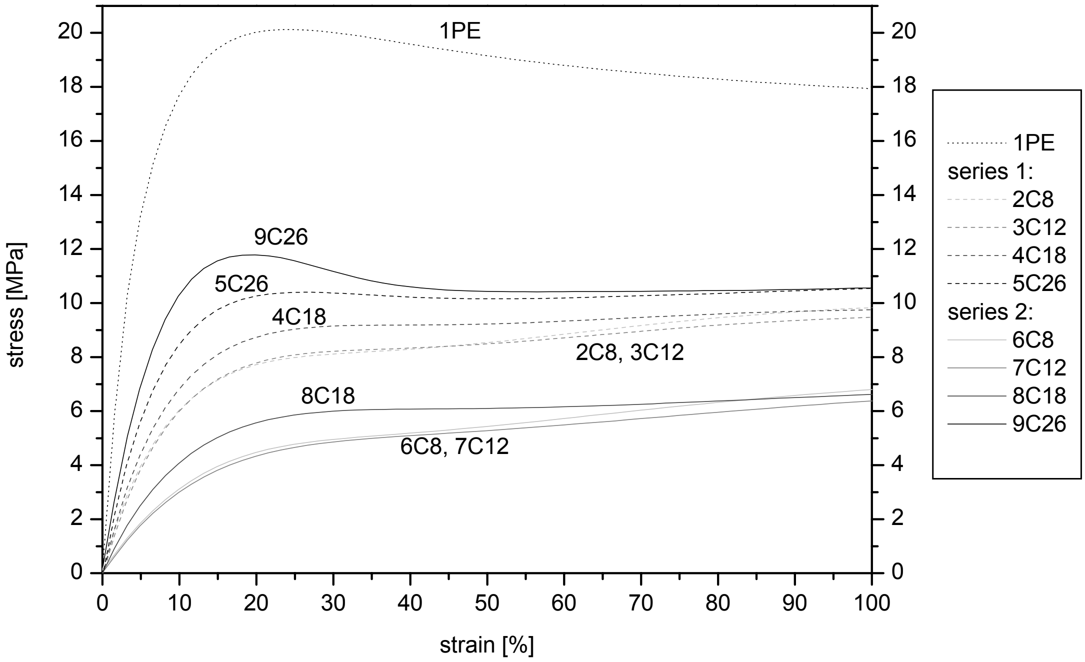

Figure 3-22: Tensile testing curves of the LLDPE series 1 and 2 and the reference PE.

3.5 Conclusion

The catalyst F provides a very good comonomer and hydrogen response and has high activities for ethene homo- and copolymerizations. It is possible to incorporate any α-olefin into the growing chain up to high degrees. The catalyst is also thermostabile and active over a long reaction period.

In this study new ethene copolymers were synthesized. The influence of the comonomer on the polymerization activity is strong. At about 10 mol-% comonomer in feed a maximum of activity can be reached. The molar masses and the thermal behavior of the materials is influenced by the amount of comonomer in feed and polymer but not by the type of comonomer. There are no or only very slight differences between 8 carbons (1-octene) and 26 carbons (1-hexacosene). The copolymers of ethene and hexacosene are new materials and not synthesized before.

For the homopolymer, a maximum degree of long-chain branching of 0.37 and 0.30 LCB/molecule was determined by melt-state NMR and SEC-MALLS, respectively. Good agreement is seen considering the small contents quantified, both being at the lower limit of detection for the techniques, and the simplifying assumptions of the Zimm-Stockmayer-theory. For the copolymers, smaller LCB contents were found with SEC-MALLS. The resolution of this classical method is not high enough for a clear discrimination of the influence of the various comonomers on the LCB-content. Therefore, rheology was used to further distinguish between the LCB-content as some rheological quantities have been proven to react very sensitively on the existence of long-chain branches. Lower degrees of LCB were detected in the copolymers than were found in the homopolymer. Higher comonomer content and comonomers of greater length were also found to result in lower degrees of LCB in qualitative agreement with the SEC-MALLS measurements. Due to the high sensitivity of rheological methods with respect to LCB a clearer discrimination could be gained from the results.

The results of the SEC-MALLS and more pronounced the rheological characterization indicate for this series of copolymers that the catalyst F produces linear and long-chain branched samples depending on the comonomer content. The ethene homopolymer showed the highest long-chain branch content. Any addition of comonomer decreased the degree of long-chain branching. For the samples with the highest comonomer content no long-chain branches were detected, neither by SEC-MALLS nor by rheology. This effect depends on both the molar mass (length) and the content of the comonomer. The LCB-content decreases with growing number of incorporated comonomers per chain and with their increase in length. For the samples with the lowest comonomer content only a very small difference to the homopolymer was found. Similar results are reported by Kokko et al.[68] and Walter et al.[138], but in these articles only one comonomer was used. The dependency of the long-chain branch incorporation (and thus of the rheological properties) on the comonomer feed was also investigated for different catalyst systems by the groups of Mülhaupt[138] and Seppälä[64,68,74,75]. The long-chain branch incorporation ceases at much higher comonomer contents than shown in this study. These differences can be related to the use of hydrogen for molar mass control and the different catalyst system in this study.

While a clear difference in LCB content was observed between the polymers copolymerized with octene and octadecene, the difference between those with hexacosene and octadecene is small. These findings can be understood when looking at the chemical mechanism of the long-chain branch incorporation. A short-chain branch of longer length provides more steric hindrance concerning the incorporation of a vinyl-terminated macromonomer into the growing chain than that of a smaller length. The effectiveness of octadecene and hexacosene seem to be above a steric threshold, where the hindrance is so strong that macromers are not attached to the backbone anymore. These conclusions could only be attained by using hexacosene as comonomer, which has not been investigated in literature before for the metallocene catalyzed synthesis of polyethylenes.

The hexacosene copolymers have side-chains of 24 carbons and they show remarkable material properties, very different from conventional LLDPEs. The side-chains of the hexacosene copolymers crystallize with each other and not only parallel to the backbone lamellar layer. This can be seen as an extra melting peak in the DSC melting endotherm, whose intensity is depending on the hexacosene concentration in the polymer. Even at low amounts of comonomer a shoulder in the melting curve is visible. These crystallizing side-chains increase strongly the materials stiffness, density and change completely the mechanical properties compared to the other LLDPEs. When the material is heated up to a temperature, where the side-chains are molten, the material behaves like the ethene/octene, ethene/dodecene or ethene/octadecene copolymers. Due to these comparisons it was also possible to explain the behavior of ethene/octadecene copolymers with higher comonomer incorporations. Some of the tendencies, which are very pronounced in case of 24 carbons side-chains, appear already at 16 carbons side-chains to a lower extent.

4. Single-site and dual-site ethene/propene copolymerizations

4.1 Introduction and materials

A promising way to understand and by that to tailor the microstructure and molar mass distribution of polyolefins is the use of mixed metallocene systems, since mixtures of well-defined single-site catalysts are good model systems. Over the last years, the number of publications on binary, dual-site or mixed catalysts for the production of polyethylene[147-158], polypropylene[159-161] and ethene/α-olefin copolymers[83,147-151,162-165] has therefore grown tremendously. To create a better understanding of dual-site catalysis with the help of single-site results, three series of ethylene-propylene copolymers were produced using the catalyst precursors 1) rac-[$Me_2Si(2\text{-}Me\text{-}4\text{-}(1\text{-}Naph)Ind)_2]ZrCl_2$, 2) [$Me_2Si(Ind)(Flu)]ZrCl_2$ and 3) a 1:5 mixture of 1 and 2, all with a broad range of (co)monomer mole fractions in the reactor and copolymers (Figure 4-1).[V] Catalyst 1 produces rather random ethylene-propylene copolymers[166] with a high affinity to incorporate propene whereas alternating copolymers with low amounts of propene are synthesized by catalyst 2[167]. The activities of the single-site series are used to calculate the contributions of the two catalysts in the dual-site experiments and ^{13}C NMR data is used for the modeling of the propene incorporation in the copolymers and the reactivity ratios of the three catalyst systems. Based on this modeling, the results of DSC and SEC measurements are interpretated. The direct peak method used here for modeling the copolymerizations is described by Karssenberg[168,XI] and a comparisson of different statistical models and their application on copolymerizations is also discussed by him.[XII] The experimental details of these copolymerization series are desribed in chapter 6, reator 2 was used and the analytics were measured on DSC 1, SEC 1 and NMR 1. The total monomer concentration and propene feed in the reactor are listed in Table 4-1.

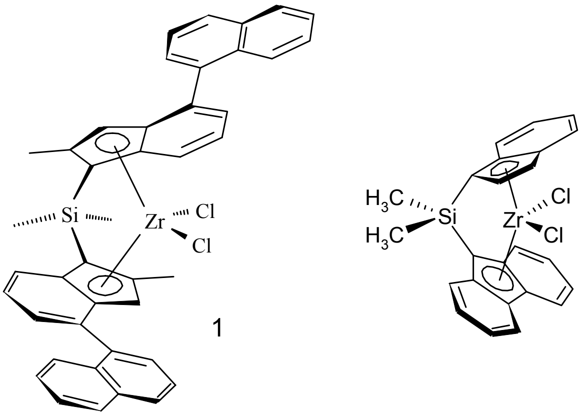

Figure 4-1: Catalyst precursors, 1: rac-$[Me_2Si(2\text{-}Me\text{-}4\text{-}(1\text{-}Naph)Ind)_2]ZrCl_2$
2: $[Me_2Si(Ind)(Flu)]ZrCl_2$.

Some of the published studies on ethene/α-olefin copolymers also investigate the possible interactions between two metallocenes, focusing on ligand exchange[162] as well as on chain transfer from site to site in solution[162-164] or on supported systems[165]. In this study though, ligand exchange is excluded because of the use of bridged metallocenes. Also the phenomenon of chain transfer is debarred, as the catalyst concentrations were kept very low to minimize the probability to incorporate a vinyl-terminated polymer-chain. For this reason we assume that each chain is build up by only one unchanging site. As will be shown, the molar mass distributions of the copolymers do not indicate otherwise.

The catalyst, the polymerization conditions, and the polymerization reactor operating condition are all significant for the comonomer incorporation. In a batch polymerization the concentrations of the (co)monomer decrease as the polymerization proceeds, but not to the same extent. In a semi-batch polymerization only the monomer concentration is constant. In the Continuous Stirred Tank Reactor (CSTR) system monomer and comonomer concentrations are both constant after the steady-state conditions are achieved. Here the semi-batch process was used as only ethene was fed during the reaction, therefore the polymerization time has an influence on the comonomer concentration and incorporation. The propene conversion was kept very low in order to achieve intermolecular homogeneous fractions for each polymer.

4.2 Results and discussion

4.2.1 Activities and contributions

The activities of all three series and the contribution of catalyst 2 to the bimodal polymers are listed in Table 4-1 and shown in Figure 4-2. For all copolymerizations catalyst 1 gives higher activities with a maximum for pure polyethylene of about 800 $t_{polymer}\cdot mol_{Zr}^{-1}\cdot h^{-1}\cdot mol_{monomer}^{-1}\cdot l$. Catalyst 2 is much less active for copolymerizations with high ethylene content, but for polypropylene and copolymers with high propylene content the activities are rather close to the ones of catalyst 1. Most of the activities of the dual-site series are in between the ones of the single-site experiments.

The contribution of catalyst 2 to the dual-site experiments is calculated from the single-site activities and the catalyst molar ratio of 1:5. Due to the non-parallel course of the activities of the two catalysts, the contribution of catalyst 2 is not only dependent on the catalysts molar ratio but also on the mole fraction of propene in feed. In the reactor feed range 0-60 mol-% the activity of catalyst 2 is more than 5 times lower then the activity of catalyst 1 and therefore the contribution of catalyst 2 to the dual-site experiments is smaller than 50%, vice versa in the reactor feed range 70-100 mol-%.

Table 4-1: Total monomer concentrations, propene reactor feed, activities of the catalysts and contribution of catalyst 2 to the dual-site polymers.

	catalyst 1		catalyst 2		dual-site series a)		
c_{tot} b)	C_3 feed c)	activity d)	C_3 feed c)	activity d)	C_3 feed c)	activity d)	contrib. e)
0.6	0	800	0	19	0	155	0.11
0.6	11	700	11	18	11	160	0.12
0.8	21	550	21	20	21	98	0.16
0.8	31	400	31	22	31	76	0.22
1.0	45	210	39	22	41	55	0.35
1.0	50	200	50	20	50	18	0.34
1.0	60	130	60	17	60	37	0.41
1.0	70	80	70	20	70	27	0.57
1.0	80	60	80	25	80	29	0.68
1.0	90	40	90	20	90	18	0.72
1.0	95	30	95	16	95	2	0.73
2.0	98	25	98	13	98	3	0.73
2.0	99	16	99	8	99	3	0.72
2.0	100	11	100	4	100	2	0.65

a) 1:5 mixture of catalyst 1 and 2

b) Total monomer concentration [$mol\cdot l^{-1}$]

c) Propene feed in the reactor [mol-%]

d) [$t_{polymer}\cdot mol_{Zr}^{-1}\cdot h^{-1}\cdot mol_{monomer}^{-1}\cdot l$]

e) Contribution of catalyst 2 to the bimodal polymers = $5 \cdot activity_{cat.2} / (activity_{cat.1} + 5\cdot activity_{cat.2})$

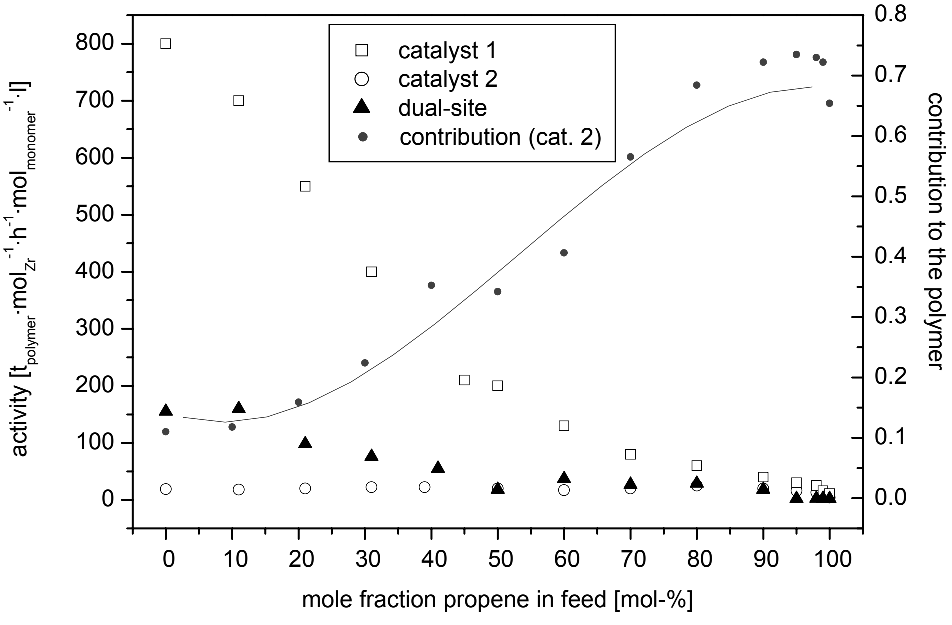

Figure 4-2: Catalyst activities and the contribution of catalyst 2 to the bimodal polymers, contribution line is added for guidance to the eye.

4.2.2 Modeling of NMR data and comonomer incorporation

The Direct Peak Method (DPM)[168] enables the modeling of comonomer incorporation and reactivity ratios of single-site catalysts based on the ^{13}C NMR data of series of homogeneous ethylene-1-alkene copolymers. This DPM has been successfully applied to series of metallocene-catalyzed ethylene-propylene copolymers before[XI,XII] and is also used here to model the single-site experiments. As will be shown, the reactivity ratios of the single-site catalysts can be used to describe the propene incorporation of the copolymers in the dual-site series.

Table 4-2 presents reactor feed and propene incorporation for the two single-site series and the second order Markov reactivity ratios of the two catalysts. As mentioned before, the experimental feed was calculated from the (co)monomer pressures and the experimental propylene incorporation from the ^{13}C NMR data using the Randall method[111]. The experimental feed and the ^{13}C NMR spectra have been used as input of the DPM for the second order Markov modeling of the reactor feed, the propene incorporation and the reactivity ratios. The use of second order Markov is justified, since first order Markov statistics do not satisfy the 99.5% reliability condition.[XII] For each of the two single-site series, the total number of equations fitted in the model is equal to 108, $(8+1)\cdot 12$, namely 8 NMR regions and 1 feed for all 12 copolymers. The number of variables is 28: per copolymer 1 reactor feed and 1 scaling factor plus 4 reactivity ratios. The total number of degrees of freedom is $108-28=80$. With χ^2 values of 40.3 and 47.8 for catalyst 1 and 2 respectively, all results reflect a reliability > 99.8%.

The experimental and modeled results presented in Table 4-2 are depicted in Figure 4-3. At high propene concentrations in the reactor, the difference between the two catalysts is very pronounced: catalyst 1 easily incorporates comonomer units while for catalyst 2 it is hardly possible to insert more than about 50 mol-% of propene even at ethene/propene ratios in the feed of [P] = 99 mol-%. In a growing chain, the addition of new monomer and comonomer units is mainly determined by the reactivity ratios of the active site(s) of the catalyst. The reactivity ratios are calculated by rhij = khii / khij with h, i, j element of {E, P} and k the reaction rate constants and are described in detail in reference [168]. The square root of the product of the 4 reactivity ratios represents the classical '$r_E \cdot r_P$' value which reveals the character of the catalyst.[168] Here the values 2.02 and 0.03 demonstrate that catalyst 1 produces rather random and catalyst 2 alternating copolymers.

Table 4-2: Experimental and modeled propene feed and propene incorporation of the single-site series and reactivity ratios of the two catalysts.

catalyst 1				catalyst 2			
feed $C_3/(C_2+C_3)$ a)		C_3 incorporation b)		feed $C_3/(C_2+C_3)$ a)		C_3 incorporation b)	
exp	model	exp	model	exp	model	exp	model
0	0.0	0.0	0.0	0	0.0	0.0	0.0
11	10.7	0.4	2.1	11	9.3	1.2	1.4
21	17.8	3.6	4.0	21	22.2	3.9	3.8
31	24.9	5.2	6.2	31	30.9	5.9	5.9
45	44.0	15.7	15.1	39	40.8	9.3	8.7
50	53.8	23.2	22.3	50	55.3	14.8	14.4
60	65.5	34.9	34.7	60	61.3	17.7	17.5
70	74.2	46.8	48.1	70	67.1	21.0	21.0
80	85.1	68.6	69.5	80	77.8	28.8	29.1
90	91.1	81.3	82.5	90	87.9	38.6	39.2
95	95.5	90.0	91.6	95	94.5	46.8	47.4
98	97.9	95.0	96.4	98	96.5	49.7	50.4
99	98.8	95.7	98.3	99	96.3	50.0	50.8
100	100.0	100.0	100.0	100	100.0	100.0	100.0

catalyst 1		catalyst 2	
r_{EEP}	5.46 (± 6.2%)	r_{EEP}	7.23 (± 4.7%)
r_{EPE}	0.37 (± 5.4%)	r_{EPE}	0.006 (± 10.0%)
r_{PEP}	3.43 (± 6.1%)	r_{PEP}	3.29 (± 5.5%)
r_{PPE}	0.59 (± 4.2%)	r_{PPE}	0.007 (± 51.4%)
‘$r_E \cdot r_P$’ c)	2.02 (± 11.2 %)	‘$r_E \cdot r_P$’ c)	0.03 (± 37.2 %)
# equations	108	# equations	108
# variables	28	# variables	28
# d.o.f.	80	# d.o.f.	80
χ^2	40.3	χ^2	47.8
reliability	99.99 %	reliability	99.84 %

a) Mole fraction propene in reactor feed [mol-%]
b) Mole fraction propylene in copolymer [mol-%]
c) See text and ref. [168]; d.o.f. = degrees of freedom

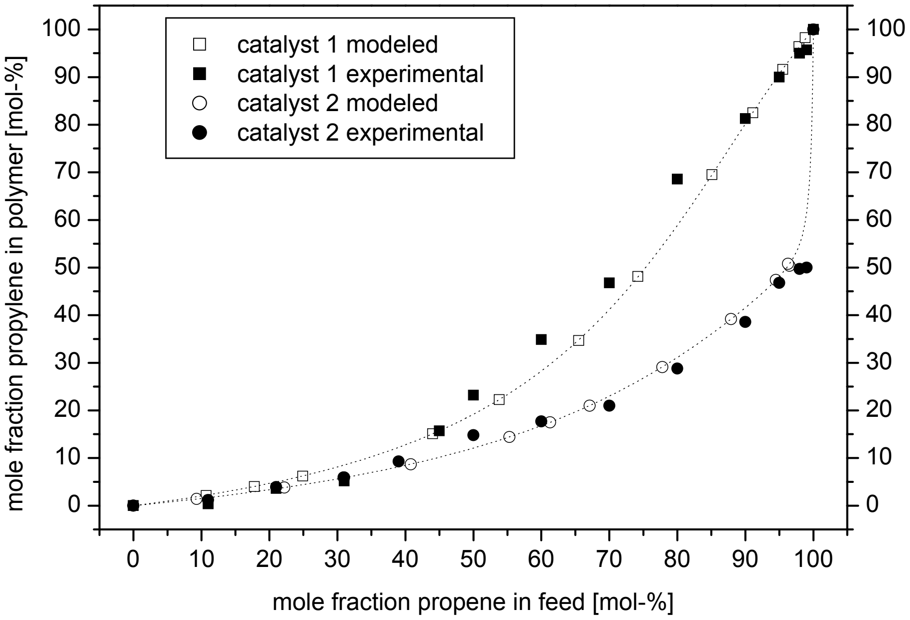

Figure 4-3: Experimental and modeled propene incorporation of the single-site series.

In the DPM for single-site copolymers, the reactivity ratios and reactor feeds determine the ^{13}C NMR spectra via propagation probabilities and diad fractions, and the theoretical spectra are multiplied by scaling factors to enable the comparison with experimental ones (see Figure 4-4a). The modeling of dual-site experiments now is rather straightforward since the copolymerization reaction at two sites is a combination of two single-site reactions. In the dual-site reactions described here, two catalysts operate independently and simultaneously, creating exactly the same copolymers as in single-site experiments. Therefore, the DPM, developed for the modeling of single-site catalysts, only needs minor changes to be able to also model dual-site catalysts. In the DPM for dual-site copolymers (Figure 4-4b), two ^{13}C NMR spectra are calculated based on two different sets of reactivity ratios, and these spectra both contribute to the overall spectrum.

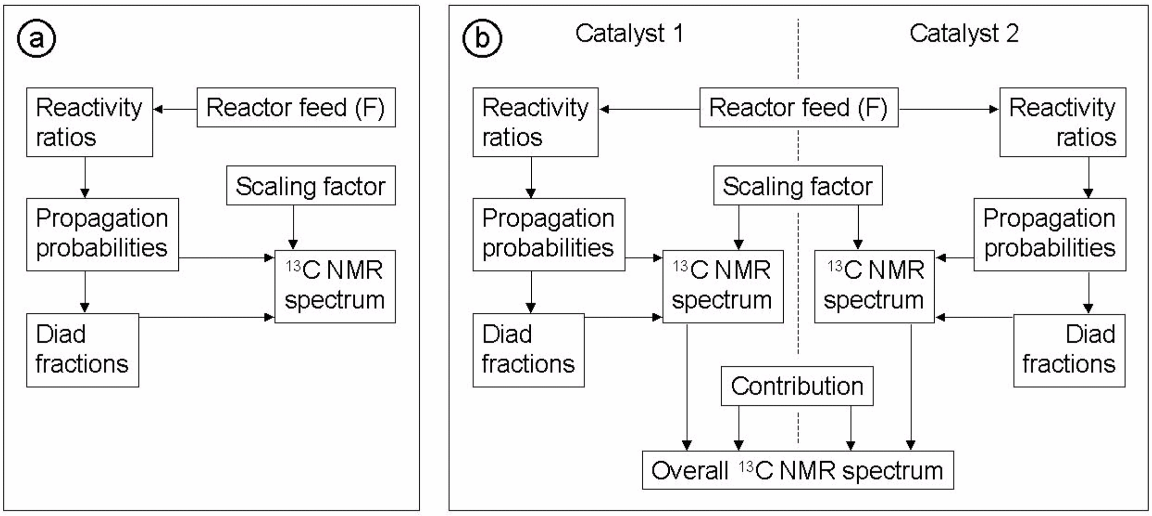

Figure 4-4: Schematics of the second order Markov Direct Peak Method for the modeling of (a) single-site and (b) dual-site copolymers.

An overview of the experimental and modeled reactor feed and propene incorporation of the dual-site experiments is shown in Table 4-3. Analogously to the single-site experiments, the experimental feed is calculated from the gas pressures, the experimental propene incorporation from the ^{13}C NMR data (Randall method). The modeled data in Table 4-3 are the results of the DPM for the modeling of dual-site copolymers using the contributions of the two catalysts (see Table 4-1) and the second order Markov reactivity ratios (see Table 4-2). The overall propylene content is calculated from the overall ^{13}C NMR spectrum, the propylene content splitted per catalyst is originating from the ^{13}C NMR spectra before applying the contributions. Note that for the catalyst 2 the modeled propylene contents at 98 and 99 mol-% propene exceed the experimental limitation of 50 mol-%.

The experimental and modeled results of the dual-site series presented in Table 4-3 are plotted in Figure 4-5 together with the second order Markov lines of the single-site series. This plot clearly shows the effect of the contribution to the dual-site results. For low propene feeds in the reactor, the contribution of catalyst 2 is low and therefore most of the copolymer chains are produced by catalyst 1, but with increasing propene feed the propylene contents of the dual-site copolymers move away from the second order Markov line of catalyst 1 towards the one of catalyst 2.

Table 4-3: Experimental and modeled propene feed and propene incorporation of the dual-site series.

feed $C_3/(C_2+C_3)$ a)		C_3 incorporation b)			
exp	model	exp	model overall	model per catalyst cat. 1	model cat. 2
0	0.0	0.0	0.0	0.0	0.0
11	9.0	0.7	1.8	1.8	1.3
21	18.6	3.0	4.1	4.3	3.1
31	29.6	7.3	7.5	8.0	5.5
41	39.9	11.6	11.5	12.7	8.4
50	48.1	14.9	15.4	17.8	11.3
60	61.9	24.8	24.5	30.4	17.8
70	73.4	33.8	34.9	46.6	25.5
80	83.7	46.0	46.7	66.5	34.7
90	89.6	52.5	53.7	83.0	38.8
95	95.5	65.3	62.6	94.8	50.5
98	98.4	72.5	69.7	97.2	56.8
99	99.4	79.9	77.6	99.0	67.6
100	100.0	100.0	100.0	100.0	100.0

a) Mole fraction propene in reactor feed [mol-%]

b) Mole fraction propylene in copolymer [mol-%]

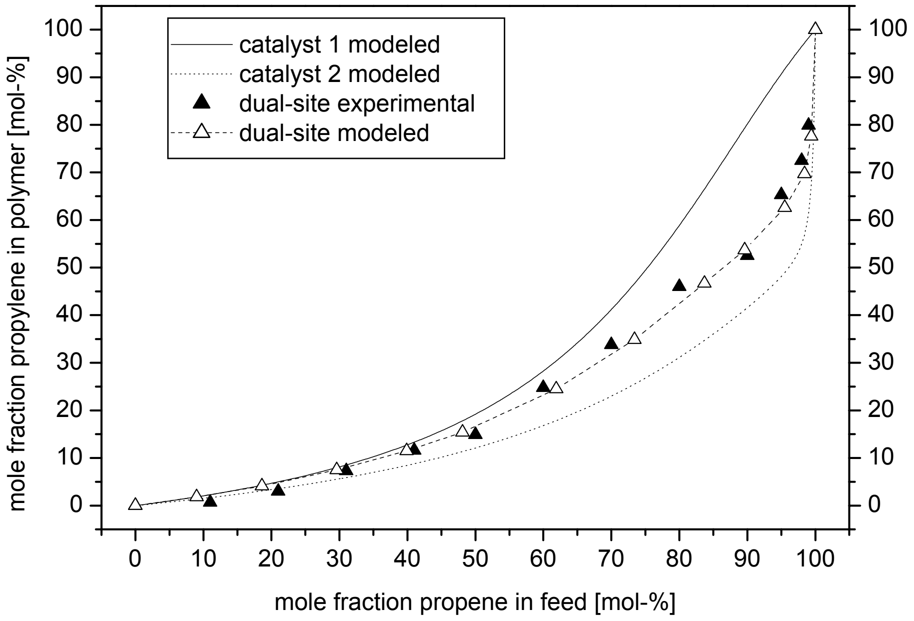

Figure 4-5: Experimental and modeled propene incorporation of the dual-site series. Outer lines represent the theoretical single-site behaviour of catalysts 1 and 2.

As an additional step, the reactivity ratios of the two metallocenes can also be estimated from the dual-site results. Therefore the modeling can be repeated without making use of the reactivity ratios found by the DPM for the single-site series. In this case, the reactivity ratios of the two catalysts are set as variables and determined via χ^2 minimalization of the overall theoretical and experimental ^{13}C NMR spectra of the series of copolymers. The activities of the two catalysts in the single-site experiments and the molar ratio 1:5 are still used to calculate the contributions (see Table 4-1). Compared to the modeling of the single-site series, the number of equations remains the same (108), the number of variables increases to 32 (8 reactivity ratios instead of 4). The results are listed in Table 4-4 in addition to the values found by the modeling of the single-site series.

Even though the reactivity ratios found by the modeling of the dual-site series are not as precise as the ones modeled by the single-site series (see Table 4-4), clearly these results are a good estimate and show great resemblance. The trends that $r_{EEP} > r_{PEP}$ and $r_{EPE} < r_{PPE}$ [XII,48] are also found. These results prove that, in the case the catalysts act independently, overall ^{13}C NMR spectra of dual-site copolymers can be split up in contributions of the two catalysts used.

Table 4-4: Reactivity ratios of the catalysts 1 and 2 obtained from the single-site and dual-site series.

	catalyst 1		catalyst 2	
	single-site[a)]	dual-site	single-site[a)]	dual-site
r_{EEP}	5.46 (± 6.2%)	5.71	7.23 (± 4.7%)	8.83
r_{EPE}	0.37 (± 5.4%)	0.25	0.006 (± 10.0%)	0.005
r_{PEP}	3.43 (± 6.1%)	2.57	3.29 (± 5.5%)	4.67
r_{PPE}	0.59 (± 4.2%)	0.86	0.007 (± 51.4%)	0.05
'$r_E \cdot r_P$'	2.02 (± 11.2 %)	1.78	0.03 (± 37.2 %)	0.10
# equations	108	108	108	108
# variables	28	32	28	32
# d.o.f.	80	76	80	76
χ^2	40.3	63.5	47.8	63.5
reliability	99.99 %	84.63 %	99.84 %	84.63 %

a) See Table 2

4.2.3 Melting temperatures and molar masses

Table 4-5 shows an overview of the melting peak temperatures of the polymers of the two single-site series. The melting temperatures of the single-site made copolymers with low propylene content are almost independent of the catalyst type. From recent Monte Carlo simulation[169] on crystallization and melting of copolymers with different distributions of the comonomer units in the chain it was expected that the influence of increasing propylene content would be slightly higher for catalyst 2 than for catalyst 1. The latter is producing more random copolymers, so longer ethylene sequences also exist for higher propene incorporation. With catalyst 2 alternating sequences in the copolymers are synthesized, so longer ethylene sequences disappear faster with increasing comonomer content. In combination with the decreasing molar masses of catalyst 2 made fractions, a slightly smaller influence of increasing propylene content on catalyst 1 compared to catalyst 2 was expected, but this is not observed indisputably.

Table 4-5: Melting points and weight average molar masses of the single-site made copolymers. Polydispersity of all polymers is close to 2.

	catalyst 1			catalyst 2	
C_3 incorp.[a)]	T_m [°C]	M_w [kg·mol^{-1}]	C_3 incorp.[a)]	T_m [°C]	M_w [kg·mol^{-1}]
0.0	131.4	345	0.0	138.3	341
2.1	110.1	218	1.4	129.9	228
4.0	114.6	219	3.8	112.8	125
6.2	107.1	290	5.9	102.5	98
15.1	59.7	162	8.7	89.6	68
22.3	44.7	144	14.4	65.4	49
34.7	--	130	17.5	41.3	43
48.1	--	130	21.0	20.1	37
69.5	--	135	29.1	--	30
82.5	83.1	185	39.2	--	25
91.6	117.2	281	47.4	--	23
96.4	139.6	469	50.4	--	23
98.3	142.7	563	50.8	--	23
100.0	152.5	888	100.0	--	43

[a)] Modeled mole fraction propylene in copolymer [mol-%]

For copolymers produced at high propene reactor feeds, the influence of catalyst type on the melting behavior is much more pronounced. If the propylene mole fraction is more than 80 mol-%, catalyst 1 is producing partly crystalline copolymers, catalyst 2 only incorporates propene up to 50 mol-% and reflects no propylene crystallinity. These results are in line with products previously made by these catalysts.[166,167] While catalyst 1 is producing highly isotactic polypropylene with a melting point over 150°C, catalyst 2 made polypropylene is rather atactic (hemiisotactic tendence). Therefore no melting point is observed for this polymer.

Table 4-6: Melting points and weight average molar masses of the dual-site made copolymers.

C_3 incorporation[a)]			T_m [°C]		M_w [kg·mol^{-1}]	
overall	catalyst 1	catalyst 2	peak 1	peak 2	mass 1	mass 2
0.0	0.0	0.0	137.9	--	331	--
1.8	1.8	1.3	130.3	--	338	--
4.1	4.3	3.1	115.5	--	292	--
7.5	8.0	5.5	95.3	--	250	--
11.5	12.7	8.4	52.7	88.0	137	--
15.4	17.8	11.3	80.4	--	82	--
24.5	30.4	17.8	62.5	--	78	--
34.9	46.6	25.5	--	--	71	--
46.7	66.5	34.7	--	--	83	--
53.7	83.0	38.8	105.6	--	27	230
62.6	94.8	50.5	133.5	--	22	471
69.7	97.2	56.8	145.0	--	24	592
77.6	99.0	67.6	150.0	--	25	649
100.0	100.0	100.0	152.7	--	41	910

[a)] Modeled mole fraction propylene in copolymer [mol-%]

The data of the dual-site series is summarized in Table 4-6, while Figure 4-6 shows the melting points of all three series versus the propylene content in the polymers. A comparison of the single-site series and the dual-site series allows an assignment of some data to catalyst 1 or 2. The observed melting peaks of the first four polymers of the dual-site series can originate either from catalyst 1 or catalyst 2, the differences in this area are too small to indisputably assign these peaks to one of the catalysts. Therefore in Figure 4-6 these points are plotted versus the overall propylene content. On the basis of the modeled propene incorporations, the double melting peak at 88.0°C and 52.7°C can be assigned to catalyst 2 and catalyst 1 respectively. The melting temperatures of 62.5°C and 80.4°C can only be originating from catalyst 2, at this propylene contents the polymers made by catalyst 1 have already lower or no melting points. Copolymers with high propylene content and crystallinity are not produced by catalyst 2, so the last four melting peaks in this series can only be originating from catalyst 1.

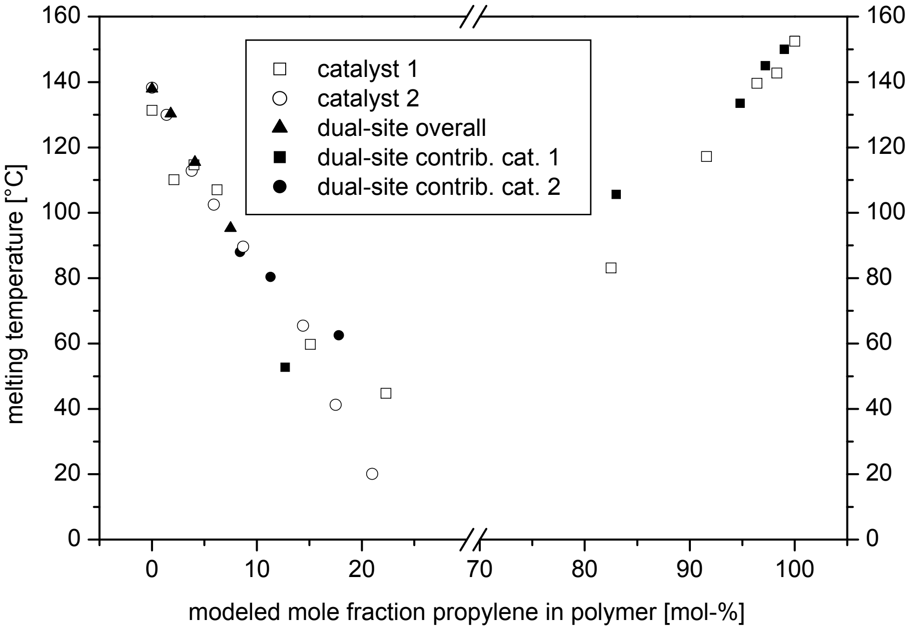

Figure 4-6: Melting temperatures versus modeled propene incorporation of the dual-site series.

As shown in Table 4-5, the molar masses of the polymers synthesized with catalyst 1 are much higher than the ones made by catalyst 2. All molar mass distributions are at about 2 as expected for single-site experiments. Catalyst 1 shows a minimum in the molar masses. The masses are high for polyethylene and copolymers with low propylene content, and high for polypropylene and copolymers with high propylene content. In between the molar masses are lower, this was also observed in previous studies.[166] Catalyst 2 shows a decrease of the molar masses with increasing comonomer content. The highest mass was reached for polyethylene and the lowest for copolymers with higher propylene content. A general trend in these series is that the polymers made by catalyst 1 have higher molar masses than those made by catalyst 2.

The SEC results of the dual-site series are given in Table 4-6. A separation of the molar masses of the samples with an overall propylene content of less than 50 mol-% was not possible. Due to the mixture of a high molar mass fraction made by catalyst 1 and a lower molar mass fraction made by catalyst 2 the non separated average molar masses are in between those of the single-site experiments. The results are plotted in Figure 4-7. The five samples with the highest overall comonomer content can be separated, and this leads to two weight average molar masses M_w. The shorter chains are originating from catalyst 2, the longer chains from catalyst 1. For these samples the MMD of each fraction was close to 2 and no peak shoulders were observed. Especially the bimodal polypropylene shows two molar masses that are very close to those of the single-site experiments, in case of catalyst 2 almost the same.

For the last two bimodal copolymers in this series the modeling predicts a propylene incorporation of more that 50 mol-% for catalyst 2 (see paragraph 4.2.2) which conflicts with the single-site experiments of this catalyst. Although in this case the modeled propylene content is too high, the measured molar masses are attributed to the proper fraction.

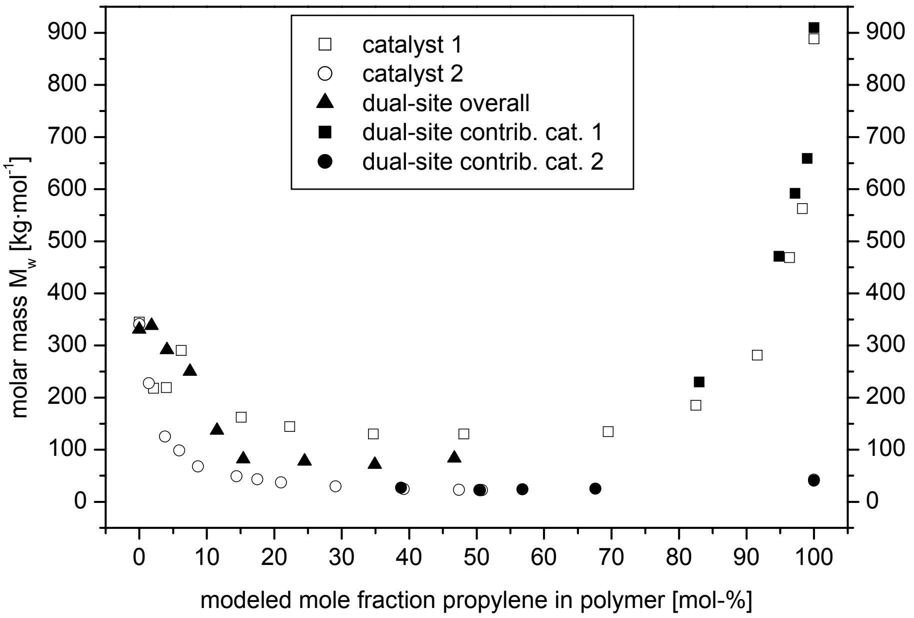

Figure 4-7: Weight average molar masses versus modeled propene incorporation of dual-site series.

4.3 Conclusion

The second order Markov reactivity ratios of the metallocene catalysts have been successfully modeled using the Direct Peak Method **X**,168 resulting in r_{EEP} = 5.46 (± 6.2%), r_{EPE} = 0.37 (± 5.4%), r_{PEP} = 3.43 (± 6.1%) and r_{PPE} = 0.59 (± 4.2%) for rac-[Me_2Si(2-Me-4-(1-Naph)Ind$)_2$]$ZrCl_2$ / MAO (catalyst 1) and r_{EEP} = 7.23 (± 4.7%), r_{EPE} = 0.006 (± 10.0%), r_{PEP} = 3.29 (± 5.5%) and r_{PPE} = 0.007 (± 51.4%) for [Me_2Si(Ind)(Flu)]$ZrCl_2$ / MAO (catalyst 2). The use of second order Markov statistics is justified since first order Markov statistics do not satisfy the condition of a 99.5% reliability of the modeling.**XII** The (product of the) reactivity ratios show that in ethene/propene copolymerizations catalyst 1 produces rather random copolymers with a high affinity to incorporate propene whereas catalyst 2 synthesizes alternating copolymers with low amounts of propylene; these observations are in line with previous work on these catalysts[166,167] which shows good reproducibility of the results.

Comparing the activities of the two metallocene catalysts used, for all copolymerizations catalyst 1 gives higher values with a maximum for pure polyethylene of about 800 $t_{polymer}\cdot mol_{Zr}^{-1}\cdot h^{-1}\cdot mol_{monomer}^{-1}\cdot l$. Catalyst 2 is much less active for copolymerizations with high ethylene content, but for polypropylene and copolymers with high propylene content the activities of the two catalysts are comparable.

The activities of the single-site experiments in combination with the 1:5 catalyst’s molar ratio for the dual-site copolymerizations can be used to calculate the contributions of the two active sites to the bimodal polymers. These contributions together with the second order Markov reactivities of the single-site series enable the modeling of the dual-site experiments based on the fitting of the ^{13}C NMR spectra. As a result, the overall propylene contents of the bimodal polymers can be splitted up into the contents of the two polymer fractions belonging to the two catalysts.

Based on these two propylene contents of the bimodal polymers the results of DSC and SEC can be interpretated in a much better way. Melting temperatures of ethylene-type and propylene-type of crystallinity as well as molar masses have been attributed to one of the two catalysts.

Finally, the second order Markov reactivity ratios of the two catalysts can also be calculated by modeling of the ^{13}C NMR spectra of the dual-site experiments by only making use of the contributions. Even though the results of this modeling are not as accurate as the reactivity ratios obtained from applying the DPM to single-site series, the rough characteristics of the two catalysts are detected and the ratios are well estimated.

5. Outlook

A variation of the polymerization conditions of the samples B6 and B7 (compare to the chapter 2.4) leads to a strong dependence of the rheological properties from the polymerization time. While the molar mass M_w is increasing only slightly (ca. 15 %) with polymerization time, the LCB content is strongly increasing. This becomes clear locking at the phase angle δ as a function of the complex modulus $|G^*|$, see Figure 5-1. At short polymerization times of about 1 hour less LCBs are formed than at polymerization times of about 4 hour. This trend can be underlined with further investigations on time dependent long-chain branching. A spezial interest thereby is also the influence of the catalyst type.

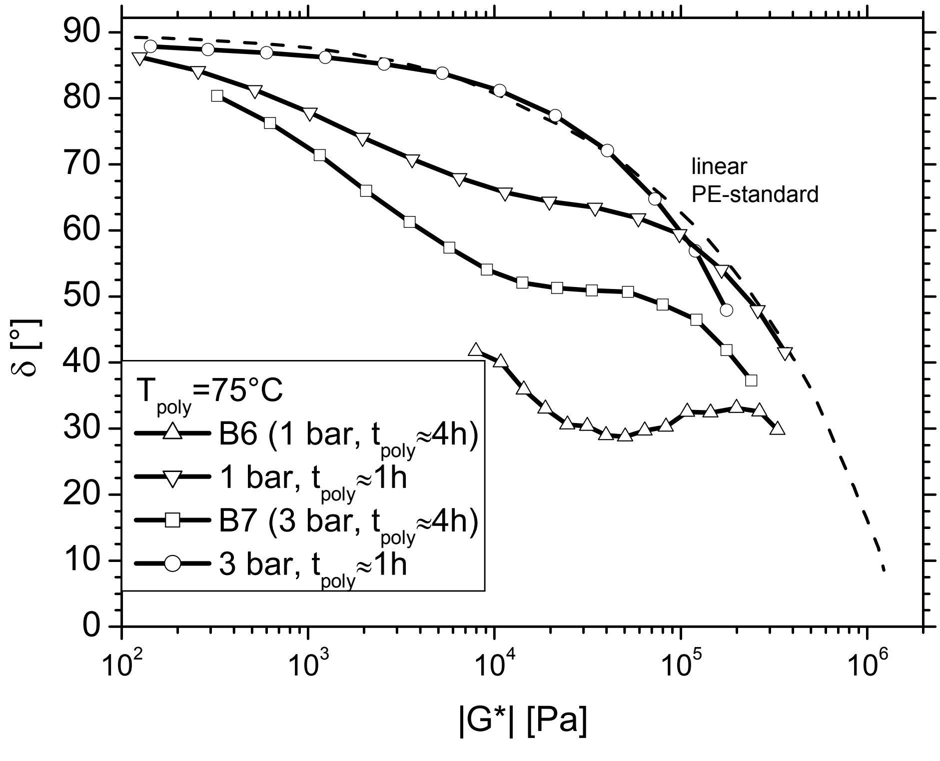

Figure 5-1: Change of rheological properties with polymerization time.

In addition to chapter 3.3 the dependency of LCB from the comonomer length can be expanded by the synthesis and characterization of ethene/1-decene and ethene/1-dodecene copolymers. Copolymers with 10 and 15 mol-% 1-decene and 1-dodecene respectively were allready produced (F10A, F10B and F12A, F12B) and the results are promissing. Figure 5-2 and Figure 5-3 show that the critical comonomer length to influence the LCB content in polyethylene is between 1-dodecene (F12A, F12B) and 1-octene (F8A, F8B, F8C). At least two more copolymers of 1-decene and 1-dodecene would help to complete these investigations. It is also of interest to expand this study to shorter comonomer copolymers like ethene/1-hexene or ethene/1-butene copolymers.

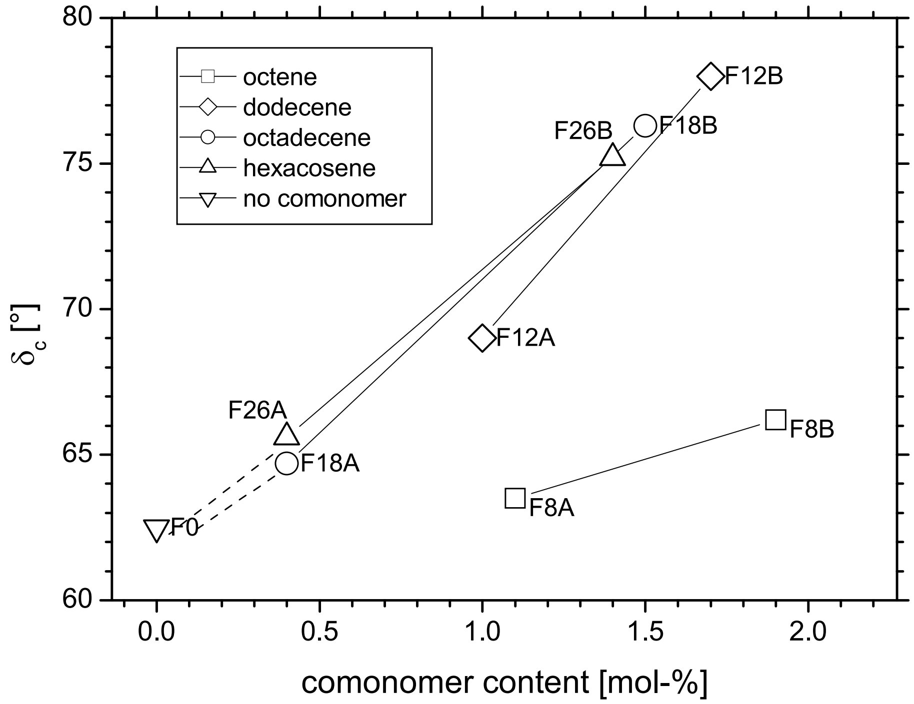

Figure 5-2: δ_c against comonomer content for LLDPEs (compare chapter 3.3.2.3).

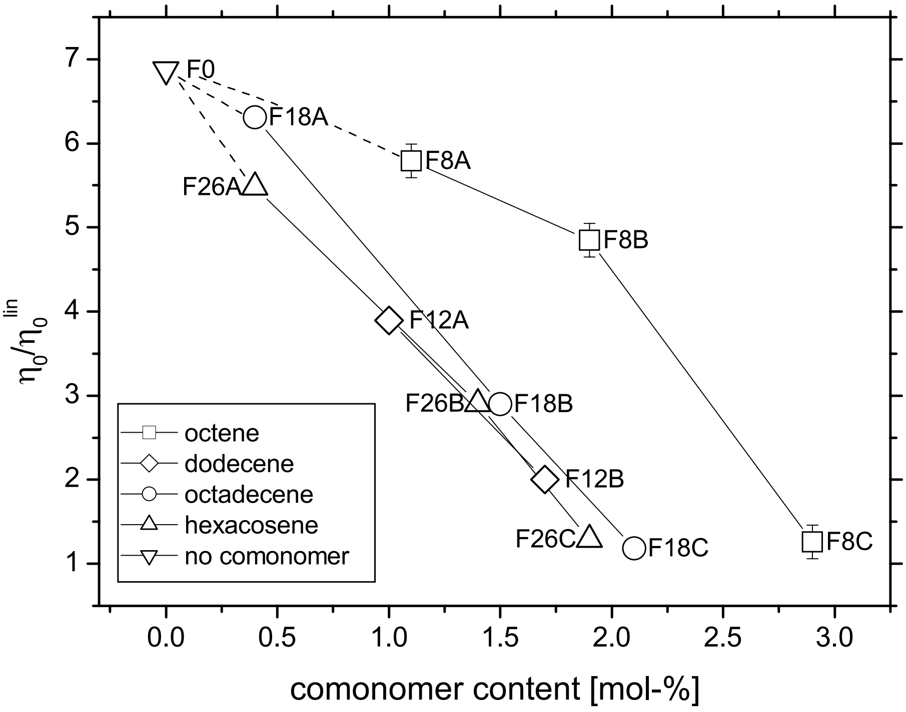

Figure 5-3: Reduced zero shear-rate viscosity for several LLDPE samples.

6. Experimental

6.1 General

All air or moisture sensitive procedures were performed under nitrogen or argon using Schlenk techniques.

6.2 Chemicals

Methylalumoxane (10 wt.-% solution in toluene, Crompton) was used as delivered for polymerizations in reactor 3. For the polymerizations made in reactor 1a, 1b and 2 the solution was filtered, the toluene and trimethylaliminium were removed in vacuo and MAO was stored as a solid. Fresh prepared solutions in dry toluene were used for polymerizations.

Ethene, propene and toluene were purified by passing through columns with copper catalyst (BASF R3-11) and 4Å molecular sieves.

1-Octene, 1-decene, 1-dodecene and 1-octadecene were degased and stored under nitrogen and molecular sieve 4Å.

Hydrogen was used without further purification.

The comonomer 1-hexacosene is a commercial available α-olefin wax fraction (mainly C_{26} to C_{28} olefins, Chevron Phillips Chemical Company LP, USA, see appendix). A defined amount was fed into the reactor and the system was evacuated and flushed with inert gas several times prior use.

The metallocene complexes $(CpMe_5)_2ZrCl_2$, Cp_2ZrCl_2, *rac*-$[Et(Ind)_2]ZrCl_2$ and $[Me_2C(Cp)_2]ZrCl_2$ were synthesized in our group according to general literature procedures. The metallocene $[Ph_2C(2,7\text{-di-}^{tert}BuFlu)(Cp)]ZrCl_2$ was also synthesized in our group[105] based on previous work by Ewen and Razavi[170,171]. The complexes *rac*-$[Me_2Si(2\text{-Me-4-(1-Naph)Ind})_2]ZrCl_2$ and $[Me_2Si(Me_4Cp)(N^{tert}Bu)]TiCl_2$ were purchased from Boulder Scientific Inc., USA and $[Me_2Si(Ind)(Flu)]ZrCl_2$ from MCAT GmbH, Germany. The catalyst precursors were stored under inert gas atmosphere and freshly prepared solutions in dry toluene were used for polymerizations.

6.3 Polymerizations

All polymerizations were carried out in toluene in Büchi reactor systems equipped with a magnetical stirrer. For the standard experiment, the reactor was evacuated at 90 °C for at least 1 h, flushed several times with inert gas and, after cooling, charged subsequently with toluene, MAO and in some cases a defined amount of comonomer. The gaseous monomer concentrations were calculated using literature data.[172] The polymerizations were started by injection of the catalyst precursor in toluene solution to the ethene saturated toluene / MAO solution. The polymerization reaction was stopped by addition of 1 ml ethanol.

6.3.1 Reactor 1a and 1b

Reactor 1a was a 1l Büchi glass reactor and reactor 1b a 3l Büchi glass reactor. The reactor was charged with toluene, MAO and comonomer. After that, the desired amount of ethene was fed. The pressure of ethene was kept constant with Brooks Mass Flow Controller. Some polymerizations were done under presence of hydrogen to reduce the molar mass of the polymer. In these cases the hydrogen pressure was fed and saturated for 5 min. before ethene was fed into the reactor.

6.3.2 Reactor 2

These polymerizations in reactor 2 were carried out in 400 ml toluene at 30°C in a 1 l Büchi glass reactor, a press flow controller and a Büchi data system bds 488 was used to record the monomer flows. The propene and ethene pressure for every run were set and the pressure was kept constant during the polymerization by feeding ethene (semi-batch process). The polymerizations were started by injection of the metallocene complex or complex mixture in toluene to the propene and ethene saturated toluene / MAO (400 mg) solution. The catalyst precursor amount for the single-site series was $5 \cdot 10^{-8}$ mol for catalyst 1) *rac*-[Me_2Si(2-Me-4-(1-Naph)Ind)$_2$]$ZrCl_2$, and $5 \cdot 10^{-7}$ mol for catalyst 2) [Me_2Si(Ind)(Flu)]$ZrCl_2$. For the dual-site series a mixture of catalyst 1) and 2) was used with a molar ratio of 1:5 and a total catalyst amount of $1.5 \cdot 10^{-7}$ mol per polymerization. The ratio of the activities of catalysts 1 and 2 for ethene reactor feeds around 50 mol-% is 5:1, so to obtain balanced bimodal copolymers the ratio 1:5 was applied. After a short polymerization period (propene conversion < 5 %) the reaction was stopped.

6.3.3 Reactor 3

This reactor 3 is located in the University of Technology (HUT), Helsinki. It is a 3 l Büchi steal reactor equipped with a press flow controller. 2000 ml toluene, 1000 mg MAO and in some cases a defined amount of comonomer were used. After reaching 60°C polymerization temperature, 13.4 mmol of hydrogen and ethene were added, such that the total monomer concentration was 0.37 mol/l. Polymerization was started by addition of $8 \cdot 10^{-7}$ mol toluenic metallocene solution. During the reaction, the total pressure was kept constant by supplying ethene and the ethene flow was recorded constantly. The polymerization was quenched after approximately 20 g of polymer was produced.

6.3.4 Post polymerization procedure

The polymer solution was stirred over night in an ethanol / HCl / water solution, filtered, washed with plenty of ethanol followed by evaporation of the solvents and drying of the polymer in vacuo at 60 °C over night. The ethene/hexacosene copolymers were in addition two times dissolved in warm toluene and filtered afterwards at room temperature and washed with ethanol before drying in order to wash out residues of comonomer.

6.4 Analytics

6.4.1 Differential scanning calorimetry

6.4.1.1 DSC 1

The thermal behavior of the polymers was measured using a Mettler-Toledo DSC 821e, in the temperature range from -100 to 200°C with a heating rate of 20 $K \cdot min^{-1}$. The calibration of temperature and melt enthalpy was done with n-heptane (T_m = -90.6 °C, 138.6 $J \cdot g^{-1}$), quicksilver (T_m = -38.8 °C, 11.5 $J \cdot g^{-1}$), gallium (T_m = 29.8 °C, 80.2 $J \cdot g^{-1}$), indium (T_m = 156.6 °C, 28.5 $J \cdot g^{-1}$) and zink (T_m = 419.5 °C, 107.5 $J \cdot g^{-1}$). To determine the melting temperatures the second heating run was used.

6.4.1.2 DSC 2

Differential scanning calorimetry curves were recorded on a Perkin Elmer DSC-7 instrument, located in HUT, calibrated with indium (T_m = 156.6 °C, 28.45 $J \cdot g^{-1}$). A heating and cooling rate of 10 K/min for all experiments and steps was used. 5-6 mg of polymer was taken for measurements. For the melting and crystallization curves of the thermal untreated samples the results of the second thermal cycle are presented exclusively. The successive self-annealing measurements were done according to the principles of Müller and Fillon.[173,174] To destroy any thermal history the samples were first heated up to 160 °C and cooled down to 30 °C again and hold there for 1 min. Subsequently, a heating was performed up to a selected self-annealing temperature donated as T_s, where the sample was isothermally kept for 5 min before cooling it again down to 30 °C. At the end of the first cooling the polymer has been self-nucleated. Then the sample was heated again to the next T_s, which is 6 °C lower than the previous T_s. This means that the unmelted crystals at this lower T_s will anneal during the 5 min at this temperature, some of the melted species will isothermally crystallize (after being self-nucleated by the unmelted crystals), while the rest of the molten crystallizable chains (or chain segments) will only crystallize during the subsequent cooling from T_s. The procedure is then repeated with T_s again being lowered at 6 °C intervals with respect to the previous step. The chosen T_s range was from 140 to 56 °C for PE, from 122 to 44 °C for series 1 and from 110 to 44 °C for series 2, for both ethene/hexacosene copolymers the last step was T_s = 38 °C. Finally, the melting behavior was recorded by a normal melting run when the thermal conditioning was over. When comparing a series of similar samples, a constant initial T_s for all samples of the series was used. The advantage of this method is that all samples will have the same thermal history and the comparison of the final curves can be more meaningful from that point of view.

6.4.2 Size exclusion chromatography

6.4.2.1 SEC 1

Size exclusion chromatography was carried out with a Waters GPCV 2000 Alliance system equipped with a refractive index detector, viscosimetric detector and a set of three columns, Styragel type (HT6, HT5, HT3). 1,2,4-Trichlorobenzene was used as solvent. The analyses were performed at 140°C and 1.0 $ml \cdot min^{-1}$ flow rate. The system was calibrated with narrow molar mass distribution polystyrene standards and their Mark-Houwink constants using the universal method.[175-177] The sample concentration was 1 mg·ml^{-1} and 2,6-di-^{tert}butyl-4-methylphenol was used as thermostabilizer (1 g·l^{-1}).

LLDPEs: The masses were calculated using the universal method and both detectors.

Ethene/propene copolymers: The molar masses were calculated using the refractive index signal and literature constants for polyethylene (K = 0.0406 ml·g^{-1}, a = 0.725) and corrected for propylene content using the method by Scholte et al.[178]

6.4.2.2 SEC 2 (SEC-MALLS)

These measurements were performed at University of Erlangen, research group of Prof. Münstedt. The molecular characterization was carried out on a Waters 150C, equipped with a refractive index (RI) detector and an additional infra-red (IR) detector (PolyChar, IR4) at 140°C for column and sample compartment using 1,2,4-trichlorobenzene (TCB) as solvent. The high temperature SEC was coupled with a multi-angle light scattering apparatus (Wyatt, DAWN EOS), which was also operated at 140°C. The samples (2 g/l) were dissolved in TCB at 160°C for three hours prior to the analysis. Irganox 1035 (Ciba SC) was added to the solution in a concentration of 1 g/l avoid degradation during analysis. The flow rate was chosen to be 0.5 ml/min in order to prevent mechanical degradation of the polymer on the columns. 300 µl of the solution was injected onto a set of 4 SEC-columns (3 Shodex columns UT 806, 1 Shodex UT807). Calibration of the SEC was performed with narrow MMD polystyrene Standards from Polymer Laboratories ranging in of molar mass from 1 kg/mol to 11 000 kg/mol. The Mark Houwink constants for the universal calibrations were K=1.21·10^{-4} ml/g and a=0.707 for PS[179] and K=4.06·10^{-4} ml/g and a= 0.725 for PE.[178] For more details see reference **I**, **II** and **IV**.

6.4.2.3 SEC 3

Size exclusion chromatography was carried out on a Waters GPCV 2000 Alliance system, located in HUT, equipped with a refractive index detector, viscosimetric detector and a set of four columns, Styragel type: HT2, HT3, HT4 and HT6. 1,2,4-Trichlorobenzene was used as solvent and 2,6-Di-^{tert}butyl-4-methylphenol as thermostabilizer. The analysis was performed at 140 °C and 1.0 mL/min. The columns were calibrated with narrow molar mass distribution polystyrene standards. The masses were calculated using the universal method and both detectors.[175-177]

6.4.3 Nuclear magnetic resonance spectroscopy

6.4.3.1 NMR 1

^{13}C NMR spectra were measured with a Bruker Ultrashield 400 spectrometer at 100.62 MHz. The samples were prepared by the dissolution of the polymers (10 mass-%) in a mixture of 1,2,4-trichlorobenzene and 1,1,2,2-tetrachloro-1,2-dideuteroethane and were measured at 100°C and referenced against $C_2D_2Cl_4$.

LLDPEs: The samples were measured at a pulse angle of 30°, delay time of 10 s, 4096 scans using the Inversed Gated Decoupling.

Ethene/propene copolymers: The samples were measured at a pulse angle of 30°, delay time of 5 s, 1024 scans, using the waltz16 decoupling method. The experimental propylene content in the copolymers was determined using the Randall method.[111]

6.4.3.2 NMR 2

^{13}C NMR spectra were measured with a Varian Gemini 2000 300 MHz spectrometer, located in HUT. Polymer samples were measured at 75 MHz at 100 °C from 300 mg of polymer in 2.5 ml of 1,2,4-Trichlorobenzene and 0.5 ml of benzene-d6. 3000 scans were measured using the waltz-16 decoupling method, 6 s delay time and 45° pulse angle.

6.4.3.3 NMR 3 (solid-state NMR)

These NMR measurements were performed at Max-Planck Institute for Polymer Research in Mainz in the research group of Prof. Wilhelm. Melt-state NMR spectroscopy was carried out on a Bruker Advance 500 dedicated solid-state NMR spectrometer operating at a proton and carbon Larmor frequency of 500.13 and 125.75 MHz respectively. All measurements were undertaken using a commercial Bruker, ^{13}C-^{1}H optimized, high temperature, 7 mm magic-angle spinning (MAS) probehead using zirconia rotors and rotor caps. Nitrogen gas was used for all pneumatics to limit thermal oxidation. All measurements were conducted at $\omega_r/2\pi = 3$ kHz spinning speed at 150°C sample temperature, whilst compensating for thermal MAS effects.

Single pulse excitation spectra were acquired using 10 µs ^{13}C $\pi/2$ excitation pulses and π pulse-train heteronuclear dipolar decoupling. For the copolymers, depending on degree of incorporation, between 16–424 scans were needed to achieve the desired signal-to-noise-ratio of the alpha peak at 34.6 ppm (SNR_α=50) using a 2 s recycle delay and 16 dummy scans. Overall measuring time of all copolymer samples was about 45 min. Short measurement times were primarily achieved due to investigation in the bulk state, combined with the use of a short recycle delay.[VIII] For the homopolymer (F0) 78 000 scans were acquired under the same conditions, and resulted in a $SNR_\alpha \approx 5$ after 48 h. For details see references **IV**, **VIII** and **XIII**.

6.4.4 Melt rheology

Rheological measurements were performed at University of Erlangen, research group of Prof. Münstedt. For these measurements different rheometers were used. Most of them were carried out with a Malvern/Bohlin CVOR "Gemini", a constant stress rheometer, using a 25 mm parallel plate geometry or a 25 mm / 2.5° cone/plate geometry. An ARES from Rheometric Scientific/TA Instruments and a Malvern/Bohlin CSM were also used (25 and 50 mm parallel plate, 50 mm/2.5° cone/plate). All experiments were performed under nitrogen atmosphere and the samples were thermostabilized. For details see reference **I**, **II** and **IV**.

6.4.5 Press

A Fontune table press TP 400, located in HUT, at 200 °C and a special mould was used for compression moulding of the DMA specimens and plates with the dimensions 2 x 80 x 80 mm^3. From these plates the tensile test specimens according to ISO 527-2:1993 (type 5A) were made using a stamping press. The polymers were thermostabilized by mixing in 0.4 wt.-% of Irganox 1010 FF and 0.2 wt.-% of Irgafos 168 (both CIBA products) before melting.

6.4.6 Dynamic mechanical analysis

Dynamic mechanic measurements were performed with a Perkin Elmer DMA-7, located in HUT. The experiments were carried out using the three-point-bending geometry. All specimens were scanned at a frequency of 1 Hz over a temperature range of -100 to 90 °C at a rate of 4 K/min under helium flow. The rectangular specimen dimensions were 2 x 4 x 17 mm^3 (by special mould using the Fontune table press). Every sample was measured at least tree times with tree different specimens and the average curves were taken for interpretation.

6.4.7 Universal testing machine

Tensile tests were performed on a Instron 4204 universal testing machine, located at HUT, equipped with a force transducer of max. 1 kN. The crosshead speed was 20 mm/min at constant 50% humidity and 23 °C. The yield stress and the Young's modulus were calculated according to ISO 527-1:1993(E).

6.4.8 Density measurements

For the density measurements the DMA specimens were taken and a Sartorius balance type LA230S equipped with the density determination kit YDK01 was used, located in HUT. The Archimedean principle is applied for determining the specific gravity of a solid, ethanol is used as liquid. Every sample was measured at least tree times with tree different specimens and the mean values are presented here.

7. References

This thesis is based on the publications **I-VI** (see list of publications on page 4), which are referred to by their Roman numbers.

1. Fawcett, E.W.; Gibson, R.O.; Perrin, M.W.; Paton, J.G.; Williams, E.G., *Ethylene polymers*, Great Britain GB 471590 (**1937**), Imperial Chemical Industries Ltd.
2. Hogan, J.P.; Banks, R.L., *Polymerization of olefins*, USA US 2825721 (**1958**), Phillips Petroleum Co.
3. Ziegler, K., *Alumino-organic syntheses in the field of olefinic hydrocarbons.* Angew. Chem. **1952**, 64, 323-329.
4. Ziegler, K.; Holzkamp, E.; Breil, H.; Martin, H., *The Mühlheim low-pressure polyethylene process.* Angew. Chem. **1955**, 67, 541-547.
5. Sinn, H.; Kaminsky, W.; Vollmer, H.J.; Woldt, R., *"Living polymers" with Ziegler catalysts of high productivity.* Angew. Chem. **1980**, 92(5), 396-402.
6. Ziegler, K., *Results and development of a discovery.* Angew. Chem. **1964**, 76(13), 545-553.
7. Ziegler, K.; Breil, H.; Holzkamp, E.; Martin, H., *Verfahren zur Herstellung von hochmolekularen Polyäthylenen*, Germany DE 973626 (**1953**).
8. Böhm, L.L., *The Ethylene Polymerization with Ziegler Catalysts: Fifty Years after the Discovery.* Angew. Chem. Int. Ed. **2003**, 42(41), 5010-5030.
9. Natta, G., *Stereospecific catalysis of isotactic polymers.* Angew. Chem. **1956**, 68, 393-403.
10. Natta, G., *From stereospecific polymerization to the asymmetric autocatalytic synthesis of macromolecules.* Angew. Chem. **1964**, 76(13), 553-566.
11. Natta, G.; Crespi, G., *Properties of ethylene-propylene copolymers and of terpolymers containing unsaturation.* J. Polym. Sci. **1962**, 61(171), 83-95.
12. Natta, G.; Pino, P.; Mazzanti, G.; Giannini, U., *A crystalline organometallic complex containing titanium and aluminum.* J. Am. Chem. Soc. **1957**, 79, 2975-2976.
13. Breslow, D.S.; Newburg, N.R., *Bis(cyclopentadienyl)titanium chloride-alkylaluminum complexes as catalysts for the polymerization of ethylene.* J. Am. Chem. Soc. **1957**, 79, 5072-5073.
14. Breslow, D.S.; Newburg, N.R., *Dicyclopentadienyltitanium dichloride-alkylaluminum complexes as soluble catalysts for the polymerization of ethylene.* J. Am. Chem. Soc. **1959**, 81, 81-86.
15. Reichert, K.H.; Meyer, K.R., *Kinetics of the low pressure polymerization of ethylene by soluble Ziegler catalysts.* Makromol. Chem. **1973**, 169, 163-176.
16. Sinn, H.; Kaminsky, W., *Ziegler-Natta catalysis.* Adv. Organomet. Chem. **1980**, 18, 99-149.
17. Kaminsky, W., *The Discovery of Metallocene Catalysts and Their Present State of the Art.* J. Polym. Sci. Part A: Polym. Chem. **2004**, 42(16), 3911-3921.

18. Kaminsky, W.; Miri, M.; Sinn, H.; Woldt, R., *Bis(cyclopentadienyl)zirconium compounds and aluminoxane as Ziegler catalysts for the polymerization and copolymerization of olefins.* Makromol. Chem., Rapid Commun. **1983**, 4(6), 417-21.

19. Wild, F.; Wasiucionek, M.; Huttner, G.; Brintzinger, H.-H., *ansa-Metallocene derivatives. VII. Synthesis and crystal structure of a chiral ansa-zirconocene derivative with ethylene-bridged tetrahydroindenyl ligands.* J. Organomet. Chem. **1985**, 288(1), 63-67.

20. Wild, F.; Zsolnai, L.; Huttner, G.; Brintzinger, H.-H., *ansa-Metallocene derivatives. IV. Synthesis and molecular structures of chiral ansa-titanocene derivatives with bridged tetrahydroindenyl ligands.* J. Organomet. Chem. **1982**, 232(3), 233-247.

21. Ewen, J.A., *"Ligand effects on metallocene catalyzed Ziegler-Natta polymerizations."* in: *Keii, T.; Soga, K.*, Catalytic Polymerization of Olefins, Studies in Surface Science and Catalysis, Eds., Elsevier, New York **1986**, p. 271-292.

22. Giannetti, E.; Nicoletti, G.; Mazzocchi, R., *Homogeneous Ziegler-Natta catalysis. II. Ethylene polymerization by IVB transition metal complexes/methyl aluminoxane catalyst systems.* J. Polym. Sci.: Part A: Polym. Chem. **1985**, 23(8), 2117-2134.

23. Ewen, J.A., *echanisms of stereochemical control in propylene polymerizations with soluble Group 4B metallocene/methylalumoxane catalysts.* J. Am. Chem. Soc. **1984**, 106(21), 6355-6364.

24. Kaminsky, W.; Külper, K.; Brintzinger, H.-H.; Wild, F., *Polymerization of Propene and Butene with a Chiral Zirconocene and Methylalumoxane as Cocatalyst.* Angew. Chem. Int. Ed. **1985**, 24(6), 507-508.

25. Coates, G.W., *Precise Control of Polyolefin Stereochemistry Using Single-Site Metal Catalysts.* Chem. Rev. **2000**, 100(4), 1223-1252.

26. Mülhaupt, R., *Catalytic polymerization and post polymerization catalysis fifty years after the discovery of Ziegler's catalysts.* Macromol. Chem. Phys. **2003**, 204(2), 289-327.

27. Lai, S.-Y.; Wilson, J.R.; Knight, G.W.; Stevens, J.C.; Chum, P.-W.S., *Elastic substantially linear olefin polymers*, U.S. Patent WO 9308221 (**1993**), Dow Chemical Co.

28. Johnson, L.K.; Killian, C.M.; Brookhart, M., *New Pd(II)- and Ni(II)-Based Catalysts for Polymerization of Ethylene and α-Olefins.* J. Am. Chem. Soc. **1995**, 117(23), 6414-6415.

29. Gibson, V.C.; Spitzmesser, S.K., *Advances in Non-Metallocene Olefin Polymerization Catalysis.* Chem. Rev. **2003**, 103, 283-315.

30. Wang, C.; Friedrich, S.K.; Younkin, T.R.; Li, R.T.; Grubbs, R.H.; Bansleben, D.A.; Day, M.W., *Neutral Nickel(II)-Based Catalysts for Ethylene Polymerization.* Organometallics **1998**, 17(15), 3149-3151.

31. Younkin, T.R.; Connor, E.F.; Henderson, J.I.; Friedrich, S.K.; Grubbs, R.H.; Bansleben, D.A., *Neutral, single-component nickel(II) polyolefin catalysts that tolerate heteroatoms.* Science **2000**, 287(5452), 460-462.

32. Soula, R.; Broyer, J.P.; Llauro, M.F.; Tomov, A.; Spitz, R.; Claverie, J.; Drujon, X.; Malinge, J.; Saudemont, T., *Very Active Neutral P,O-Chelated Nickel Catalysts for Ethylene Polymerization.* Macromolecules **2001**, 34(8), 2438-2442.

33. Soula, R.; Novat, C.; Tomov, A.; Spitz, R.; Claverie, J.; Drujon, X.; Malinge, J.; Saudemont, T., *Catalytic Polymerization of Ethylene in Emulsion.* Macromolecules **2001**, 34(7), 2022-2026.

34. Soula, R.; Saillard, B.; Spitz, R.; Claverie, J.; Llauro, M.F.; Monnet, C., *Catalytic Copolymerization of Ethylene and Polar and Nonpolar α-Olefins in Emulsion.* Macromolecules **2002**, 35(5), 1513-1523.

35. Matsui, S.; Tohi, Y.; Mitani, M.; Saito, J.; Makio, H.; Tanaka, H.; Nitabaru, M.; Nakano, T.; Fujita, T., *New Bis(salicylaldiminato) Titanium Complexes for Ethylene Polymerization.* Chem. Lett. **1999**, 1065-1066.

36. Matsui, S.; Mitani, M.; Saito, J.; Tohi, Y.; Makio, H.; Tanaka, H.; Fujita, T., *Post-Metallocenes: A New Bis(salicylaldiminato) Zirconium Complex for Ethylene Polymerization.* Chem. Lett. **1999**, 1263-1264.

37. Chen, E.Y.-X.; Marks, T.J., *Cocatalysts for Metal-Catalyzed Olefin Polymerization: Activators, Activation Processes, and Structure-Activity Relationships.* Chem. Rev. **2000**, 100(4), 1391-1434.

38. Alt, H.G.; Köppl, A., *Effect of the Nature of Metallocene Complexes of Group IV Metals on Their Performance in Catalytic Ethylene and Propylene Polymerization.* Chem. Rev. **2000**, 100(4), 1205-1222.

39. Resconi, L.; Cavallo, L.; Fait, A.; Piemontesi, F., *Selectivity in Propene Polymerization with Metallocene Catalysts.* Chem. Rev. **2000**, 100(4), 1253-1345.

40. Imanishi, Y.; Naga, N., *Recent developments in olefin polymerizations with transition metal catalysts.* Prog. Polym. Sci. **2001**, 26(8), 1147-1198.

41. Cossee, P., *Ziegler-Natta catalysis I. Mechanism of polymerization of α-olefins with Ziegler-Natta catalysts.* J. Catal. **1964**, 3, 80-88.

42. Arlman, E.J.; Cossee, P., *Ziegler-Natta catalysis III. Stereospecific polymerization of propene with the catalyst system* $TiCl_3$-$AlEt_3$. J. Catal. **1964**, 3, 99-104.

43. Busico, V.; Cipullo, R.; Cutillo, F.; Vacatello, M., *Metallocene-catalyzed propene polymerization: from microstructure to kinetics. 1.* C_2*-symmetric ansa-metallocenes and the "trigger" hypothesis.* Macromolecules **2002**, 35, 349-354.

44. Kaminsky, W.; Lüker, H., *Influence of hydrogen on the polymerization of ethylene with the homogeneous Ziegler system bis(cyclopentadienyl)zirconium dichloride/aluminoxane.* Macromol. Rapid Commun. **1984**, 5(4), 225-228.

45. Schneider, M.J.; Mülhaupt, R., *Influence of indenyl ligand substitution pattern on metallocene-catalyzed propene copolymerization with 1-octene.* Macromol. Chem. Phys. **1997**, 198, 1121-1129.

46. Heuer, B.; Kaminsky, W., *Alternating Ethene/Propene Copolymers by C1-Symmetric Metallocene/MAO Catalysts.* Macromolecules **2005**, 38(8), 3054-3059.

47. Sperber, O.; Kaminsky, W., *Synthesis of long-chain branched comb-structured polyethylene from ethylene by tandem action of two single-site catalysts.* Macromolecules **2003**, 36(24), 9014-9019.

48. Koivumäki, J.; Fink, G.; Seppälä, J.V., *Copolymerization of Ethene/1-Dodecene and Ethene/1-Octadecene with the Stereorigid Zirconium Catalyst Systems iPr[FluCp]ZrCl2/MAO and Me2Si[Ind]2ZrCl2/MAO: Influence of the Comonomer Chain Length.* Macromolecules **1994**, 27, 6254-6258.

49. Hoff, M.; Kaminsky, W., *Syndiospecific homopolymerisation of higher 1-alkenes with two different bridged* $[(RPh)_2C(Cp)(2,7\text{-}^{tert}\text{-}BuFlu)]ZrCl_2$ *catalysts.* Macromol. Chem. Phys. **2004**, 205(9), 1167-1173.

50. Mülhaupt, R.; Engelhardt, T.; Schall, N., *Nanocomposites - auf dem Weg zur Anwendung.* Kunststoffe **2001**, 91(10), 178-190.

51. Imuta, J.; Todo, A.; Tsutsui, T.; Hachimoei, T.; Kashiwa, N., *Development of polyethylene copolymers manufacturing technologies and synthesis of new functionalized polyolefins with designed catalysts.* Bull. Chem. Soc. Jpn. **2004**, 77(4), 607-615.

52. Perez, E.; VanderHart, D.L.; Crist, B.; Howard, P.R., *Morphological partitioning of ethyl branches in polyethylene by carbon-13 NMR.* Macromolecules **1987**, 20, 78-87.

53. McFaddin, D.C.; Russell, K.E.; Kelusky, E.C., *Morphological location of ethyl branches in carbon-13-enriched ethylene/1-butene random copolymers.* Polym. Commun. **1988**, 29(9), 258-260.

54. Dealy, J. M.; Wissbrun, K. F., *Melt Rheology and its Role in Plastics Processing: Theory and Applications*, Van Nostrand Reinhold, New York **1990**, 665.

55. Macosko, C. W., *Rheology: Principles, Measurements, and Applications*, Wiley-VCH, New York **1994**, 550.

56. Laun, H. M., *Orientation of macromolecules and elastic deformations in polymer melts. Influence of molecular structure on the reptation of molecules.* Prog. Colloid Polym. Sci. **1987**, 75, 111-139.

57. Gahleitner, M., *Melt rheology of polyolefins.* Prog. Polym. Sci. **2001**, 26, 895-944.

58. Brant, P.; Canich, J. A. M.; Dias, A. J.; Bamberger, R. L.; Licciardi, G. F.; Henrichs, P. M., *Long chain branched polymers and a process to make long chain branched polymers*, Int. Pat. Appl. WO 94/07930 (**1994**), Exxon Chemical.

59. Woo, T.K.; Margl, P.M.; Ziegler, T.; Blochl, P.E., *A Static and ab Initio Molecular Dynamics Study of the Titanium(IV)-Constrained Geometry Catalyst (CpSiH2NH)Ti-R+. 2. Chain Termination and Long Chain Branching.* Organometallics **1997**, 16(15), 3454-3468.

60. Harrison, D.; Coulter, I.M.; Wang, S.T.; Nistala, S.; Kuntz, B.A.; Pigeon, M.; Tian, J.; Collins, S., *Olefin polymerization using supported metallocene catalysts: development of high activity catalysts for use in slurry and gas phase ethylene polymerizations.* J. Mol. Cat. A: Chem. **1998**, 128(1-3), 65-77.

61. Malmberg, A.; Kokko, E.; Lehmus, P.; Löfgren, B.; Seppälä, J.V., *Long-chain branched polyethene polymerized by metallocene catalysts* $Et[Ind](2)ZrCl_2/MAO$ *and* $Et[IndH(4)](2)ZrCl_2/MAO$*.* Macromolecules **1998**, 31(24), 8448-8454.

62. Beigzadeh, D.; Soares, J. B. P.; Hamielec, A. E., *Study of long-chain branching in ethylene polymerization.* Polym. React. Eng. **1997**, 5(3), 141-180.

63. Kim, Y.S.; Chung, C.I.; Lai, S.Y.; Hyun, K.S., *Melt rheological and thermodynamic properties of polyethylene homopolymers and poly(ethylene/*α*-olefin) copolymers with respect to molecular composition and structure.* J. Appl. Polym. Sci. **1996**, 59, 125-137.

64. Kokko, E.; Lehmus, P.; Malmberg, A.; Löfgren, B.; Seppälä, J.V., *"Long-Chain Branched Polyethene via Metallocene-Catalysis: Comparison of Catalysts"*, in:

Organometallic Catalyst and Olefin Polymerization, Catalysts for a New Millenium, Blom, R.; Follestad, A.; Rytter, E.; Tilset, M.; Ystenes, M., Eds., Springer, **2001**, p. 335-345.

65. Vega, J.F.; Muñoz-Escalona, A.; Santamaría, A.; Muñoz, M.E.; Lafuente, P., *Comparison of the Rheological Properties of Metallocene-Catalyzed and Conventional High-Density Polyethylenes.* Macromolecules **1996**, 29(3), 960-965.

66. Kolodka, E.; Wang, W.-J.; Charpentier, P.A.; Zhu, S.; Hamielec, A.E., *Long-chain branching in slurry polymerization of ethylene with zirconocene dichloride/modified methylaluminoxane.* Polymer **2000**, 41(11), 3985-3991.

67. Gabriel, C.; Kokko, E.; Löfgren, B.; Seppälä, J.V.; Münstedt, H., *Analytical and rheological characterization of long-chain branched metallocene-catalyzed ethylene homopolymers.* Polymer **2002**, 43(24), 6383-6390.

68. Kokko, E.; Malmberg, A.; Lehmus, P.; Löfgren, B.; Seppälä, J.V., *Influence of the catalyst and polymerization conditions on the long-chain branching of metallocene-catalyzed polyethenes.* J. Polym. Sci., Part A: Polym. Chem. **2000**, 38(2), 376-388.

69. Kokko, E.; Wang, W.-J.; Zhu, S.; Seppälä, J.V., *Structural analysis of polyethene prepared with rac-dimethylsilylbis(indenyl)zirconium dichloride/methylaluminoxane in a high-temperature, continuously stirred tank reactor.* J. Polym. Sci., Part A: Polym. Chem. **2002**, 40(19), 3292-3301.

70. Wood-Adams, P.M.; Dealy, J. M.; deGroot, A.W.; Redwine, O.D., *Effect of Molecular Structure on the Linear Viscoelastic Behavior of Polyethylene.* Macromolecules **2000**, 33(20), 7489-7499.

71. Beigzadeh, D.; Soares, J. B. P.; Hamielec, A. E., *Recipes for synthesizing polyolefins with tailor-made molecular weight, polydispersity index, long-chain branching frequencies, and chemical composition using combined metallocene catalyst systems in a CSTR at steady state.* J. App. Pol. Sci. **1999**, 71(11), 1753-1770.

72. Wang, W.J.; Yan, D.J.; Zhu, S.P.; Hamielec, A.E., *Kinetics of Long Chain Branching in Continuous Solution Polymerization of Ethylene Using Constrained Geometry Metallocene.* Macromolecules **1998**, 31(25), 8677-8683.

73. Soga, K.; Uozumi, T.; Nakamura, S.; Toneri, T.; Teranishi, T.; Sano, T.; Arai, T.; Shiono, T., *Structures of polyethylene and copolymers of ethylene with 1-octene and oligoethylene produced with the* Cp_2ZrCl_2 *and* $[(C_5Me_4)SiMe_2N(t\text{-}Bu)]TiCl_2$ *catalysts.* Macromol. Chem. Phys. **1996**, 197(12), 4237-4251.

74. Kokko, E.; Pietikainen, P.; Koivunen, J.; Seppälä, J.V., *Long-chain-branched polyethene by the copolymerization of ethene and nonconjugated* α,ω*-dienes.* J. Polym. Sci., Part A: Polym. Chem. **2001**, 39(21), 3805-3817.

75. Lehmus, P.; Kokko, E.; Härkki, O.; Leino, R.; Luttikhedde, H.J.G.; Näsman, J.; Seppälä, J.V., *Homo- and Copolymerization of Ethylene and* α*-Olefins over 1- and 2-Siloxy-Substituted Ethylenebis(indenyl)zirconium and Ethylenebis(tetrahydroindenyl) zirconium Dichlorides.* Macromolecules **1999**, 32(11), 3547-3552.

76. Gabriel, C; Münstedt, H., *Influence of long-chain branches in polyethylenes on linear viscoelastic flow properties in shear.* Rheol. Acta **2002**, 41(3), 232-244.

77. Münstedt, H.; Steffl, T.; Malmberg, A., *Correlation between rheological behaviour in uniaxial elongation and film blowing properties of various polyethylenes.* Rheol Acta **2005**, 45(1), 14-22.

78. Knuttila, H.; Lehtinen, A.; Nummila-Pakarinen, A., Adv. Polym. Sci. **2004**, 169, 13.

79. Knuttila, H.; Lehtinen, A.; Salminen, H., Metallocene-based polyolefins, ed. Scheirs J.; Kaminsky, W., Wiley, Chichester **2000**, p 364-378.

80. Scheirs, J.; Böhm, L.L.; Boot, J.C.; Leevers, P.S., *PE100 resins for pipe applications: continuing the development into the 21st century.* Trends in Polym. Sci. **1996**, 4(12), 408-415.

81. Mathot, V.B.F.; Pijpers, T.F.J., *Crystallization and melting behavior of polyethylene fractions obtained by various fractionation methods.* Polym. Bull. **1984**, 11(3), 297-304.

82. Mathot, V.B.F., *Chapter 9*, in *Calorimetry and Thermal Analysis of Polymers*, Mathot, V.B.F., Editor, Hanser Publishers: München **1994**, p. 368 pp.

83. Böhm, L.L.; Enderle, H.F.; Fleißner, M., *High-density polyethylene pipe resins.* Adv. Mater. **1992**, 4(3), 234-238.

84. De Souza, R.F.; Casagrande, Jr. O.L., *Recent advances in olefin polymerization using binary catalyst systems.* Macromol. Rapid Commun. **2001**, 22(16), 1293-1301.

85. Komon, Z.J.A.; Bazan, G.C., *Synthesis of branched polyethylene by tandem catalysis.* Macromol. Rapid Commun. **2001**, 22(7), 467-478.

86. Freedonia Group, The, *Metallocene & Single Site Polymers to 2009*, Distributed by: Global Information, Inc., Editor. **2005**, http://www.the-infoshop.com/.

87. Vega, J.F.; Santamaria, A.; Munoz-Escalona, A.; Lafuente, P., *Small-amplitude oscillatory shear flow measurements as a tool to detect very low amounts of long chain branching in polyethylenes.* Macromolecules **1998**, 31(11), 3639-3647.

88. Malmberg, A.; Liimatta, J.; Lehtinen, A.; Löfgren, B., *Characteristics of long chain branching in ethene polymerization with single site catalysts.* Macromolecules **1999**, 32(20), 6687-6696.

89. Ferry, J.D., *Viscoelastic Properties of Polymers*, John Wiley and Sons, New York **1980**, 672.

90. Graessley, W.W.; Edwards, S.F., *Entanglement interactions in polymers and the chain contour concentration.* Polymer **1981**, 22(10), 1329-1334.

91. Zang, Y.H.; Carreau, P.J., *A correlation between critical end-to-end distance for entanglements and molecular chain diameter of polymers.* J. Appl. Polym. Sci. **1991**, 42(7), 1965-1968.

92. Wasserman, S.; Graessley, W.W., *Prediction of linear viscoelastic response for entangled polyolefin melts from molecular weight distribution.* Polymer Eng. Sci. **1996**, 36(6), 852-861.

93. Bersted, B.H., *On the effects of very low levels of long chain branching on rheological behavior in polyethylene.* J. App. Pol. Sci. **1985**, 30(9), 3751-3765.

94. Bersted, B.H.; Slee, J.D.; Richter, C.A., *Prediction of rheological behavior of branched polyethylene from molecular structure.* J. App. Pol. Sci. **1981**, 26(3), 1001-1014.

95. Gabriel, C.; Münstedt, H., *Creep recovery behavior of metallocene linear low-density polyethylenes.* Rheol. Acta **1999**, 38(5), 393-403.

96. Tobita, H., *Dimensions of branched polymers formed in simultaneous long-chain branching and random scission.* J. Polym. Sci., Part B: Polym. Phys. **2001**, 39(23), 2960-2968.

97. Beer, F.; Capaccio, G.; Rose, L., *High molecular weight tail and long-chain branching in SRM 1476 polyethylene.* J. App. Pol. Sci. **1999**, 73(14), 2807-2812.

98. Alamo, R.G.; Mandelkern, L., *Thermodynamic and structural properties of ethylene copolymers.* Macromolecules **1989**, 22, 1273-1277.

99. Höhne, G.W.H., *Another approach to the Gibbs-Thomson equation and the melting point of polymers and oligomers.* Polymer **2002**, 43(17), 4689-4698.

100. Alizadeh, A.; Richardson, L.; Xu, J.; McCartney, S.; Marand, H.; Cheung, Y.W.; Chum, S., *Influence of Structural and Topological Constraints on the Crystallization and Melting Behavior of Polymers. 1. Ethylene/1-Octene Copolymers.* Macromolecules **1999**, 32(19), 6221-6235.

101. Stadler, F., *Ph.D. thesis in preparation*, Department of Materials Science, Friedrich-Alexander University Erlangen-Nürnberg, Erlangen.

102. Trinkle, S.; Walter, P.; Friedrich, C., *Van Gurp-Palmen Plot II - classification of long chain branched polymers by their topology.* Rheol. Acta **2002**, 41(1-2), 103-113.

103. Zimm, B.H.M; Stockmayer, W. H., *The dimensions of molecules containing branching and rings.* Journal of Chemical Physics **1949**, 17(12), 1301-1314.

104. McLeish, T. C. B.; Allgaier, J.; Bick, D. K.; Bishko, G.; Biswas, P.; Blackwell, R.; Blottiere, B.; Clarke, N.; Gibbs, B.; Groves, D. J.; Hakiki, A.; Heenan, R. K.; Johnson, J. M.; Kant, R.; Read, D. J.; Young, R. N., *Dynamics of entangled H-polymers: Theory, rheology, and neutron-scattering.* Macromolecules **1999**, 32(20), 6734-6758.

105. Hopf, A., *Ph.D. thesis: Homo- und Copolymerisation von Propen/Ethen mit C_s-symmetrischen Metallocen/MAO-Katalysatoren*, University of Hamburg, Hamburg, **2002**.

106. Quijada, R.; Dupont, J.; Miranda, M.S.L.; Scipioni, R.B.; Galland, G.B., *Copolymerization of ethylene with 1-hexene and 1-octene: correlation between type of catalyst and comonomer incorporated.* Macromol. Chem. Phys. **1995**, 196(12), 3991-4000.

107. Chien, J.C.W.; Nozaki, T., *Ethylene-hexene copolymerization by heterogeneous and homogeneous Ziegler-Natta catalysts and the "comonomer" effect.* J. Polym. Sci. Part A: Polym. Chem. **1993**, 31(1), 227-237.

108. Seppälä, J.V.; Koivumäki, J.; Liu, X., *Co- and terpolymerization of ethylene with 1-butene and 1-decene by using Cp_2ZrCl_2-methylaluminoxane catalyst.* J. Polym. Sci., Part A: Polym. Chem. **1993**, 31(13), 3447-3452.

109. Koivumäki, J.; Seppälä, J.V., *Observations on the rate enhancement effect with magnesium chloride/titanium tetrachloride and dicyclopentadienylzirconium dichloride (Cp_2ZrCl_2) catalyst systems upon 1-hexene addition.* Macromolecules **1993**, 26(21), 5535-5538.

110. Villar, M.A.; Ferreira, M.L., *Co- and terpolymerization of ethylene, propylene, and higher α-olefins with high propylene contents using metallocene catalysts.* J. Polym. Sci. Part A: Polym. Chem. **2001**, 39(7), 1136-1148.

111. Randall, J. C., *A review of high-resolution liquid carbon-13 nuclear magnetic resonance characterizations of ethylene-based polymers.* J. Macromol. Sci. - Rev. Macromol. Chem. Phys. **1989**, C29(2&3), 201-317.

112. Keating, M.; Lee, I.H.; Wong, C.S., *Thermal fractionation of ethylene polymers in packaging applications.* Thermochim. Acta **1996**, 284, 47-56.

113. Müller, A.J.; Arnal, M.L., *Thermal fractionation of polymers.* Prog. Polym. Sci. **2005**, 30, 559-603.

114. Zhang, M.; Wanke, S.E., *Quantitative Determination of Short-Chain Branching Content and Distribution in Commercial Polyethylenes by Thermally Fractionated Differential Scanning Calorimetry.* Polym. Eng. Sci. **2003**, 43(12), 1878-1888.

115. Klimke, K., *Ph.D. thesis in preparation*, Max Planck Institute for Polymer Research, Mainz, **2005**.

116. Tackx, P.; Tacx, J.C.J.F., *Chain architecture of LDPE as a function of molar mass using size exclusion chromatography and multi-angle laser light scattering (SEC-MALLS).* Polymer **1998**, 39(14), 3109-3113.

117. Zimm, B.H.M.; Stockmayer, W.H., *The dimensions of chain molecules containing branches and rings.* J. Chem. Phys. **1949**, 17(12), 1301-1314.

118. Sun, T.; Brant, P.; Chance, R.R.; Graessley, W.W., *Effect of Short Chain Branching on the Coil Dimensions of Polyolefins in Dilute Solution.* Macromolecules **2001**, 34(19), 6812-6820.

119. Adisson, E.; Ribeiro, M.; Deffieux, A.; Fontanille, M., *Evaluation of the heterogeneity in linear low-density polyethylene comonomer unit distribution by differential scanning calorimetry characterization of thermally treated samples.* Polymer **1992**, 33(20), 4337-4342.

120. Starck, P., *Studies of the Comonomer Distributions in Low-Density Polyethylenes using Temperature Rising Elution Fractionation and Stepwise Crystallization by DSC.* Polym. Int. **1996**, 40, 111-122.

121. Starck, P.; Malmberg, A.; Löfgren, B., *Thermal and Rheological Studies on the Molecular Composition and Structure of Metallocene and Zeigler-Natta-Catalyzed Ethylene-α-Olefin Copolymers.* J. Appl. Polym. Sci. **2002**, 83, 1140-1156.

122. Starck, P.; Rajanen, K.; Löfgren, B., *Comparative Studies of Ethylene-α-Olefin Copolymers by Thermal Fractionations and Temperature Dependent Crystallinity Measurements.* Thermochim. Acta **2002**, 7042, 1-13.

123. Starck, P.; Lehmus, P.; Seppälä, J.V., *Thermal Characterization of Ethylene Polymers prepared with Metallocene Catalysts.* Polym. Eng. Sci. **1999**, 39, 1444-1455.

124. Starck, P.; Löfgren, B., *Thermal Properties of Ethylene / Long Chain α-Olefin Copolymers produced by Metallocenes.* Europ. Polym. J. **2002**, 38, 97-107.

125. Lehtinen, C.; Starck, P.; Löfgren, B., *Co- and Terpolymerizations of Ethene and α-Olefins with Metallocenes.* J. Polym. Sci., Part A: Polym. Chem. **1997**, 35, 307-318.

126. Benavente, R.; Pérez, E.; Yazdani-Pedram, M.; Quijada, R., *Viscoelastic relaxations in poly(ethylene-co-1-octadecene) synthesized by a metallocene catalyst.* Polymer **2002**, 43, 6821-6828.

127. Starck, P., *Dynamic Mechanical Thermal Analysis on Ziegler-Natta and Metallocene type Ethylene Copolymers.* Europ. Polym. J. **1997**, 33, 339-348.

128. Yoon, J.-S.; Lee, D.-H.; Park, E.-S.; Lee, I.-M.; Park, D.-K.; Jung, S.-O., *Thermal and mechanical properties of ethylene/α-olefin copolymers produced over (2-MeInd)$_2$ZrCl$_2$/MAO system.* Polymer **2000**, 41(12), 4523-4530.

129. Clas, S.-D.; McFaddin, D.C.; Russell, K.E., *Dynamic Mechanical Properties of Homogeneous Copolymers of Ethylene and 1-Alkenes.* J. Polym. Sci., Part B: Polym. Phys. **1987**, 25, 1057-1069.

130. Boyd, R.H., *Relaxation processes in crystalline polymers: molecular interpretation - a review.* Polymer **1985**, 26(8), 1123-1133.

131. Popli, R.; Mandelkern, L., *The transition in ethylene copolymers: the β-transition.* Polym. Bull. **1983**, 9(6-7), 260-267.

132. Alamo, R.; Domszy, R.; Mandelkern, L., *Thermodynamic and structural properties of copolymers of ethylene.* J. Phys. Chem. **1984**, 88(26), 6587-6595.

133. Popli, R.; Glotin, M.; Mandelkern, L., *Dynamic mechanical studies of α and β relaxations of polyethylenes.* J. Polym. Sci., Part B: Polym. Phys. **1984**, 22(3), 407-448.

134. Khanna, Y.P.; Turi, E.A.; Taylor, T.J.; Vickroy, V.V.; Abbott, R.F., *Dynamic mechanical relaxations in polyethylene.* Macromolecules **1985**, 18, 1302-1309.

135. Flory, P.J.; Yoon, D.Y.; Dill, K.A., *The interphase in lamellar semicrystalline polymers.* Macromolecules **1984**, 17, 862-868.

136. Strobl, G.R.; Hagedorn, W., *Raman spectroscopic method for determining the crystallinity of polyethylene.* J. Polym. Sci., Part B: Polym. Phys. **1978**, 16(7), 1181-1193.

137. Alamo R.G., Mandelkern L., *Thermodynamic and structural properties of ethylene copolymers.* Macromolecules **1989**, 22, 1273-1277.

138. Walter, P.; Trinkle, S.; Suhm, J.; Mader, D.; Friedrich, C.; Mülhaupt, R., *Short and long chain branching of polyethene prepared by means of ethene copolymerization with 1-eicosene using MAO activated* $Me_2Si(Me_4Cp)(N^tBu)TiCl_2$. Macromol. Chem. Phys. **2000**, 201, 604-612.

139. Anal, M.L.; Balsamo, V.; Ronca, G.; Sanchez, A.; Müller, A.J.; Canizales, E.C.; de Navarro, C.U., J. Therm. Anal. **2000**, 59, 451.

140. Müller, A.J.; Arnal, M.L.; Spinelli, A.L.; Cañizales, E.; Puig, C.C.; Wang, H.; Han, C.C., *Morphology and Crystallization Kinetics of Melt Miscible Polyolefin Blends.* Macromol. Chem. Phys. **2003**, 204(12), 1497-1513.

141. Hosoda, S., *Structural Distribution of Linear Low-Density Polyethylenes.* Polym. J. **1988**, 20(5), 383-397.

142. Mirabella, F.M., *Correlation of the Melting Behavior and Copolymer Composition Distribution of Ziegler-Natta-Catalyst and Single-Site-Catalyst Polyethylene Copolymers.* J. Polym. Sci., Part B: Polym. Phys. **2001**, 39, 2800-2818.

143. Flory, P.J., *Theory of Crystallization in Copolymers.* Faraday Soc. Transact. **1955**, 51, 848-875.

144. Zhang, F.; Liu, J.; Fu, Q.; Huang, H.; Hu, Z.; Yao, S.; Cai, X.; He, T., *Polydispersity of Ethylene Sequence Length in Metallocene Ethylene/α-Olefin Copolymers. I. Characterized by Thermal-Fractionation Technique.* J. Polym. Sci., Part B: Polym. Phys. **2002**, 40, 813-821.

145. Chen, F.; Shanks, R.A.; Amarasinghe, G., *Molecular distribution analysis of melt-crystallized ethylene copolymers.* Polym. Int. **2004**, 53(11), 1795-1805.

146. Russell, K.E.; McFaddin, D.C.; Hunter, B.K.; Heyding, R.D., *Crystallization of Side Chains in Copolymers of Ethylene and 1-Alkenes.* J. Polym. Sci., Part B: Polym. Phys. **1996**, 34, 2447-2458.

147. Heiland, K.; Kaminsky, W., *Comparison of zirconocene and hafnocene catalysts for the polymerization of ethylene and 1-butene.* Makromol. Chem. **1992**, 193, 601-610.

148. Chu, K.-J.; Soares, J.B.P.; Penlidis, A., *Variation of molecular weight distribution (MWD) and short chain branching distribution (SCBD) of ethylene/1-hexene copolymers produced with different in-situ supported metallocene catalysts.* Macromol. Chem. Phys. **2000**, 201, 340-348.

149. Soares, J.B.P.; Kim, J.D., *Copolymerization of ethylene and α-olefins with combined metallocene catalysts. I. A formal criterion for molecular weight bimodality.* J. Polym. Sci., Part A: Polym. Chem. **2000**, 38, 1408-1416.

150. Kim, J.D.; Soares, J.B.P., *Copolymerization of ethylene and α-olefins with combined metallocene catalysts. II. Mathematical modeling of polymerization with single metallocene catalysts.* J. Polym. Sci., Part A: Polym. Chem. **2000**, 38, 1417-1426.

151. Kim, J.D.; Soares, J.B.P., *Copolymerization of ethylene and α-olefins with combined metallocene catalysts. III. Production of polyolefins with controlled microstructures.* J. Polym. Sci., Part A: Polym. Chem. **2000**, 38, 1427-1432.

152. Ahlers, A.; Kaminsky, W., Makromol. Chem., Rapid Commun. **1998**, 9, 457.

153. D'Agnillo, L.; Soares, J.B.P.; Penlidis, A., *Controlling molecular weight distributions of polyethylene by combining soluble metallocene/MAO catalysts.* J. Polym. Sci., Part A: Polym. Chem. **1998**, 36, 831-840.

154. Han, T.K.; Choi, H.K.; Jeung, D.W.; Ko, Y.S.; Woo, S.I., *Control of molecular weight and molecular weight distribution in ethylene polymerization with metallocene catalysts.* Macromol. Chem. Phys. **1995**, 196, 2637-2647.

155. Kim, J.D.; Soares, J.B.P.; Rempel, G.L., *Synthesis of tailor-made polyethylene through the control of polymerization conditions using selectively combined metallocene catalysts in a supported system.* J. Polym. Sci., Part A: Polym. Chem. **1999**, 37, 331-339.

156. Liu, J.; Rytter, E., *Bimodal Polyethylenes Obtained with a Dual-Site Metallocene Catalyst System. Effect of Trimethylaluminium Addition.* Macromol. Rapid Commun. **2001**, 22, 952-956.

157. Beigzadeh, D.; Soares, J.B.P.; Duever, T.A., *Combined metallocene catalysts: an efficient technique to manipulate long-chain branching frequency of polyethylene.* Macromol. Rapid Commun. **1999**, 20, 541-545.

158. Beigzadeh, D.; Soares, J.B.P.; Duever, T.A., *Production of polyolefins with controlled long chain branching and molecular weight distributions using mixed metallocene catalysts.* Macromol. Symp. **2001**, 173, 179-194.

159. Lieber, S.; Brintzinger, H.-H., *Propene Polymerization with Catalyst Mixtures Containing Different ansa-Zirconocenes: Chain Transfer to Alkylaluminum Cocatalysts and Formation of Stereoblock Polymers.* Macromolecules **2000**, 33, 9192-9199.

160. Chien, J.C.W.; Iwanoto, Y.; Rausch, M.D., *Homogeneous binary zirconocenium catalysts for propylene polymerization. II. Mixtures of isospecific and syndiospecific zirconocene systems.* J. Polym. Sci., Part A: Polym. Chem. **1999**, 37, 2439-2445.

161. Chien, J.C.W.; Iwanoto, Y.; Rausch, M.D.; Wedler, W.; Winter, H.H., *Cationic Initiation of Vinyl Ether Polymerization Induced by* $(4\text{-}R^1C_6H_4)(4\text{-}R^2C_6H_4)R^3CX$ *in Conjunction with Silica: Producing Highly Head Group Functionalized Polymers.* Macromolecules **1997**, 30, 3447-3458.

162. Bruaseth, I., *Ph.D. thesis: Towards tailoring of ethene/1-hexene copolymers by dual-site metallocene catalysis*, Norwegian University of Science and Technology, Trondheim, **2003**.

163. Bruaseth, I.; Rytter, E., *Dual Site Ethene/1-Hexene Copolymerization with MAO Activated* $(1,2,4\text{-}Me_3Cp)_2ZrCl_2$ *and* $(Me_5Cp)_2ZrCl_2$ *Catalysts. Possible Transfer of Polymer Chains between the Sites.* Macromolecules **2003**, 36(9), 3026-3034.

164. Bruaseth, I.; Rytter, E., *Relative reactivity enhancement of* $(Me_5Cp)_2ZrCl_2$ *in mixture with* $(1,2,4\text{-}Me_3Cp)_2ZrCl_2$ *during ethene/1-hexene copolymerization.* Macromol. Symp. **2004**, 213, 69-78.

165. Przybyla, C.; Fink, G., *Two different, on the same silica supported metallocene catalysts, activated by various trialkylaluminums. A kinetic and morphological study as well as an experimental investigation for building stereoblock polymers.* Acta Polym. **1999**, 50(2-3), 77-83.

166. Arrowsmith, D.; Kaminsky, W.; Schauwienold, A.-M.; Weingarten, U., *EP(D)M-synthesis with highly active homogeneous and heterogeneous metallocene/MAO-catalysts.* J. Mol. Catal. A: Chem. **2000**, 160(1), 97-105.

167. Fan, W.; Waymouth, R. M., *Alternating Copolymerization of Ethylene and Propylene: Evidence for Selective Chain Transfer to Ethylene.* Macromolecules **2001**, 34, 8619-8625.

168. Karssenberg, F.G.; Mathot, V.B.F.; Zwartkruis, T.J.G., *Chain Microstructure of Homogeneous Ethylene-1-Alkene Copolymers and Characteristics of Single Site Catalysts using a Direct 13C NMR Peak Method. Part I: Theory and Models.* Polym. Sci., Part B: Polym. Phys. **2005**, in press.

169. Hu, W.; Karssenberg, F.G.; Mathot, V.B.F., *How restriction of sliding diffusion of comonomers affects crystallization and melting of homogeneous copolymers.* Polymer **2005**, in press.

170. Ewen, J.E.; Jones, R.L.; Razavi, A.; Ferrara, J.D., *Syndiospecific propylene polymerizations with Group IV metallocenes.* J. Am. Chem. Soc. **1988**, 110(18), 6255-6258.

171. Razavi, A.; Ferrara, J., *Preparation and crystal structures of the complexes (η5-C5H4CMe2-η5-C13H8)MCl2 (M = zirconium, hafnium) and their role in the catalytic formation of syndiotactic polypropylene.* J. Organomet. Chem. **1992**, 435, 299-310.

172. Landolt-Börnstein, *Physikalisch-Chemische Tabellen, Band IV, Technik, 4. Teil, Band C: Wäremetechnik.* 6th edition eds. Vol. C2, Springer, Berlin **1976**, 126-129.

173. Fillon, B.; Wittmann, J.C.; Lotz, B.; Thierry, A., *Self-Nucleation and Recrystallization of Isotactic Polypropylene (α Phase) Investigated by Differential Scanning Calorimetry.* J. Polym. Sci., Part B: Polym. Phys. **1993**, 31, 1383-1393.

174. Müller, A.J.; Hernández, Z.H.; Arnal, M.L.; Sánchez, J.J., *Successive self-nucleation/annealing (SSA): A novel technique to study molecular segregation during crystallization.* Polym. Bull. **1997**, 39, 465-472.

175. Grubisic, Z.; Rempp, P.; Benoit, H.C., *A Universal Calibration for Gel Permeation Chromatography.* J. Polym. Sci., Part B: Polym. Phys. **1996**, 34, 1707-1713.

176. Barth, H.G., *Comments on "Universal Calibration for Gel Permeation Chromatography", by Z. Grubisic, P. Rempp, and H. Benoit, J. Polym. Sci., 5, 753 (1967).* J. Polym. Sci., Part B: Polym. Phys. **1996**, 34, 1705-1706.

177. Benoit, H.C., *Reflections on "Universal Calibration for Gel Permeation Chromatography", by Z. Grubisic, P. Rempp, and H. Benoit, J. Polym. Sci., 5, 753 (1967).* J. Polym. Sci., Part B: Polym. Phys. **1996**, 34, 1703-1704.

178. Scholte, T.G.; Meijerink, N.L.J.; Schoffeleers, H.M.; Brands, A.M.G., *Mark-Houwink Equation and GPC Calibration for Linear Short-Chain Branched Polyolefins, Including Polypropylene and Ethylene-Propylene Copolymers.* J. Appl. Polym. Sci. **1984**, 29, 3763-3782.

179. Coll, H.; Gilding, D.K., *Universal calibration in gel-permeation chromatography: study of polystyrene, poly(α-methylstyrene), and polypropylene.* J. Polym. Sci., Polym. Phys. Ed. **1970**, 8, 89-103.

8. Appendix

8.1 Abbreviations and symbols

^{13}C NMR	carbon13 nuclear magnetic resonance
CGC	constrained geometry catalyst
c_n	number of carbons in the comonomer chain
CP MAS	cross polarization magic angle spinning
CSTR	continuous stirred tank reactor
DI	DSC relative index
DMA	dynamic mechanical analysis
DPM	direct peak method
DSC	differential scanning calorimetry
ESL	ethylene sequence length
EPDM	ethene propene dien monomer (rubber)
$\lvert G^*\rvert$	complex modulus
HDPE	high density polyethylene
HUT	Helsinki University of Technology
J_e^0	linear steady-state elastic compliance
mPE	metallocene catalyzed polyethylene
L_c	crystalline lamellar thickness
LCB	long-chain branching
LDPE	low density polyethylene
LLDPE	linear low density polyethylene
MAO	methylaluminoxane
m_c	molar mass of the comonomer
M_c	critical molar mass
MDPE	medium density polyethylene
M_e	entanglement molar mass
M_{LS}	molar mass determined by light scattering
MMD	molar mass distribution = M_w/M_n = polydispersity
M_n	number average molar mass
MSL	methylene sequence length
M_w	weight average molar mass
n_c	molar fraction of the comonomer content in the polymer
SC	step crystallization from the melt
SCB	short-chain branching
SEC-MALLS	size exclusion chromatography – multi angle laser light scattering
SNR	signal to noise ratio
SSA	successive self-nucleation and annealing
T_c	crystallization peak temperature
TCB	1,2,4-trichlorobenzene
T_g	glass transition temperature
T_m	melting peak temperature
T_m^0	equilibrium melting temperature
TMA	trimethylaluminium
T_m^f	final melting temperature
T_m^c	copolymer melting temperature
TPE	thermoplastic elastomer

t_{poly}	polymerization time
T_{poly}	polymerization temperature
T_s	step temperature in SSA method
UHMWPE	ultra high molecular weight polyethylene
VLDPE	very low density polyethylene
w_c	weight fraction of the comonomer content in the polymer
X	CH_2 molar fraction
X_e	copolymer composition
Z-N	Ziegler-Natta (catalysis)

δ	phase angle
ΔH	enthalpy of fusion
ΔH_u	volumetric heat of fusion
η_0	zero shear-rate viscosity
η_0^{lin}	zero shear-rate viscosity of a linear polymer
σ_e	basal surface free energy

$(CpMe_5)_2ZrCl_2$	Di-[η5-(penta-methyl)cyclopentadienyl] zirconiumdichloride
Cp_2ZrCl_2	Zirconocene, Di-(η5-cyclopentadienyl) zirconiumdichloride
rac-$[Et(Ind)_2]ZrCl_2$	*rac*-[Ethylen-di-(1-η^5-indenyl)] zirconiumdichloride
$[Me_2C(Cp)_2]ZrCl_2$	[Isopropyliden-bis-(η5-cyclopentadienyl)] zirconiumdichloride
$[Ph_2C(2,7\text{-di-}^{tert}BuFlu)(Cp)]ZrCl_2$	[Diphenylmethylen(2,7-bis(1,1-di-methylethyl)-9-η^5-fluorenyl)(η5-cyclopentadienyl)] zirconiumdichloride
$[Me_2Si(Ind)(Flu)]ZrCl_2$	[Dimethylsilyl(1-η^5-indenyl)(9-η^5-fluorenyl)] zirconiumdichloride
$[Me_2Si(Me_4Cp)(N^{tert}Bu)]TiCl_2$	[Dimethylsilylen-(^{tert}butylamido)-(2,3,4,5-tetramethyl-1-η^5-cyclopentadienyl)] titaniumdichloride
rac-$[Me_2Si(2\text{-}Me\text{-}4\text{-}(1\text{-}Naph)Ind)_2]ZrCl_2$	*rac*-[Dimethylsilylbis(2-methyl-4-(1-naphtyl)-1-η^5-indenyl)] zirconiumdichloride

8.2 1-Hexacosene comonomer specifications

This wax is used as comonomer for polymerizations and within this thesis it is named as 1-hexacosene. It is a fraction for differenent α-olefins. The product name from Chevron Phillips Chemical Company LP is “Alpha Olefin 26-28”, obtained from distillation. The following information is taken from the product data sheet, for more information see: http://www.cpchem.com.

CHARACTERISTIC	METHOD	SPECIFICATION
Carbon Number, wt. % C_{24}, max.	GLC	3.0
Carbon Number, wt. % C_{26}, min.-max.	GLC	50-62
Carbon Number, wt. % C_{28}, min.-max.	GLC	30-42
Carbon Number, wt. % C_{30}, max.	GLC	6.0
Color, Saybolt, min.	ASTM D 156	+30
Appearance	ASTM D 4176	Bright & Clear

ADDITIONAL INFORMATION	METHOD	TYPICAL VALUE
n-Alpha Olefin, wt. %	NMR	83
Vinylidene, wt. %	NMR	15
cis- and trans-2-Olefin, wt. %	NMR	2
Paraffin, wt. %	Calculated	0.3
API Gravity, 15.6°C/15.6°C (60°F/60°F)	ASTM D 287	40.4
Specific Gravity (Solid), 15.6°C/15.6°C (60°F/60°F)	ASTM D 287	0.822
Specific Gravity (Liquid), 71°C/15.6°C (160°F/60°F)	SM 350-4	*
Density, lb./gal., 15.6°C (60°F)		6.48
Congealing Point, °C (°F)	ASTM D 938	*
Drop Melt Point, °C (°F)	ASTM D 127	56.7 (134)
Flash Point, PM, °C (°F)	ASTM D 93	227
Viscosity, 99°C (210°F)		
- Kinematic, cSt	ASTM D 445	*
- Saybolt, SUS	ASTM D 2161	*
Penetration, 0.10 mm, 25°C (77°F)	ASTM D 1321	63
Distillation, °C (°F)	ASTM D 1160/5mm	
IBP		*
5%		*
95%		*
EP		*

* = Data incomplete to-date

8.3 Safety instructions

chemical substance	symbol	risks	safety
acetone	Xi, F	11-36-66-67	(2-)9-16-26
argon	A	-	-
catalyst BASF R3-11	A	-	-
1-decene	A	-	-
2,6-Di^{tert}butyl-4-methyl-phenol	Xn	20/21/22-38	36/37
1-dodecene	A	-	-
ethanol	F	11	2-7-16
ethene	F^+	12	2-9-16-33
1-hexacosene	A	-	-
hydrochloric acid (36 wt.-%)	C	35-37	7/9-26-44
hydrogen	F^+	12	2-9-16-33
methylalumoxan	F, C	14/15-17-35	16-23-30-36-43
1-octadecene	A	-	-
1-octene	F	11	-
iso-propanol	F, Xi	11-36-67	7-16-24/25-26
propene	F^+	12	2-9-16-33
1,1,2,2-tetrachloro-1,2-dideuteroethane	T	26/27	2-38-45
1,2,3-trichlorobenzene	Xn, N	22-38-50/53	2-23-37/39-60-61
toluene	F, Xn	11-20	16-25-29-33

Declaration

I declare to have developed the results presented in this thesis myself, and with the help of no other than the cited references and resources.

This work has not been presented to any inspecting authority in the same or a similar form before.

Erklärung

Der Verfasser erklärt, die vorliegende Arbeit selbständig und ohne fremde Hilfe verfasst zu haben. Andere als die angegebenen Hilfsmittel und Quellen wurden nicht benutzt und die benutzten wörtlich oder inhaltlich entnommen Stellen sind als solche kenntlich gemacht.

Diese Arbeit hat in gleicher oder ähnlicher Form noch keiner Prüfungsbehörde vorgelegen.

Hamburg, den 15. Oktober 2005 ___________________________

(Christian Piel)